Characteristics of Brown Carbon Present in Ambient Aerosols Over Different Regions in India

A Thesis

submitted for the Award of Ph. D. degree of

MOHANLAL SUKHADIA UNIVERSITY

in the

Faculty of Sciences

By

Rangu Venkata Satish Kumar

Under the supervision of

Dr. Neeraj Rastogi
Associate Professor
Physical Research Laboratory,
Ahmedabad-380 009, India

Department of Chemistry
Mohanlal Sukhadia University, Udaipur
2018

CERTIFICATE

I feel great pleasure in certifying that the thesis entitled "**Characteristics of brown carbon present in ambient aerosol over different regions in India**" by Mr. Rangu Venkata Satish Kumar has been completed under my guidance.

He has completed the following requirements as per the Ph.D. regulations of the University:

(a)Completion of the Course Work as per the university rules.

(b)Residential requirements as per the university rules.

(c)Regular submission of six monthly progress reports.

(d)Presentation of his/her work in the Departmental Committee

(e)Publication of at least one research paper in a refereed research journal.

I am satisfied with the analysis of data, interpretation of results and conclusions drawn. I recommend the submission of the thesis.

Date:2018

Name and Designation of the supervisor

Dr. Neeraj Rastogi

Associate Professor

Countersigned by

ABSTRACT

Brown carbon (BrC) is a part of organic carbon (OC) which efficiently absorbs light at near UV and visible region, and it is characterized by an absorption spectrum that smoothly increases from the visible to UV wavelengths. BrC immersed in cloud droplets can absorb light and facilitate evaporation/dispersion of clouds. It contributes ~35% of the direct radiative forcing warming caused by carbonaceous aerosols. However, to better assess the effects of BrC on air quality and climate, a proper understanding of its sources and characteristics on temporal and spatial scales is very important. In this study, we have characterized atmospheric BrC using both offline and online techniques. With an aim to understand the characteristics of BrC over different regions dominated by different emission sources and/or meteorological conditions, many regions (Patiala, Delhi, Kanpur, Ahmedabad, Shillong, and Port Blair) and sampling periods were selected for particulate matter smaller than 2.5 µm aerodynamic diameter ($PM_{2.5}$) sampling. Absorption coefficient at 365 nm is used as a general measure of water-soluble (($b_{abs\_365\_Water}$) and methanol soluble ($b_{abs\_365\_Methanol}$) BrC. Further, BrC characteristics were investigated concerning its sources, chemical composition, optical properties, and atmospheric evolution. Results from this study suggest that primary emissions from biomass burning (BB) and fossil fuel burning (FFB) are the major sources of highly absorbing BrC, and BB emits significant fraction of water-insoluble BrC. Further, secondary BrC and aged/oxygenated OA are found to be relatively less absorbing. BrC absorption decreases as the day progresses achieving a minimum during afternoon hours, which is ascribed to photo-bleaching/volatilization of BrC. It is also shown that BrC composition is not uniform throughout the day. Our observations suggest that BrC chromophores are a variable mixture of at least HULIS and nitrogen-containing organic compounds over the study regions. Mass absorption efficiency (MAE) of water-soluble and methanol-soluble BrC is found to be significant compare to that of elemental carbon over most of the study sites. These results have important implications in estimating regional radiation budget.

TABLE OF CONTENTS

LIST OF TABLES

LIST OF FIGURES

CHAPTER 1

Introduction

1.1 What are atmospheric aerosol?

Aerosol are technically defined as a suspension of liquid and/or solid particles in the air. In day-to-day life, they are seen as dust, fume, smoke, mist, fog, haze, and smog (Jacobson et al., 2000). John Aitken, a Scottish meteorologist, considered one of the founders of cloud physics and aerosol science, began his pioneering research on condensation nuclei in 1875, and he published several of his significant findings concerning atmospheric aerosol in the 1880s. In his phenomenal paper "On the Number of Dust Particles in the Atmosphere" (1888), Aitken devised the first laboratory apparatus to measure the dust concentrations in the atmosphere and his instruments serve as the models for precise aerosol measurements even today. Studying the aerosol particles in the atmosphere is important because they influence our environment by affecting Earth's radiation balance, cloud chemistry as well as air quality. These particles are emitted to the atmosphere directly as a primary aerosol from different natural sources like sea spray, terrestrial dust, volcano ash emissions, bacteria, microscopic fungi, spores and pollen, emissions from forest fires, etc. (Seinfeld and Pandis, 2006). A secondary aerosol particle are formed in the atmosphere through different processes. The dispersal of material creates them at the pre-existing surface (primary aerosol), or by reaction of gases in the atmosphere (Hoyle et al., 2011; Spracklen et al., 2011). Secondary aerosol predominantly includes sulfates from the oxidation of sulfur-containing gases, nitrates from gaseous nitrogen species, and organic products from the oxidation of volatile organic compounds (VOCs).

1.2 Aerosol size distribution

Particle size is one of the most important parameters for characterizing the behavior of aerosol. The size of aerosol particles varies from a few nanometers (nm) to several micrometers (μm) depending upon their sources. In Fig. 1, a schematic view of multi-modal particle size distribution showing the different growth and shrink processes is presented. In the atmosphere, each particle mode has its specific sources. Nucleation particles form by condensation of super-

saturated gases, Aitken particles form from the nucleation mode particles or, by incomplete combustion (e.g., soot), accumulation mode particles form from Aitken particles or, intensive mechanical processes, and coarse particles form from accumulation mode particles and moderate mechanical processes (e.g., abrasion of mineral dust, volcanic ash, sea spray). Based on size, aerosol are defined as nucleation mode (~1 to 10 nm); Aitken mode (~10-100 nm); Accumulation mode (~100-1000 nm); and Coarse mode (1000-10000 nm). As the size of the particle grows, the residence time of the particle in the atmosphere also decreases. The residence time of aerosol particle is defined as the average time spent by an aerosol in the atmosphere before it is removed.

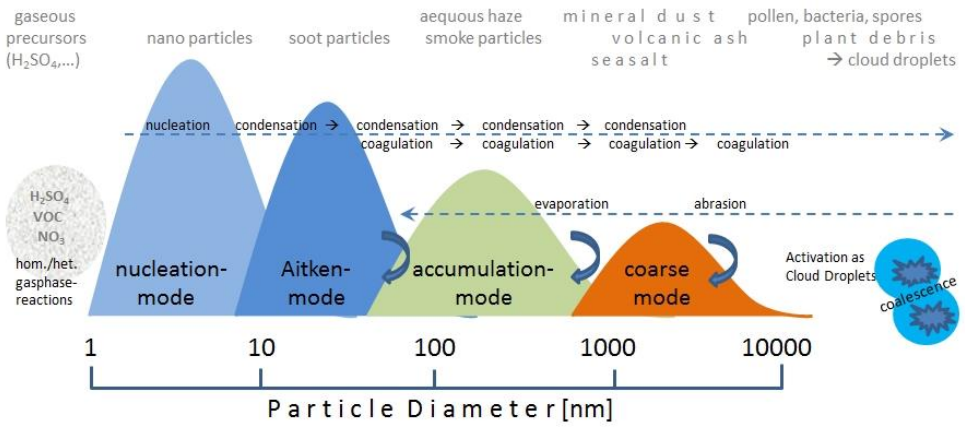

Figure 1.1: Schematic multi-modal particle size distribution with typical transformation processes and example particle types within each mode; Image courtesy: Deutscher Wetterdienst Institute

The particles are removed from the atmosphere mainly by two processes - dry deposition and wet deposition. Dry deposition of atmospheric aerosol critically depends on their sizes (Stoke's law) and hence, smaller particles have longer residence times in the atmosphere.

Dry deposition mainly consists of two processes – gravitational sedimentation and impaction. In gravitational sedimentation, the settling of particles occur due to the

gravity. In case of impaction, small particles interfacing a bigger obstacle are not able to follow the curved streamlines of the flow due to their inertia, so they hit or impact the droplet. The larger the masses of the small particles facing the big one, the greater the displacement from the flow streamline.

In wet removal, there are two mechanisms - washout by rain and washout by clouds. The removal rate by washout with rain depends on raindrop size distribution as well as aerosol size distribution. In washout by cloud process, they take part in cloud formation (acting as cloud condensation nuclei (CCN)) and are carried away by clouds as winds move them. In general, the lifetime of atmospheric aerosol varies from a few days to weeks and thus, have local to regional effects on air quality and climate (Seinfeld and Pandis, 2006). A typical residence time of atmospheric aerosol particles not only depends on their size but also their altitude. In the planetary boundary layer, the residence time of aerosol particles is usually less than a week depending on aerosol properties and meteorological conditions. In the free troposphere, the typical particle lifetime is 3–10 days on average (Williams et al., 2002). Given this long residence time, the particle can easily be transported to long distances. Therefore, we could see the variability in particle concentrations in the free troposphere, reflecting the geographical distribution of sources and sinks. In the stratosphere, aerosol particles have a much longer lifetime (up to 1 to 2 year) than the tropospheric particles, due to the lack of removal by precipitation.

1.3 Why do we study Aerosol?

People use aerosol for various purposes in the day to day life. For example, they use it for calibrating instruments, performing research, and testing sampling equipment and air filters. They use it as deodorants, paints, and other consumer products in sprays. They use it for dispersal and agricultural application. They also use it in medical treatment of respiratory disease. They use it in fuel injection systems and other combustion technology. However, people started working on atmospheric aerosol because aerosol affects Earth's climate directly or

indirectly. Atmospheric aerosol also affects air quality, human health, and biogeochemistry of surface ocean/lakes.

1.3.1 Direct and indirect effects on climate

Aerosol can absorb or scatter incoming solar radiation, thereby affecting Earth's radiative balance - the "direct effect." They can, thus, influence global temperature, rainfall, and dynamical circulations. Aerosol also influence the formation of clouds by acting as CCN and thereby causing indirect radiative forcing - the "indirect effect." The aerosol indirect effect has two components. An increase in aerosol concentration (CCN) increases droplet concentration and thereby reducing the droplet size. The resulting larger cross-sectional area for a fixed water content increases the cloud albedo significantly. Secondly, the lifetime of the clouds depends upon the size of droplets. If droplets are smaller, then they don't precipitate easily and decrease the amount of rainfall. The accompanying higher cloud lifetime and thickness also results in an increased cloud albedo. The aerosol indirect effect is considerably more complex and uncertain than the direct impact, and contributes significantly to the total aerosol radiative forcing. In addition to their role in climate, a scattering of radiation by aerosol particles decrease atmospheric visibility, a phenomenon more prominent during winter periods due to the higher relative humidity and lower temperature. (Hallquist et al., 2009; Kaul et al., 2011).

1.3.2 Effects on air quality

Aerosol undergoes both homogeneous (same phase) and heterogeneous chemical reactions. Aerosol particles also provide a surface media upon which chemical reactions can occur. For example, volcanic eruption emits vast amounts of sulfur dioxide (SO_2) into the atmosphere. Further, this SO_2 get converted to the H_2SO_4 aerosol in the atmosphere. Sulfur dioxide and nitrogen oxides (NO, NO_2) are also emitted in large amounts by anthropogenic sources like thermal power plants, from base-metal smelting, and fuel combustion in vehicles. Once released into the atmosphere, they form secondary pollutants like nitric acid and sulfuric acid, both

of which dissolve quickly in water. Hydrochloric acid (HCl), another volcanic gas, is also rapidly removed by liquid water due to its substantial solubility. These droplets can cause acid rain and thereby causes atmospheric pollution in various ways. In addition to this, ambient air pollution from particulate matter (PM) components also exists. The health impacts of aerosol include both short-term acute symptoms like asthma and bronchitis as well as long-term effects like chronic irritation and inflammation of the respiratory tract that can potentially lead to cancer (Jiang et al., 2016). Air pollution is known to affect the respiratory system (coughing, wheezing, reduced lung function), reproductive system (congenital disabilities), cardiovascular system (atherosclerosis, myocardial infarctions, and systemic inflammation) and nervous system (cerebrovascular impairment) (Wang et al., 2013; Pope et al., 2009).

1.3.3 Effects on biogeochemistry of aquatic systems

In addition to the air quality, aerosol deposition onto the land or ocean surfaces can impact various biogeochemical cycles by acting as either a source of nutrients or pollutants (Hamilton et al., 2013). In twentieth-century, rapid increase of industrialization and increase in the food production for the sustainability of rapidly growing world population had resulted in widespread changes in the sources and transport pathways of bioactive nutrients such as nitrogen (N), phosphorus (P), iron (Fe) and silicon (Si) (Krishnamurthy et al., 2010 and references are therein). Anthropogenic activities enhance Nitrogen (N) supply to coastal and open oceans (Luo et al., 2007). The increased N which released from the land due to agricultural use and fossil fuel consumption had resulted in a change in nutrient supply to the oceans (De Leeuw et al., 2001). Anthropogenic N inputs in the form of strong acid (HNO_3) and base (NH_3) dissociation products alter surface seawater alkalinity, pH, and inorganic carbon storage, increasing ocean acidification and affecting ecosystems, especially in coastal regions, which could have a significant effect on human populations (Doney et al., 2007).

1.4 Carbonaceous aerosol

Atmospheric PM mainly consists of carbonaceous matter, inorganic salts, siliceous crustal minerals, and water (Seinfeld and Pandis, 2006; Jacobson, 2014). Their chemical composition is highly variable on spatial and temporal scales. The variables include geographical location, urban/rural setting, altitude, sources and their emission strength, meteorological conditions and transport patterns towards the sampling sites. Over the past twenty years, studies on the chemical composition of inorganic salts and dust have made significant progress. However, due to their compositional complexity, atmospheric carbonaceous aerosol are still difficult to understand. Carbonaceous aerosol constitutes a substantial fraction of the total aerosol mass over urban and rural atmosphere (~20-80%), followed by water-soluble inorganic species (WSIS) and mineral aerosol (Kanakidou et al., 2005; Fuzzi et al., 2006; Tripathi et al., 2006; Rengarajan et al., 2007; Rastogi and Sarin, 2009; Rastogi et al., 2016).

Carbonaceous aerosol exerts a significant influence on atmospheric chemistry, climate forcing, and human health. Organic aerosol (OA) can be emitted from both primary and secondary sources. Primary OA is directly emitted into the atmosphere by fossil fuel burning (FFB), bio-fuel emission, trash burning, and biomass burning (BB). A set of directly emitted organic compounds and precursor gases (VOCs) undergo aging or atmospheric oxidation with species such as the hydroxyl radical (OH), nitrate radical (NO_3) and ozone (O_3) to produce secondary organic aerosol (SOA, Ng et al., 2008; Karl et al., 2009). The oxidation of VOC's generates low volatile organic compounds with long chains of different chemical moieties (such as CO_2, CH_2O, etc.) (Al et al., 2007; Robinson et al., 2011). Due to the chemical complexity of these oxidation processes, the exact chemical mechanisms leading to changes in the volatility of atmospheric organics (and in particular the formation of SOA) remains poorly constrained. In recent studies, it is reported that SOA accounts for a large, and often dominant, fraction of total organic particulate mass (Jimenez et al., 2009).

Over the last few years, it has been established that BC absorbs significant amounts of solar radiation and causes atmospheric warming. It absorbs light strongly over the broad spectral region from ultra-violet to infrared region (UV-IR). Typical BC absorption wavelengths are shown in Figure. 2. The BC is directly emitted into the atmosphere from a variety of combustion sources like crop-residue burning, diesel engines, industries, residential solid fuel, and open trash burning. Black carbon is co-emitted with a mixture of precursor gases and particles, and over time, BC particles get mixed with other aerosol components and develop a coating (Lack et al., 2013; Forrister et al., 2015). This coating on BC enhances its absorption. The enhancement of BC light absorption by coating depends upon the chemical composition of the components it gets mixed within the atmosphere. The hydrophobic (water repellent) BC particle can be changed to hydrophilic (water-loving) by coating with polar organic compounds (Ackerman and Toon, 1981). This allows BC particles to act as cloud condensation nuclei (CCN). Due to its hydrophilic nature, they influence cloud processes and alters the melting of snow and ice cover (Abbatt et al., 2012). The total direct radiative forcing by all black carbon (including preindustrial background sources) sources is +0.88 Wm^{-2} with 90% uncertainty bounds of +0.17 to +1.48 Wm^{-2} (Bond et al., 2006; 2013).

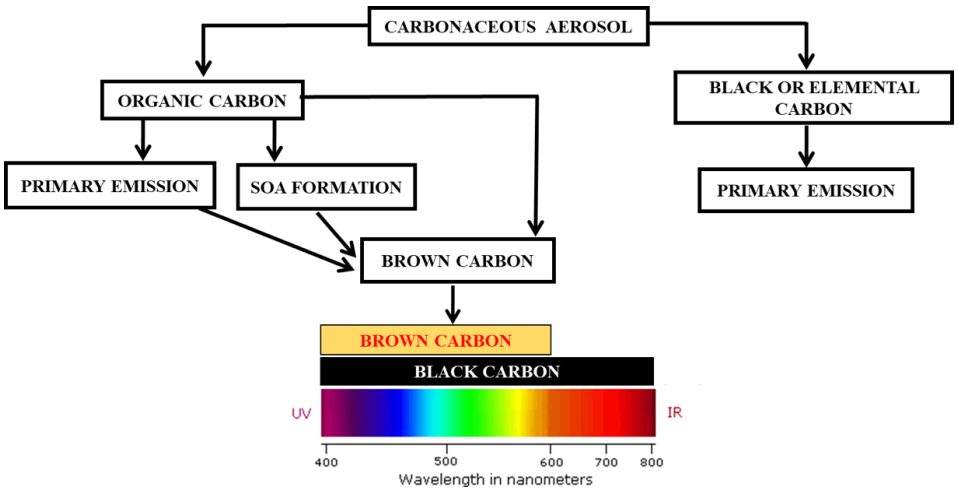

Figure 1.2: Types of carbonaceous aerosol and their absorption characteristics

OA constitute a significant fraction of airborne particulates and also play an important role in atmospheric chemistry and climate forcing. OC is composed of a wide variety of organic species including primary oxygenated organics such as humic-like substances (HULIS), which are similar to terrestrial and aquatic humic and fulvic acids. Organic aerosol related observations have been made not only confined to the surface but also in the free and the upper troposphere (Froyd et al., 2010). OA dominates the tropospheric aerosol mass concentration with varying regional levels, accounting for 20-60% of total suspended particulates (TSP) over continental mid-latitude regions (Seinfeld and Pankow, 2003), 20-80% over Indo-Gangetic Plain (Ram et al., 2011; Rastogi et al., 2016) and up to 90% over tropical rainforests (Kanakidou et al, 2005). Health-related impacts of OA and its formation pathways in the atmosphere are still challenging to comprehend (Mauderly and Chow, 2008; Chanpimol et al., 2017). It has been shown that OA poses adverse physiological effects on human health, mainly by causing asthma, bronchitis, heart disease and cancer (Pope et al., 2009).

The large uncertainty found in composite aerosol radiative forcing estimated by climate models since they consider BC only the absorbing species and they consider OC as purely scattering (Bond et al., 2013). Over the last two decades, considerable efforts have been made to understand the OA optical properties (Dusek et al., 2006; Riipinen et al., 2011). Despite fundamental advances having been made in these studies, our understanding of the climate-related properties of atmospheric OA still is incomplete, and the specific ways in which OA impacts the atmospheric chemistry and climate forcing due to OA are only beginning to be understood (Laskin et al., 2015). The scattering and absorbing nature of OA exerts a dominant impact on regional atmospheric chemistry and radiative forcing (RF). Often, OA considered as 'white,' i.e., it scatters the incoming solar radiation in most climate models. Recent studies have documented that a particular type of organic carbon significantly absorb light at near-UV (300-400nm) and visible regions and is termed as ''Brown Carbon'' (BrC) (Andreae and Gelencsér, 2006; Bond et al., 2006; Gustafsson et al., 2009; Laskin et al., 2015; Sun et al., 2017; Yan et al., 2018). This class of organic carbon, known for its light brownish color, is emitted from incomplete biomass and fossil fuel burning, while secondary

processes are also suggested as a significant source of BrC in the ambient atmosphere. Water-soluble organic carbon (WSOC) predominantly consists of secondarily formed oxygenated organic aerosol (Ervens et al., 2008; 2011). There is evidence from laboratory studies that secondary BrC is produced from a variety of chemical aging processes that often involve nitrogenous compounds (Laskin et al., 2015; Sun et al., 2017; Yan et al., 2018). Formation of light-absorbing nitro-aromatic compounds has been demonstrated in photooxidation of various aromatic precursors including benz[a]pyrene, naphthalene, catechol and guaiacol, and toluene in the presence of NOx (Lu et al., 2011; Ofner et al., 2011; Lambe et al., 2013; Lin et al., 2017; Wang et al., 2017).

BrC species may consist of a variety of organic chromophores with variable concentrations and different absorbing characteristics. The identification of molecular markers in BrC corresponding to the source of emission is a relatively new and vital area of research. BrC is a highly complex and dynamic mixture of organic compounds (Lin et al., 2017), although little is known about the relationship between its chemical composition and the source of emission. Different BrC chromophores can absorb at different wavelengths. Sun et al. (2007) suggested two kinds of organic carbon: a water-soluble organic mixture with some UV-visible absorption, and water-insoluble organic carbon with higher absorption (Hoffer et al., 2006; Chen and Bond, 2009). The BrC absorption at UV and visible region mainly associated with the functional groups (-OH, -NO_2, -NH_4, etc.) or conjugated double bonds which are attached to organic compounds. In the literature, BrC compounds may also be comprised of highly oxygenated (3 or more O atoms), are large (18+ carbon atoms), or contain one or more nitrogen atoms. High absorption also requires conjugation of unsaturated bonds or non-bonding electron pairs. The UV and visible absorption results from electronic transitions. These are often $\pi \rightarrow \pi^*$ transitions at UV and near-UV wavelengths, and $n \rightarrow \pi^*$ transitions at visible wavelengths. If BrC compounds containing O or N, non-bonding orbitals allow the $n \rightarrow \pi^*$ transition that occurs at visible wavelengths (Sun et al., 2007). In the presence of functional groups (-OH, -NO_2, -NH_4, etc.) they tend to have a low energy gap and higher λ. Jacobson et al. (1999) identified nitrated and aromatic compounds as likely absorbers. Bond et al. (2001)

suggested differing levels of aromatization to explain wavelength-dependent absorption.

It has been also demonstrated that the optical properties of BrC might evolve in the atmosphere due to various processes like oxidation, other chemical reactions, solar irradiation, temperature, and relative humidity. Lee et al. (2014) reported that chemical composition and optical properties of BrC could not be viewed as static, as they may change with time. Light-absorbing compounds (responsible for the color of BrC) can be potentially photo-bleached in sunlight and lose their ability to absorb visible radiation (Lee et al., 2014). Some of the laboratory studies also have suggested that photo-bleaching was due to degradation of BrC chromophores (Lee et al., 2014; Zhong and Jang, 2011, 2014). Further, photo-bleaching observed through an aerosol mass spectrometer (AMS) data shows that decrease in organic nitrogen to organic matter (ON to OM) ratio (Lee et al., 2014). Some studies showed that high O:C ratios correspond to less absorption during day hours, suggesting that highly oxidized species are less absorbing (Satish et al., 2017).

BrC was first described in the literature in some experimental studies where the spectral dependence of their light-absorption distinguished carbonaceous aerosol, represented using an empirically defined power law relationship (Bond et al., 2006; Ram and Sarin, 2009; Drozd et al., 2014; Bergstrom et al., 2002). The wavelength exponent of the aerosol absorption power law, Absorption Angstrom Exponent (AAE), was used to describe the aerosol absorption optical depths and thereby estimate dominant aerosol type. Kirchstetter & Novakov (2004) showed that low-temperature, incomplete burning processes such as BB produce a light-absorbing aerosol with much stronger spectral dependence than high-temperature combustion processes such as fossil fuel burning (Kirchstetter et al., 2004). They found that when absorption is dominated by only graphitic-like BC aerosol, the corresponding AAE values are close to 1. The steep increase of absorption at shorter wavelengths with characteristic values of AAE more than one was attributed to aerosol organic constituents from inefficient combustion at lower temperatures, such as BB. This was the earliest studies in which BC and BrC

components of biomass emissions were separated from insoluble soot-like carbon using solvent extraction. Following this pioneering work, the spectral dependence of light absorption became a standard method for identifying BC and BrC components. However, recent studies have shown that enhancement of BC absorption by coating can introduce considerable uncertainty into this method (Lack et al., 2013). Lack and Cappa, (2010) recent modeling study showed that AAE values ranging from 1−1.6 could be observed for internally mixed OC/BC particles and suggested that aerosol with AAE exceeding 1.6 should be classified as BrC. These studies together suggest that simple application of AAE method to distinguish absorbing and non-absorbing OC is not ideal and corroborating measurements are necessary.

Recent global models estimate that atmospheric absorption by BrC ranges from +0.22 to +0.57 Wm^{-2}, corresponding to 27-70% of that predicted by BC (Lin et al., 2014). On the other hand, BrC is shown to result in an overall cooling effect in the winter season, reaching close to −1.0 Wm^{-2}. Regional impacts of BrC on radiative forcing over major areas of BB and biofuel combustion, such as South and East Asia, South America, and subtropical Africa, may be substantially higher than 0.25 W m^{-2} (Feng et al., 2013). They suggest that BrC may be the significant atmospheric light-absorbing material in these regions. Over the Indo-Gangetic Plain (IGP), the direct radiative forcing of BrC showed a monthly warming effect up to 0.5 Wm^{-2} during the spring season. Several studies have documented that, due to the widespread crop-reside burning and unique cultural rituals in the area, BrC is a significant climate-warming agent in the area (Chakrabarty et al., 2014; Shamjad et al., 2015). Since most of the BrC are derived from BB aerosol, they are more likely to be elevated to higher altitudes and transported long distances than surface-emitted aerosol, resulting in a fundamentally different and complicated life cycle as well as more widespread and efficient warming. It has been demonstrated that aging during long-range atmospheric transport is significant in the outflows from the IGP (Srinivas et al., 2016). Despite several studies in this direction to understand the light-absorbing properties of water-soluble BrC over the IGP, the Bay of Bengal and the Indian Ocean, the spatial and temporal variability of BrC characteristics in this globally relevant region is still

poorly constrained (Bosch et al, 2014; Kirillova et al, 2014; Srinivas & Sarin, 2014; Srinivas et al, 2016).

Carbonaceous aerosol in the South-Asian region, originating from a variety of anthropogenic sources, are gaining considerable importance because of their potential impact on regional climate. In this context, systematic measurements of relevant optical parameters OA (BrC) from Indian region are essential. These type of studies are very limited in the Indian subcontinent.

1.5 Major objectives of the study:

Many of the studies mentioned above indicated large uncertainties and a lack of fundamental data on BrC variability concerning its sources, chemical composition, optical properties, formation mechanisms, atmospheric evolution, and scavenging processes (Laskin et al., 2015). Increasing evidence for the effect of BrC on climate and on the atmospheric environment has motivated a range of focused analytical and physical chemistry studies. There is still a substantial discrepancy between model predictions and observational data on aerosol absorption and radiative forcing and there exists little comprehensive studies on quantifying BrC in aerosol over the Indian subcontinent. This thesis aims to contribute to this knowledge gap in the existing literature by undertaking a focused study of chemical characteristics and optical properties of BrC in atmospheric aerosol over different regions of India.

The specific objectives of this thesis are the following:

- To investigate the abundances and characteristics of carbonaceous aerosol over regions dominated by different emission sources,
- To understand the primary and secondary sources of BrC in ambient aerosol and their temporal and spatial variability, and
- To compare the optical properties of BrC and BC over different regions of India

1.6 Thesis Outline:

Chapter 1 provides an introduction of the subject and review of previous research work in brief. ***Chapter 2*** describes relevant analytical details on aerosol sampling and analysis of its various chemical constituents. The significance of sampling locations in the context of this study will also be discussed. ***Chapter 3*** describes the offline BrC measurements made over different sites, and its compositional characteristics deduced using different offline techniques. ***Chapter 4*** describes the online BrC measurements and its characteristics over different sites. ***Chapter 5*** summarizes the essential findings of the thesis and their implications in assessing the impact of carbonaceous aerosol on regional climate as well as the present scope for future research in this field of study.

CHAPTER 2

Instrumentation & Methodology

2.1 Sites for ambient aerosol sampling

With an aim to understand the characteristics of BrC over different regions dominated by different emission sources and/or meteorological conditions, many sampling regions and periods for sampling were selected, as listed in Table 2.1. Sampling sites were chosen in northern, western and northeastern India, as well as in south Andaman, as shown in Fig. 2.1. Most of the selected locations, except Port Blair and Ahmedabad, fall in the Indo-Gangetic Plain (IGP). Among the study sites, Patiala is a semi-urban city affected majorly by BB during October-November. Delhi and Kanpur both are urban sites with significant levels of atmospheric pollution from fossil fuel burning as well as BB. Further, Shillong (a high-altitude site located in the foothills of Himalaya) and Port Blair (the capital of the Andaman and Nicobar Islands in the Bay of Bengal) both sites are affected by long-range transported aerosol. The meteorology of each sampling site is explained in the results section.

2.2 Site description

2.2.1 Patiala:

Patiala (30.33^{o}N, 76.4^{o}E, 250 m above mean sea level (amsl) is a semi-urban city surrounded by agricultural areas. It is situated in the western part of the IGP, close to Shivalik Hills in the east and the Thar Desert in the southwest. This study was carried out during the months of October- November 2014 and December, 2015 to February, 2016. The emissions from large-scale paddy residue burning in the open fields are the major contributor to the aerosol loading during autumn (October-November), and the remnant of agriculture waste burning and emission from thermal power plants, bio- and fossil-fuel combustion coupled with a shallower boundary layer are responsible for high aerosol loading during winter (Rastogi et al., 2014; Singh et al., 2015). The farmers of this region and nearby states (Haryana and Uttar Pradesh) grow both wheat and rice crops in the rotation in a year, and the harvesting leaves huge quantities of straw over the fields. The large fraction of wheat residue, after harvesting, is used as cattle feed but the rice

stubble, being unfit for cattle feed, is burnt in the open fields, which emits a large amount of submicronic particles and trace gases to the atmosphere during autumn (Sahai et al., 2007; Rastogi et al., 2016).

2.2.2 Kanpur:

The sampling site is located in the campus of Indian Institute of Technology, Kanpur (26.5°N, 80.3°E, 142 m amsl) and sampling carried out during 20-December-2015 to 6-February-2016. Being located in the middle of the IGP, Kanpur is a big urban city with a population of ~4.5 million, and reported to be among cities with the worst air quality in India. The sampling site receives emissions from several sources in and around the city, and from north and northwestern IGP through long-range transport during the study period. During winter, regional BB is among the major contributors to aerosol loadings at this location. Other sources of pollution in the Kanpur city are emissions from vehicles, bio-fuel, wood and coal burning, industrial activities, brick kilns and thermal power plant plumes. Further, meteorological conditions in winter (low wind speeds and shallow boundary layer heights) favors the accumulation of pollutants over the region. The study period was characterized by high RH (up to 100%) and low temperature conditions (lowest temperature: approximately 4 °C).

2.2.3 Shillong:

Barapani (25.7 °N; 91.9 °E; 1064 m amsl) is situated in the foothills of NE–Himalaya (NE–H), ~ 50 km north-east of the Cherrapunji–Maysynram, one of the heaviest rainfall region in the world and ~20 km to nearest town Shillong. The sampling was carried out during the months of January to April, 2017. The study region is influenced by North-West (NW)-winds during January to March, and NE-winds during April. Influence of local sources are expected to be insignificant (Rajput et al., 2013). The total annual rainfall in this region is ~1200 mm, spread over June–September (SW–monsoon) and October–December (NE–monsoon) (Mahanta et al., 2013). The driest month is December, with 8 mm of rainfall and the most precipitation occur during June, averaging 851 mm. In January (15 mm),

February (20 mm), March (80 mm) and April (150 mm) relatively less rainfall occurs.

2.2.4 Port Blair:

The sampling site located in Port Blair region (PB) (11.63°N; 92.71°E) and it is the capital of the Andaman and Nicobar Islands, a union territory of India situated in the Bay of Bengal (Fig. 2.1). Samples were collected from the building of ISTRAC (Indian Space Research Organization's Telemetry, Tracking and Command Network), on a hillock, ~60 m MSL. The sampling carried out during the months of February to April, 2013 when the site receives air masses from India and Southeast Asia.

2.2.5 Delhi:

The sampling site located in the campus of Indian Institute of Technology, Delhi (28.4 °N, 77.1 °E, 230m amsl) and the sampling was carried out during 10-January to 28-February, 2018. According to a world health organization (WHO) survey of 1600 world cities, Delhi is the worst of any major city in the world in terms of air quality. Delhi as a megacity, suffers from the intense pressure of urbanization, industrialization and densely populated regions. These potential factors have caused subsequent degradation of ambient air quality and have been estimated to cause ~12000 premature deaths per year (Chaudhary et al., 2017). Additionally, high pollutant concentration also leads to urban and regional haze, and has a deleterious impact on the local ecosystem, crop yield and climate change. During winter, regional BB is among the significant contributors to aerosol loadings at this location. Other sources of pollution in the Delhi city are vehicles, bio-fuel, wood and coal burning, industrial activities, etc. Further, meteorological conditions in winter (low wind speeds and shallow boundary layer heights) favors the accumulation of pollutants over the region. The study period was characterized by high RH (up to 100%) and low-temperature conditions (lowest temperature: approximately 6 °C).

2.2.6 Ahmedabad:

The sampling site was located in the campus of Physical Research Laboratory, Ahmedabad (23.0ºN, 72.6ºE, 49 m amsl) and sampling was carried out in November, 2015. Ahmedabad is a big urban city located in western India with about 8 million populations in 2018. It located in western India, ~500 km southeast of the Thar Desert. The nearest distance to the Arabian Sea, in the southwest direction, is ~100 km. The local climate is typical of semi-arid type. The sampling location is surrounded by various emission sources both anthropogenic and natural. Typically, during December-February winds are north-easterly, whereas during June-August south-westerly (Rastogi et al., 2005; Sudheer and Rengarajan, 2015; Rastogi et al., 2018).

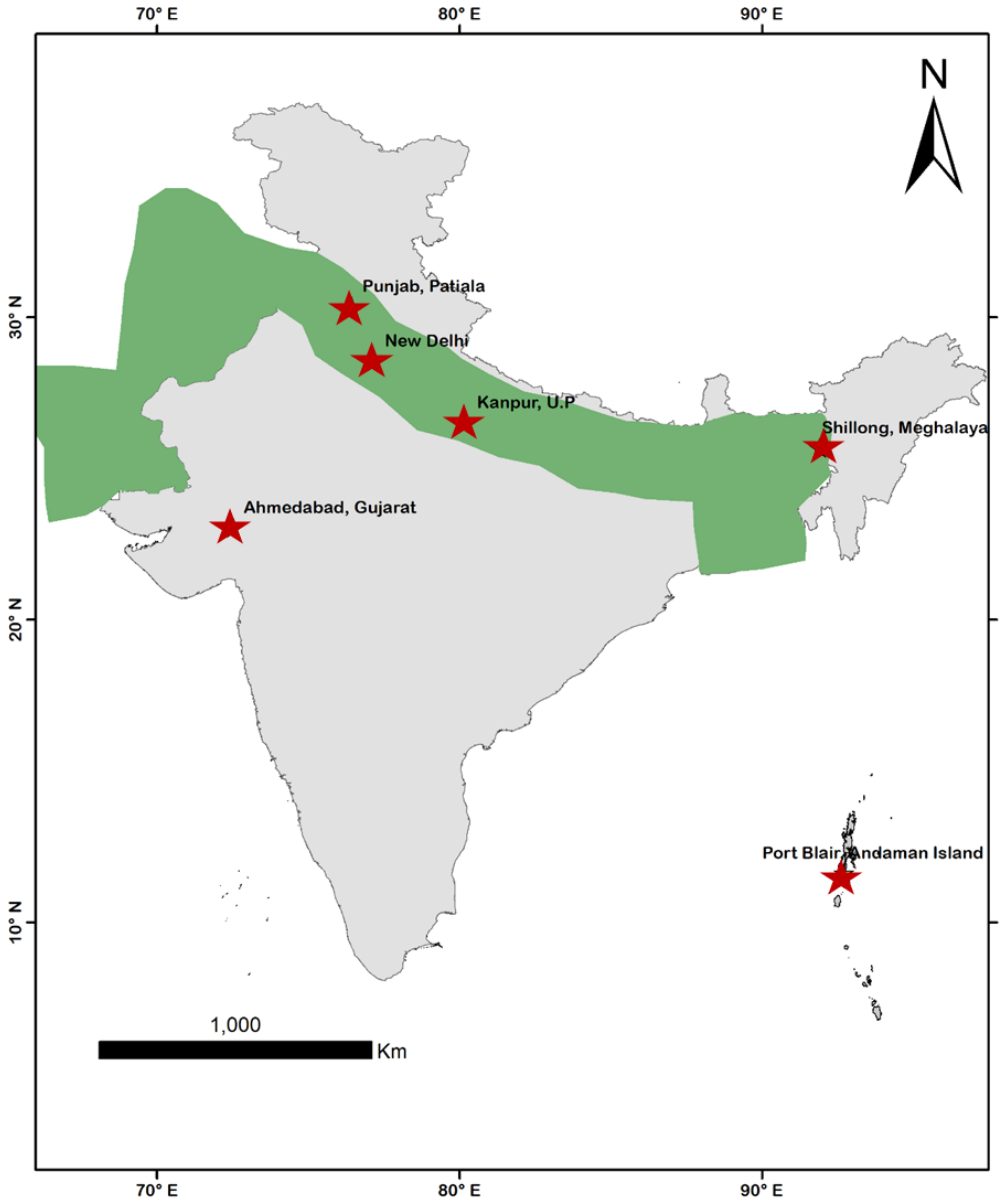

Figure 2.1: A map showing all the sampling locations (denoted by star legend). The shaded green region is Indo-Gangetic Plain (IGP) where Patiala (semi-urban), Delhi (urban), Kanpur (urban) and Shillong (high altitude) sites are located; whereas, other two sites were Ahmedabad (urban) and Port Blair (Island).

Table 2.1: List of the sampling sites, sampled period, geographical location, measurement type (online/offline sampling), number of samples (n), and frequency of sample collection.

Sampling site	**Sampling period**	**Geographical location Latitude, Longitude, and Altitude (m)**	**Measurement type (Online and/or Filter based)**	**Number of Samples**	**Sampling frequency, Integration Time**
Patiala	Oct-Nov, 2014	30.35° N, 76.44° E; 255 m amsl	$PM_{2.5}$ Filter Sampling	69	Daily (day-night) every12 Hrs
Patiala	Dec, 2015-Feb, 2016	30.35° N, 76.44° E; 255 m amsl	$PM_{2.5}$ Filter Sampling	43	Daily, 24 Hrs
Kanpur	Dec, 2015-Feb, 2016	26.51° N, 80.23° E; 150 m amsl	$PM_{2.5}$ Filter Sampling	59	Daily, 24 Hrs
Shillong	Jan-Apr-2017	25.67° N, 91.91° E; 1430 m amsl	$PM_{2.5}$ Filter Sampling	35	Every 3rd day, 24 Hrs
Port Blair	Feb-Mar, 2013	11.62° N, 92.72° E; 50 m amsl	PM_{10} Filter Sampling	50	Daily, 24 Hrs
Kanpur	Dec, 2015-Feb, 2016	26.51° N, 80.23° E; 150 m amsl	$PM_{2.5}$ Real-Time Analysis	13265	4 min
Ahmedabad	Nov-14	23.03° N, 72.54° E; 60 m amsl	$PM_{2.5}$ Real-time analysis	3949	4 min
Delhi	Jan-Mar-2018	28.5° N, 77.2° E; 220 m amsl	$PM_{2.5}$ Real-Time Analysis	11635	4 min

amsl #: above mean sea level

2.3 Instrumentation & Methodology

The following offline and online measurement techniques were employed in this thesis work. Filter-based ambient aerosol samples were collected using high volume air sampler and analyzed for the particulate matter (PM) mass, the concentrations of elemental carbon (EC), organic carbon (OC), Water-soluble organic carbon (WSOC) and water-soluble organic nitrogen (WSON), water-soluble inorganic constituents (cations: NH_4^+, Na^+, K^+, Mg^{2+}, and Ca^{2+} and anions: Cl^-, NO_3^-, and SO_4^{2}), Anhydrous-sugars as well as water-soluble and methanol-soluble BrC. The sampling and measurements schemes adopted for the chemical species and optical properties of aerosol are shown in a schematic flow-chart (Fig 2.2).

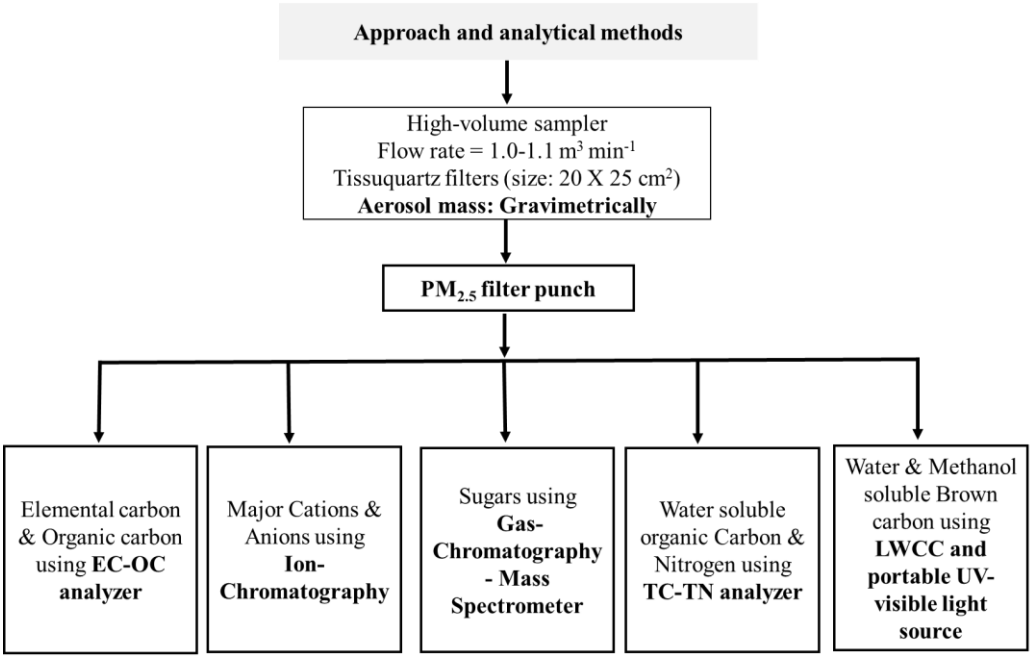

Figure 2.2: Schematic representation of analytical approaches

2.3.1 Particulate matter sampling:

The ambient particulate matter smaller than 2.5 µm aerodynamic diameter ($PM_{2.5}$) were collected using a high-volume air sampler (Thermo-Anderson, HVS) with the flow rate of ~1.13 m^3 min^{-1} at various sampling locations (Fig 2.1). Samples were collected on pre-combusted (at 450 °C for 10-12 hours) tissuquartz filters (PALLFLEX®TM, 25X20 cm^2). Soon after their collection, filters were wrapped in aluminum foils, sealed in plastic zip-lock bags, and stored in the deep freezer (-19 °C) until the time of analysis.

2.3.1.1 Maintenance of HVS:

It is essential to clean the pistons inside the HVS sampler once in a week. Otherwise, pistons may get choked and don't allow all the particulate matter to be collected on the filter. Similarly, the Teflon ring needs cleaning from time to time followed by application of silicone oil/Grease.

2.3.1.2 Assessment of PM Mass:

The $PM_{2.5}$ mass concentrations were assessed gravimetrically from the weights of the filters before and after the particulate collection on an electronic balance (Saratorius, Model LA130S-F). Before their weighing, aerosol filters were equilibrated to ambient room temperature (~23 °C) under constant relative humidity (~35-40%). To ensure the precision, we have repeated weighing one sample after every five samples, and weights were found within 5%.

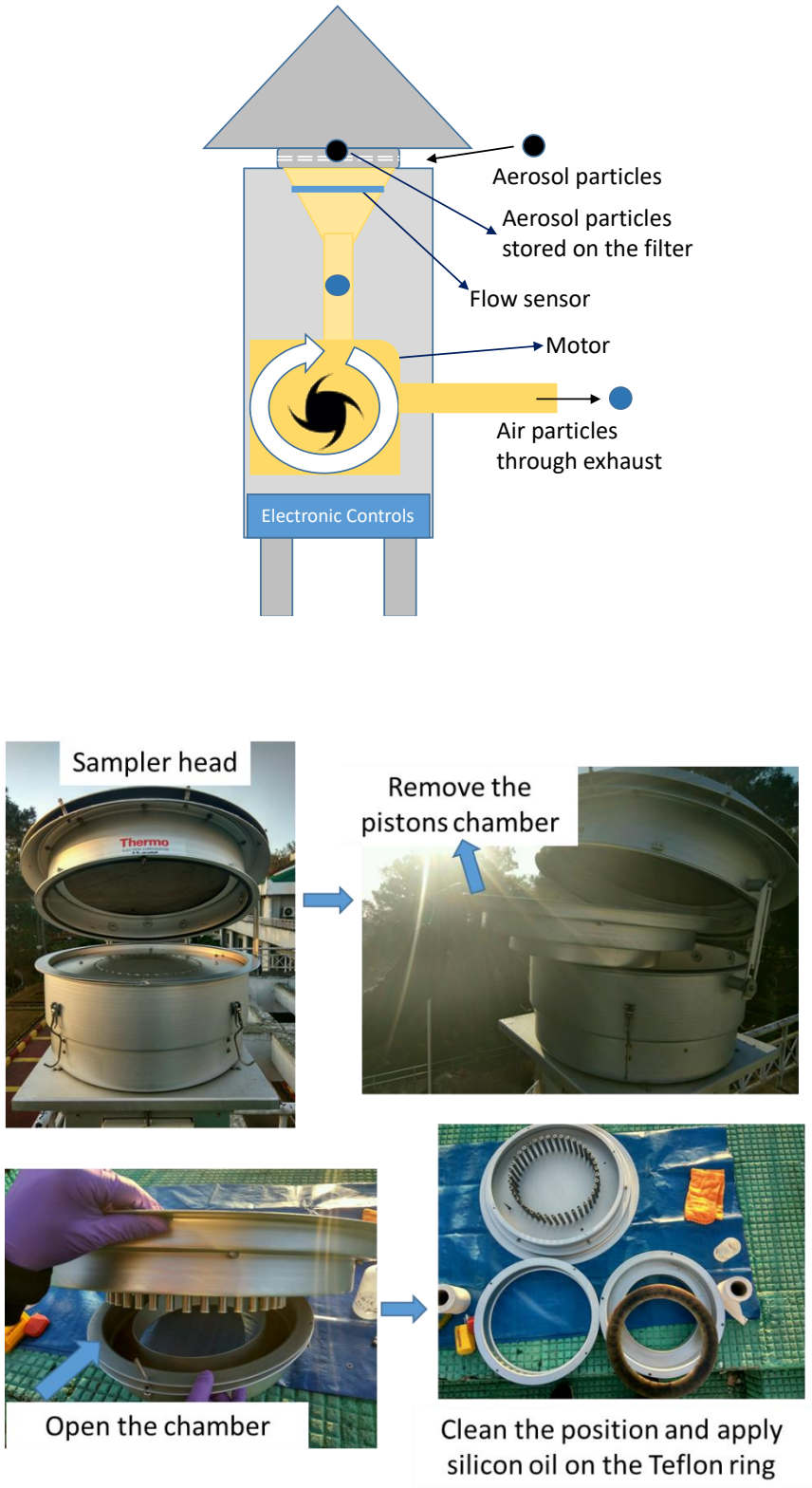

Figure 2.3: Schematic representation of HVS and cleaning procedure

2.3.2 Analysis of OC and EC using a thermal-optical EC-OC analyzer

The concentrations of Elemental Carbon (EC) and Organic Carbon (OC) were measured with an EC-OC analyzer (*Model 2000, Sunset Laboratory, Forest Grove, USA*) using a temperature gradient (NIOSH-5040) Thermo-Optical Transmittance (TOT) protocol (Birch and Cary, 1996; Rastogi and Sarin, 2009; Rengarajan et al., 2007).

The schematic diagram of the EC-OC analyzer is depicted in Fig. 2.4, the instrument made up of the following:

1. ***Sample oven***: It consists of a front oven where the temperature ramping (25°C to 880°C) is performed during the analysis, and a back oven where the temperature is constantly maintained (at 880°C).
2. ***Manganese dioxide (MnO_2) catalyst***: It converts all the combusted carbon from sample into carbon dioxide (CO_2) at 880°C in the back oven.
3. ***Methanator***: It reduces CO_2 to CH_4 (Methane) in the presence of nickel catalyst (Ni) at 550°C.
4. ***Flame Ionization Detector***: It measures the carbon signal coming from samples and calibration gas (5 % CH_4)

Measurement of EC-OC:

- Set the gas flows
- Ignite the FID
- Clean the oven (Run clean)
- Insert the blank filter and run the analysis
- Load the check standard on the filter (To ensure system stability and accuracy)
- Run the samples: A filter-punch (Area=1.5 cm^2) has to be placed on a quartz boat and gently inserted into the front oven of the EC-OC analyzer.
- Instrument run as per the parameter file (quartz.par) which consists of a pre-defined program for temperature ramp and hold time. By changing the parameter commands, one can use different parameter run file.

Principle:

The analytical procedure for OC-EC analysis consists of two-stage thermal analysis. During first stage, OC volatilizes from filter punch in the inert atmosphere (100% He) through step-wise heating (from room temperature to 850 °C), whereas during the second stage, the front oven is cooled to below 550 °C and filter punch is heated again in an oxidizing atmosphere (98% He + 2% O_2) through step-wise heating. Here, EC is evolved. The evolved carbon during each temperature step gets oxidized to CO_2 by passing it through manganese dioxide (MnO_2) oxidizing oven (kept at 880°C) where it further gets reduced to CH_4 for quantification by passing it through Flame-Ionization Detector (FID). To set the OC-EC split point and correcting for pyrolyzed carbon (PC), the transmittance of light from a He-Ne laser source (λ = 678 nm), passing through the filter-punch is monitored continuously. The transmittance first decreases and then increases, so at a point of time when the optical transmittance becomes equal to the initial transmittance (at time t = 0, transmittance due to EC in the sample), that point is referred as the split-point between OC and EC. At the end of every analysis, a known amount of methane (5% CH_4 + 95% He; methane in Helium gas as an internal standard) was injected to check the response of detector (FID) whereas the known amount of sucrose solution was used as an external standard every day before and after analyses to check the response of the detector. Blank filters were analyzed to obtain a blank concentration for OC. The OC concentration in each sample was corrected for blank concentration. Replicate analysis of the samples results in limiting the uncertainty on the analytical precision of ±7% for OC and ±6% for EC.

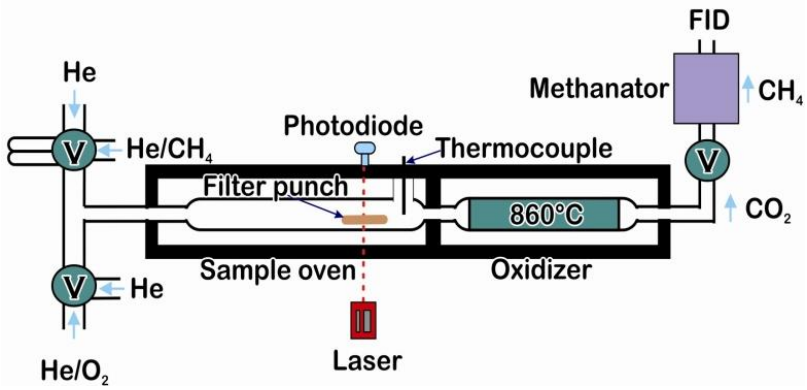

Figure 2.4: The schematic diagram of the thermos-optical EC-OC analyzer (Reference: Sunset Laboratory manual).

2.3.3 Determination of Water-Soluble Inorganic Species (WSIS)

Chromatography is the technique used for separating and analyzing the mixed compounds or ions in a sample. In this study, both mobile phase and stationary phase are used. The stationary phase is bound inside the column and mobile phase pass through it along with the sample. The compounds or ions are separated based on retention time. The separation depends on the molecular weight or charge of the compounds or ions. In Ion chromatography, two columns are used, one consists of cation exchange resin and second consists of anion exchange resin. The mobile phase used for cation column is methane sulphonic acid (MSA), and that for anion column is the mixture of sodium carbonate/bicarbonate.

Principle:

The exchanges of ions between the stationary phase and mobile phase occur in the column, and they are separated from the column based on their retention time. The detector used in the IC is the conductivity detector.

The analysis of water-soluble cations (Na^+, K^+, NH_4^+, $Ca^{2+,}$ and Mg^{2+}) and anions (Cl^-, SO_4^{2-} and NO_3^-) in water-extracts of aerosol were performed with dual channel Ion Chromatograph (Dionex, ICS-5000, DC). For water-soluble inorganic

species (WSIS) analysis, 2 punches (6 cm^2 each) of sample filter were sonicated for 30 minutes (10 minutes, 3 times) in 15 ml Milli-Q water (Resistivity: 18.2 MΩ cm). Subsequently, the filtered water extract was transferred to pre-cleaned two mL vials and used for analysis on Ion Chromatograph. The instrument is well calibrated before the analysis using external standards of both cations and anions. A mixture of sodium carbonate (Na_2CO_3) and sodium bicarbonate ($NaHCO_3$) was used as an eluent for the study of anions, and an anion self-regenerating suppressor (ASRS) was used to suppress the conductivity. For the analysis of cations, methane sulphonic acid (MSA) was used as an eluent, and the conductivity was suppressed with the help of a cation self-regenerating suppressor (CSRS). The anions and cations were separated using analytical and guard columns. Here we have used Ionpac-CG16, CS16 (Serial no: 006532) for cations, and for anions Ionpac-AG23, AS23 (Serial no: 005206) as a guard and analytical columns, prior to their determination using conductivity detector. More details of the analytical procedure for water-soluble ionic constituents are described in earlier publications (Rastogi et al., 2016 and references therein).

Charge Balance: It means the total sum of all the positive charges (cations) must equal the total sum of all negative charges (anions). After completing the analysis, we calculated the charge balance (ratio of Σ^+/Σ^-). The fair charge balance of ambient aerosol samples should be within ~5%.

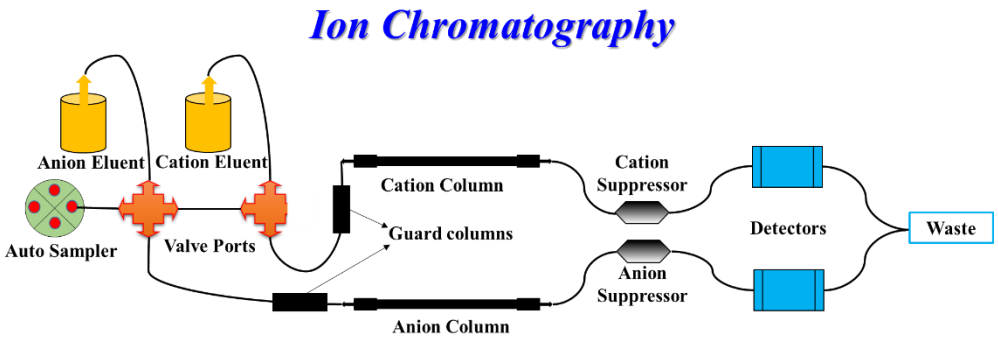

Figure 2.5: Schematic representation IC working principle

2.3.4 Gas chromatography-mass spectrometry (GC-MS)

GC-MS is a combination of two different analytical techniques, Gas Chromatography (GC) and Mass Spectrometry (MS), and it is used to analyze complex organic mixtures. GC can separate the various organic compounds with high resolution, but it cannot identify. MS can give the information of many compounds so that we can identify and quantify them, but it cannot separate them. A GC-MS gives a complete picture of organic speciation of interest.

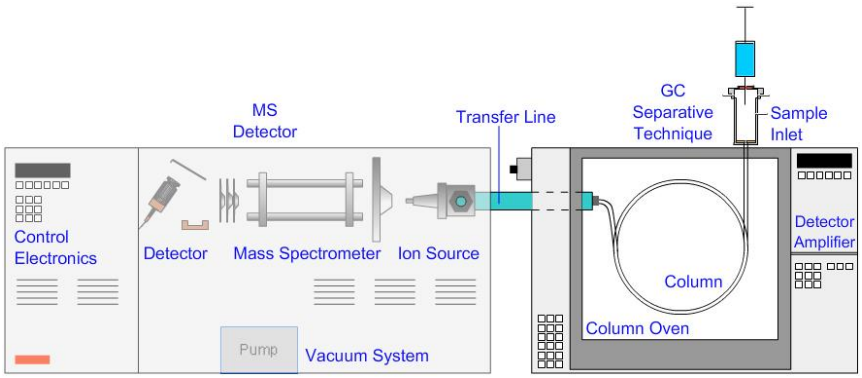

Figure 2.6: GC-MS schematic view (Reference: Semantic scholar, Syed Zameer Hussain)

For organic speciation, the Levoglucosan, Mannose, Galactose, Arabitol, Mannitol, Erythrose, and Glucose mass concentrations were measured and quantified using a GC-MS (Agilent, 7890A/5975C). The complete analytical procedure is adopted from Pietrogrande et al. (2013) and Pietrogrande et al. (2016). Briefly, PM samples were extracted in 30 mL of methanol: dichloromethane (9:1) solvent mixture using an accelerated solvent extractor (ASE 200, Dionex Corporation, at 1500 psi and 100°C using three static cycles 5 minute each), followed by evaporation in an evaporator (Turbo Vap LV® II, Caliper Life Sciences, Hopkinton, USA).

Before GC-MS analysis, the sample extracts were submitted to a silylation reaction for 70 min at 75 ^{o}C. For the silylation, 45 µL of N, O-bis-(trimethylsilyl) trifluoroacetamide (BSTFA) containing 1% of trimethylchlorosilane (TMCS) and 15 µL of pyridine and 40 µL of iso-octane were added to extracted PM samples. The non-polar stationary phase column used was a DB-5MS column (L = 30 m,

I.D. = 0.25 mm; J&W Scientific, Rancho Cordova, CA, USA). High-purity helium was the carrier gas at a velocity of 1.5 ml min^{-1}. The temperature program conditions were optimized for the analysis of a wide range of target polar organic compounds. The initial temperature of 70 °C was raised to 125 °C at 2.5 °C min^{-1}, followed by an isothermal hold for 7 min; after that, the temperature was increased to 145 °C at 2 °C min^{-1}, an isothermal hold for 5 min; then further raised to 170 °C at 2.5 °C min^{-1} and finally led to 300 °C at 7 °C min^{-1}; this temperature was maintained for 1 minute. All samples were injected in pulsed splitless mode (splitless time: 60 seconds); the injector temperature was 250 °C. Quality control was assessed by the reproducibility of ≤ 12% (RSD%) attained on external standards and sample repeats suitable for applicability in environmental monitoring.

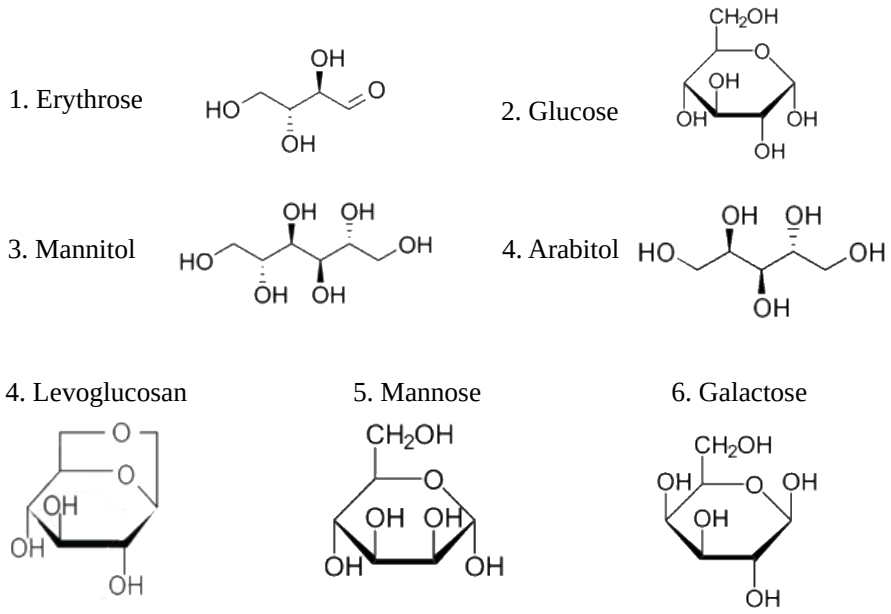

Figure 2.7: Organics speciated using Gas Chromatography-Mass Spectrometry (GC-MS)

2.3.5 Determination of total water-soluble organic carbon (WSOC) and total nitrogen (TN)

The mass concentrations of total water-soluble organic carbon (WSOC) and total nitrogen (TN) was determined using TOC/TN analyzer (Shimadzu, model-TOC-LCPH with AS-L auto-sampler). For TOC and TN analysis, one punch (6 cm^2) of the $PM_{2.5}$ filter was sonicated for 30 minutes with 14 mL Milli-Q (Resistivity: 18.2 MΩ cm) water and filtered using syringe filter. The filtered solutions were lined up in the auto-sampler of the analyzer for the simultaneous measurements of WSOC and TN.

2.3.5.1 WSOC measurement can be performed in two ways:

1. **Direct injection:**

Water extract (50 µl) is injected into combustion tube (heated at 680°C) and oxidized to CO_2 using oxidation catalyst. Carrier gas carries the sample combustion product (flow rate of 150 ml min^{-1}) from combustion tube to an electronic dehumidifier, where gas gets cooled and dehydrated. After that, it passes through the halogen scrubber to remove chlorine and other halogens. Finally, the carrier gas delivers the sample combustion product to the cell of a Non-Dispersive Infrared Detector (NDIR) gas analyzer, where the carbon dioxide is detected, and the concentration of total carbon (TC) is quantified. Usually, in the fine particulates, the contribution of inorganic carbon to TC is negligible (<5%). Thus, total carbon concentration can be considered as representing the mass concentration of Water-Soluble Organic Carbon (WSOC). The response of the NDIR detector was checked using a standard solution of sucrose. The average ratios of measured carbon to expected carbon is 0.99 ± 0.05. The WSOC in blank filters was simultaneously measured and utilized for blank correction to derive the WSOC concentrations in aerosol samples. Replicate analysis of samples shows the uncertainty of WSOC measurement within ±5%.

2. Non-purgeable organic carbon (NPOC):

In some environmental water and other samples in which the IC component of the TC may be high, significant errors may be there if the method mentioned above was used for TOC measurement. Organic carbon in such sample can be measured via an NPOC measurement as shown in Figure 2.8. This method is similar to TOC measurement methods, but it also uses acidification and sparging (IC removal) of the sample as described in TOC manual measurement methods.

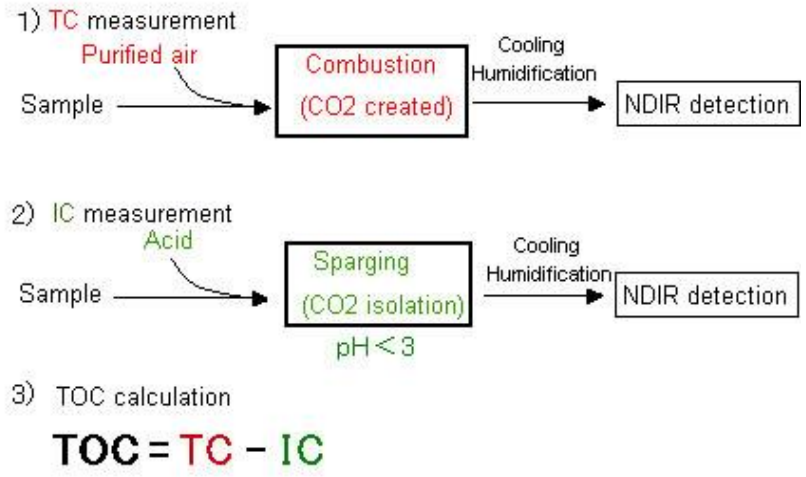

Figure 2.8 Working principle of TOC

TN measurement:

When a sample is introduced into the combustion tube and heated at 720 ^{o}C, the TN in the sample decomposes to become nitrogen monoxide. The carrier gas, which contains the nitrogen monoxide, is cooled and dehumidified by the dehumidifier and then enters a chemiluminescence gas analyzer where the nitrogen monoxide is detected**.**

2.3.6 NOx Measurement

The Serinus 40 Oxides of Nitrogen Analyzer uses gas phase chemiluminescence detection to perform continuous analysis of nitrogen oxide (NO), and nitrogen dioxide (NO_2). The measurement of the Oxides of Nitrogen is performed using the gas phase chemiluminescence method. The steps of detection are:

1. Sample air enters the reaction cell via two separate (alternating) paths; the NO and NO_X channels
2. NO in the first path reacts with ozone according to the following reaction

$$\mathbf{NO + O_3 \longrightarrow NO_2^* + O_2}$$

3. The second path travels through a delay loop and the NO2 to NO converter such that it reaches the reaction cell after the first path. At this point, the NOx measurement (the combined concentration of NO and NO_2) is taken
4. This reaction releases the energy in the form of chemiluminescent radiation, which is filtered by the optical bandpass filter and detected by the photomultiplier tube (PMT
5. The level of chemiluminescence detected is directly proportionally to the NO in the sample.
6. The concentration of NO_2 is calculated by subtracting the NO measurement from NOx measurement

   $NO_X = NO + NO_2$ or $NO_2 = NO_X - NO$

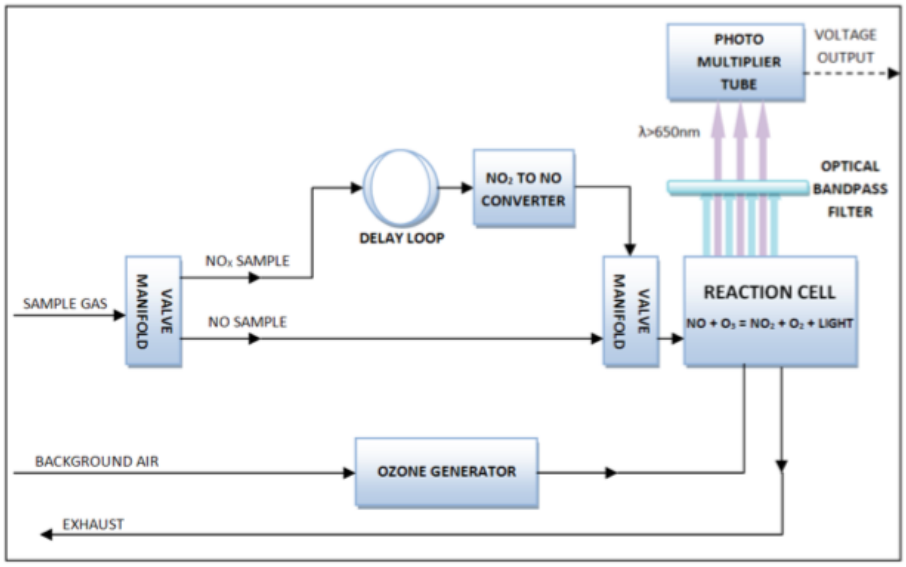

Figure 2.9: NO_X analyzer flow chart and working principle

Analyzer Calibration:

1. Thermo gas calibrator has three ports named as A, B, and C. Using any one of them, connect it to the standard gas (NO_X cylinder) for calibration.
2. Calibrator main display→ Mode→Press Standby Mode
3. To edit the span calibration, the instrument should be kept in ‘’Standby Mode’’ then press page up button just below the play button→gas setup→Select Gas (A or B or C)→Here we can edit the Gas name, and Set standard cylinder tank Concentration.
4. After that zero dilution adjusts automatically depends on tank concentration, we have given already.
5. Now edit the span calibration (1, 2...5), here also depending on tank concentration and dilution capacity of the calibrator the span calibration range will be displayed just above.
6. Save after every parameter that has been changed (save symbol)
7. Now click on Operation (OPER)→Using left and right arrows one can change span mode(zero, span 1,...5)

8. Analyzer part: Calibration→ Calibration mode→ Span mode; Sample mode should be closed and calibration port of analyzer connected to calibrator output port

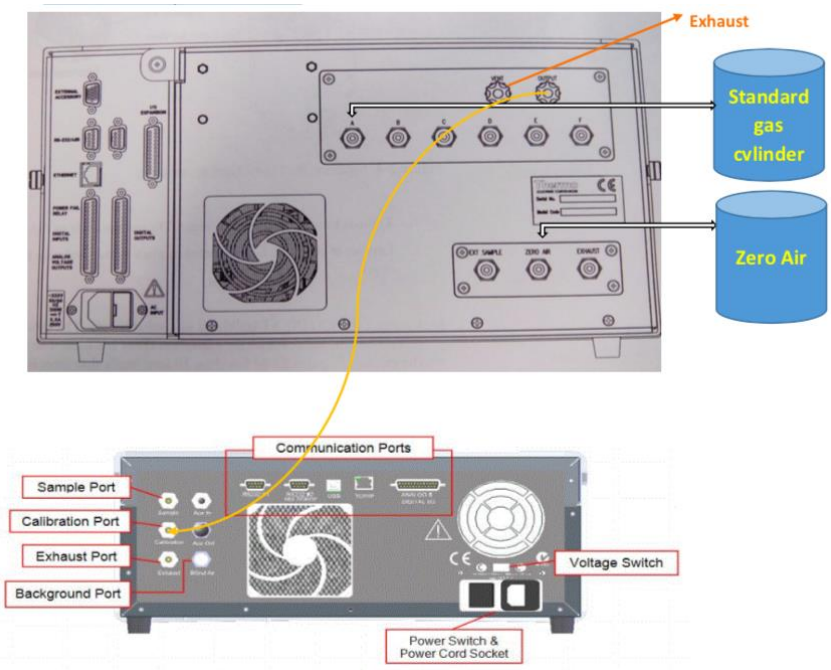

Figure 2.10: NOx analyzer calibration setup

2.3.7 CO Measurement

CO absorbs infrared radiation (IR) at a wavelength near 4.7 microns. IR radiation (at 4.7 microns) is passed through a 5-meter folded path length through sample air. The strength of the signal received is proportional to the amount of CO in the sample as shown in the Beer-Lambert Law. A bandpass filter is fitted to the signal detector to ensure only light near 4.7 microns' wavelength is detected.

1. A gas filter correlation wheel is combined with this system.
2. This wheel contains three parts to increase measurement accuracy; CO, N_2 and the mask.
3. The CO window contains a saturation (40%) of CO which acts as a reference beam – absorbing a known amount of light.

4. The N_2 window, containing 100% N_2, does not absorb IR at 4.7 microns at all and is used during standard CO measurement.
5. The mask entirely blocks the light source and is used to determine background signals and the strength of other signals relative to each other and the background.

Analyzer Calibration:

1. Change sampling mode of the instrument from 'measure' to 'span mode.'
2. Close sample port, connect the standard gas cylinder to span port.
3. Let analyzer run in the span mode for 10 min.
4. Adjust or set true value of the standard tank concentration in the span window and press enter.

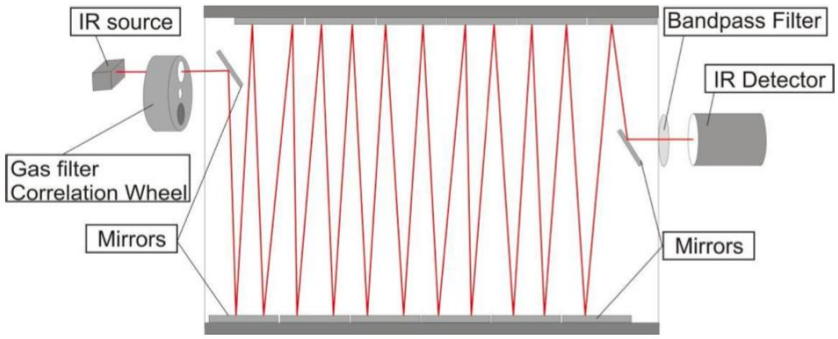

Figure 2.11: CO analyzer cell working principle

2.3.8 Black Carbon

The atmospheric Black Carbon (BC) was monitored online using an Aethalometer (AE-31, Magee Scientific, USA). It observes optical attenuation (absorbance) of light at seven wavelengths (370, 470, 520, 590, 660, 880 and 950 nm) with a typical half-width of 20 nm (Hansen et al., 2005). However, the measured mass concentration at 880 nm is considered as the standard BC since, among dominant

aerosol species in the atmosphere, BC has maximum absorption at this wavelength. The principle of Aethalometer is to measure the change in attenuation of light passing through a spot (where the aerosol is being continuously collected) on the filter for a given interval of time.

Assuming that BC is the only absorbing component in the atmospheric aerosol, a linear relationship of BC mass concentration with the change in attenuation of light is used to determine the BC mass concentration (Snyder and Schauer, 2007). In the present study, the attenuation signal has been integrated for 1 minute, and the flow rate was maintained at 3 L min^{-1}. Aethalometer uses a constant attenuation cross section of 16.6 m^2 g^{-1} to determine the BC mass concentration. However, sometime the BC mass concentration can be overestimated due to the presence of another absorbing aerosol in the atmosphere (Hansen et al., 1993). The analytical uncertainty in BC measurements is about ±2% (as reported in the manual).

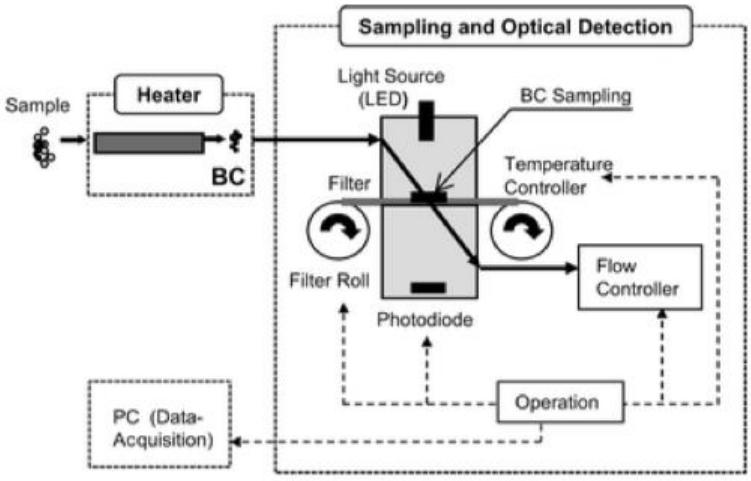

Figure 2.12: Flow diagram of Aethalometer operation.

2.3.9 Hybrid single–particle lagrangian integrated trajectory (HYSPLIT)

The Air Resources Laboratory's (ARL's) Hybrid Single–Particle Lagrangian Integrated Trajectory (HYSPLIT) model is a tool that helps to explain how, when, and where various constituents are atmospherically transported, dispersed, and

deposited. It is a complete system for computing simple air parcel trajectories, complex dispersion, and deposition simulations. The model calculation method is a hybrid between the Lagrangian approach, which uses a moving frame of reference for the advection and diffusion calculations as the air parcels move from their initial location, and the Eulerian approach, which uses a fixed three–dimensional grid as a frame of reference to compute the pollutant air concentrations (ARL's, NOAA). HYSPLIT model has been employed in this study to calculate 5-days air mass back trajectories. They are calculated at 00:00 h (local time) using NOAA–Air Resource Laboratory HYSPLIT–Model (GADS data set) at arrival heights of 100 m, 200 m and 500 m (above ground level; AGL) (Draxler and Rolph, 2003).

2.3.10 Measurement of BrC

BrC is still a qualitative and descriptive term due to the lack of an analytical reference method. There are four available BrC techniques in the literature (Cheng et al., 2016). First is the molecular level identification of BrC. The methods in this category aim to attribute observed OA absorption to individual organic compounds (e.g., Zhang et al., 2013; Lin et al., 2015). Until recently, however, quantification of ambient OA on a molecular level remains a difficult challenge (Nozie re et al., 2015) whereas identified organic compounds can explain only a small fraction of measured OA absorption (Mohr et al., 2013; Zhang et al., 2013; Cheng et al., 2016). The second method is the observation of individual BrC particles. Techniques in this category, such as transmission electron microscopy (TEM; e.g., Alexander et al., 2008) and scanning electron microscopy (SEM; e.g., Chakrabarty et al., 2010), typically focus on a single type of BrC particles, i.e., tarballs. These methods can provide particle morphology information, whereas a more comprehensive characterization of tar balls will be possible when using TEM or SEM in combination with other techniques (Alexander et al., 2008). The third method is optical estimation of BrC un-isolated from BC. Techniques in this category involve attribution of total aerosol absorption, which is typically measured by an optical instrument (either filter-based or not), to BrC and BC absorption (Sandradewi et al., 2008; Wonaschütz et al., 2009; Yang et al., 2009;

Favez et al., 2010; Chen et al., 2015; Massabo et al., 2015). These methods commonly assume that the wavelength dependence of BC absorption is independent of BC mixing state, which might be invalid. An in-depth discussion of uncertainties associated with this assumption is provided by Lack and Langridge (2013). The fourth method is an optical measurement of isolated BrC. In this method, BrC isolation is most frequently achieved by water or organic solvent extraction, followed by BrC absorption measurement either in the filtered extracts or on atomized BrC particles (the former approach has been most commonly used). An advantage of these methods is that BrC absorption can be measured without any interference from BC. Some studies (e.g., Powelson et al., 2013) have used UV-Vis and fluorescence spectroscopy to characterize brownness of organic compounds.

In this study, we used a spectrometric technique to measure BrC absorption using offline and online methods.

2.3.10.1 Online BrC measurements:

BrC absorption spectra (300-700 nm) and WSOC mass concentration in ambient $PM_{2.5}$ have been measured semi-continuously using an assembled system (PILS-LWCC-TOC) consisting of a particle-into-liquid sampler (PILS, Model ADI 2081, Application Analytical) coupled to a liquid waveguide capillary cell (LWCC, World Precision Instrument, Sarasota, FL, 2m path length) and total organic carbon (TOC, Sievers 900 Portable with Turbo, GE Analytical Instruments) analyzer. The ambient air was drawn through a cyclone inlet ($PM_{2.5}$ URG, model no. URG-2000-30EH) coupled to a PILS-LWCC-TOC system at 16.7 lpm airflow rate. Aerosol water-extract from the sample line coming out of PILS was passed through a disposable syringe filter (with GHP Membrane, 0.45μm porosity, 25mm diameter, Acrodisc) to remove all the insoluble particles (including BC and dust) prior to injecting it in LWCC and TOC analyzers. The BrC absorption spectra (300-800 nm) were measured using portable UV-Vis Spectrophotometer (Model: USB-4000) and deuterium and tungsten halogen lamps (DT-Mini-2, Ocean Optics), and saved every 2 min; whereas, WSOC

concentrations were measured with 4 min integration time. The PILS-LWCC-TOC system setup was similar to that reported by Hecobian et al. (2010). Background measurements were performed every day by putting a high-efficiency particulate air (HEPA) filter to the cyclone inlet for about an hour and reported concentrations are corrected for blanks. Rastogi et al. (2015) have described details of the semi-continuous measurement of WSOC. In the present study, the light absorption coefficient at a given wavelength (b_{abs_λ}) was calculated as follows (as described in Hecobian et al., 2010; Satish et a., 2017).

$$b_{abs\_\lambda} = (A_\lambda - A_{700}) * (\frac{V_l}{V_a * l}) * ln10 \quad (1)$$

Here, A_λ is the absorbance at a given wavelength, A_{700} is the absorbance at 700 nm to account for any baseline drift, V_l is the PILS liquid sample flow rate (0.7mL min^{-1}), and V_a is air sampling flow rate (16.7 L min^{-1}). The absorbing path length '*l*' is 2 m.

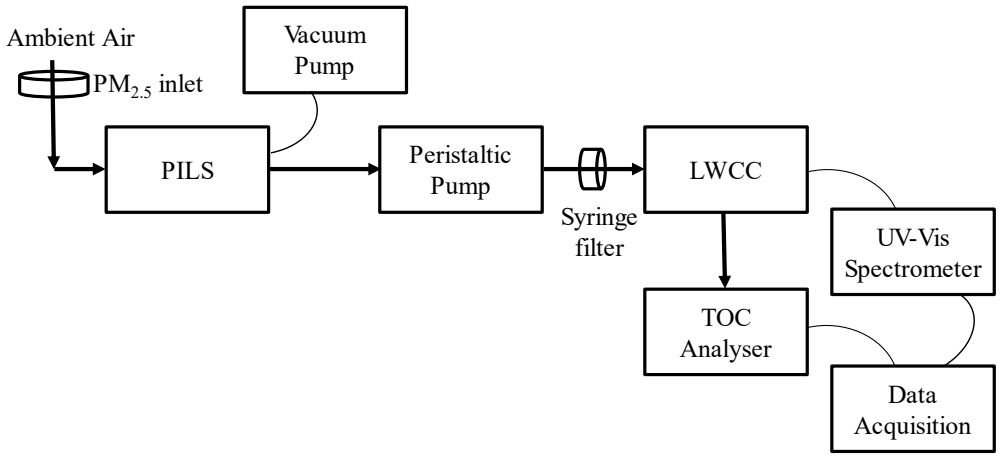

Figure 2.13: Schematic diagram of an assembled PILS-LWCC-TOC system used for online the measurements of BrC and WSOC

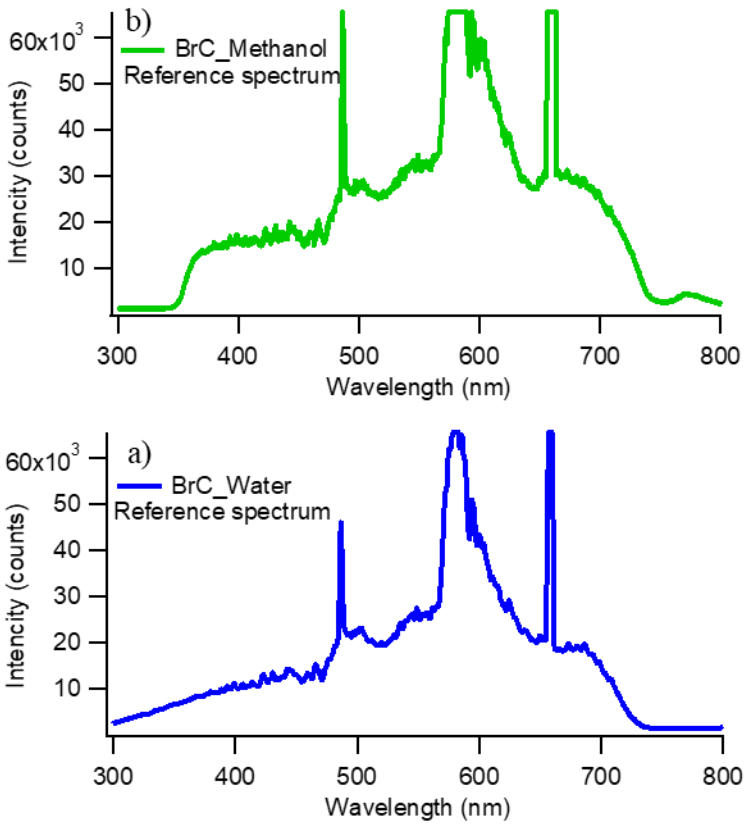

Figure 2.14: Typical reference spectrum of a) Water and b) Methanol for BrC measurements

2.3.10.2 Offline BrC analysis:

For BrC spectra, a 3 cm^2 punch of sample filters was extracted with water, and another 3 cm^2 punch with methanol using ultrasonication. The extract was introduced into the liquid waveguide capillary cell coupled to a portable UV−visible spectrophotometer and deuterium and tungsten halogen lamps via a syringe filter (Acrodisc syringe filters with GHP membrane, 0.45 μm, 25 mm) to remove insoluble particles (including BC and dust), and the high-resolution absorption spectra were saved from 300-700 nm for each filter extract using the portable UV-visible spectrophotometer. Spectrum of water-extracts was

referenced with water and that of methanol-extracts with methanol to remove any possible effect of absorbance from solvent on the observed spectrum of samples. This also enables one to compare the spectra of different solvents. Several blanks filters were also treated like samples, and reported values are corrected for blanks. The analysis of about 20% samples were also repeated for absorption spectra, and found to be within 8%. The detailed analytical protocol for the assessment of optical properties of BrC were described elsewhere (Srinivas et al., 2016). Further, Chen and Bond (2010) found that when using methanol approximately 98% of BB OC could be extracted from filters. It also says that strongly light-absorbing water-insoluble components are likely large molecular weight PAHs, such as quinones from BB and fossil fuel combustion. A recent study by Cheng et al. (2016), suggests that 85% of the OC mass can be dissolved in methanol.

Absorption coefficient at a given wavelength (b_{abs_λ}) was estimated as follows:

$$b_{abs\_\lambda} = (A_\lambda - A_{700}) * V_{ext} * \frac{Total\ filter\ area}{Area\ of\ filter\ aliquot\ used} * \frac{ln(10)}{Va*l}\ Mm^{-1} \qquad (2)$$

Here, A_λ is the absorbance at wavelength λ, A_{700} is an absorbance at the reference wavelength (700 nm) to account for any baseline drift, V_{ext} = volume of water (or methanol) used for the extraction of the aerosol filter punch, V_a = volume of air filtered during sampling, and l = path length (2 m). Here, λ = 365 nm was used. The b_{abs_365} is the absorption coefficient at 365 nm (expressed in M m^{-1} = 10^{-6} m^{-1}). This wavelength was chosen because it is far enough from the UV region to avoid interferences from nonorganic compounds (e.g., nitrate), HUMIC like substances (HULIS) absorb at this wavelength, and it is similar to earlier reported studies (Hecobian et al., 2010; Hoffer et al., 2006; Lukács et al., 2007). The A_{700} is an absorbance at the reference wavelength (700 nm) to account for any baseline drift. V_{ext} is the volume of water used for the extraction of the aerosol filter V_a is the volume of air filtered through the quartz filters during sampling and l is path length (2 m). The Absorption Ångstrom exponent (AAE), reflecting the

wavelength (λ) dependence of particulate absorption, is often fitted with a power law of the form

$$b_{abs\_\lambda} = K\lambda^{-\alpha} \quad (3)$$

Where, K = constant, α = Aerosol Angstrom Exponent (AAE), and b_{abs} is the absorption coefficient of a light-absorbing species at a given wavelength (λ). In this study, the AAE for BrC (AAE_{BrC}) is determined from the slope of a linear regression fit between ln (b_{abs_λ}) and ln (λ) for the λ ranging from 360 and 480 nm (Liu et al., 2014; Yan et al., 2015; Cheng et al., 2016).

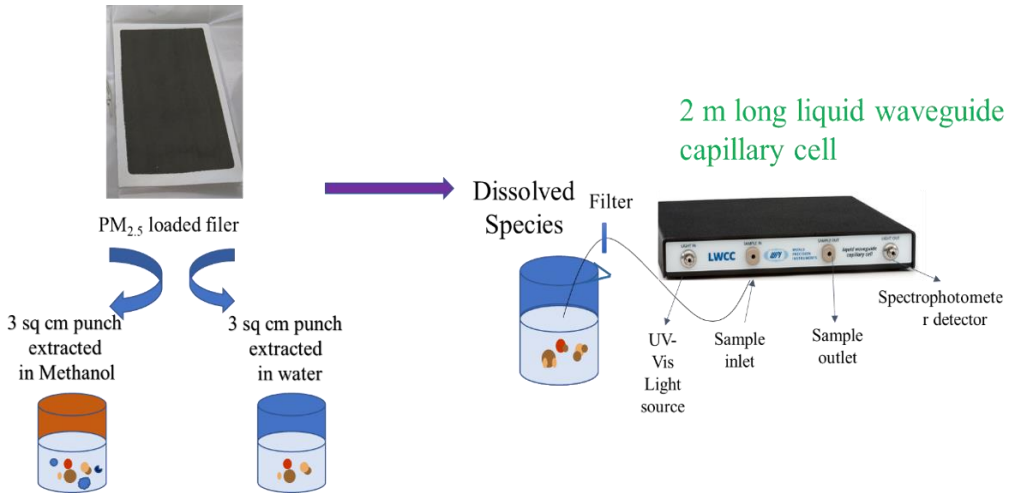

Figure 2.15: Schematic view of offline absorption measurement

2.3.10.3 Mass absorption efficiency of WSOC and OC

Using b_{abs_365} (Mm^{-1}), WSOC (μg m^{-3}), and OC, mass absorption efficiency (MAE or σ, m^2 g^{-1}) was calculated as follows for both water-soluble and methanol soluble extracts:

$$\sigma_{abs\_365\_Water} = \frac{b_{abs\_365Water}}{WSOC} \quad (4)$$

$$\sigma_{abs\_365\_Methanol} = \frac{b_{abs\_365\_Methanol}}{OC} \quad (5)$$

2.3.10.4 b_{abs} and MAE of EC:

The MAE of EC (σ_{EC}) was assessed from its attenuation coefficient and concentration measured on Sunset-EC-OC analyzer using the NIOSH protocol, as per the procedure described by Ram and Sarin (2009). The analytical instrument (EC-OC analyzer) provides absorbance (initial transmittance) at 678 nm by measuring intensities of the incident and transmitted light through the filter loaded with aerosol. The absorption signal is represented by optical-attenuation (ATN, a unitless parameter) and is governed by the Beer-Lambert's law. Thus, the measured ATN through the sample filter is attributed to the presence of light absorbing carbon and is equivalent to in situ EC concentration in aerosol (Sciare et al., 2001). The attenuation (ATN) of an EC can be used to determine the b_{abs} and σ of EC.

$$\textit{Absorption coefficient}\ (b_{abs\_EC}\ Mm^{-1}) = ATN * \frac{A}{V} \quad (6)$$

Here ATN = initial absorbance; A = filter area (cm^2); V = volume of air (m^3)

$$\textit{Mass absorption efficiency of EC } (\sigma_{EC}) = \frac{b_{abs\_EC}}{EC} \quad (7)$$

Here EC is in μg m^{-3} (obtained at 678 nm). However, the σ_{EC} needs to be corrected for shadowing (i.e., decrease in absorption signal) and multiple scattering effects (which enhances the absorption signal) arising from artifacts associated with the filter-based measurements (Ram and Sarin, 2009). The correction relies on normalizing the mass absorption efficiency with two empirical factors suggested for shadowing effects R(ATN) and multiple scattering effects (C) (Weingartner et al.,2003). Here we have used C = 2.14 as a correction factor for enhancement in the absorption signal arising from multiple scattering effects (Ram and Sarin, 2009).

$$\sigma_{EC\ corrected}\ (m^2g^{-1}) = \frac{\sigma_{EC}}{(C*R(ATN))} \quad (8)$$

2.3.10.5 Relative absorptions of BrC over EC:

Carbonaceous aerosol were distinguished by the spectral dependence of their light-absorption concerning the empirically defined power law relationship as follows.

$$\text{Mass absorption efficiency (MAE or } \sigma) \; \alpha \; \lambda^{-\alpha} \qquad (9)$$

In the above equation, α refers to the Angstrom exponent of BrC. To estimate the relative absorption of BrC (Water and Methanol) over EC, we have compared their mass absorption efficiency using their wavelength-dependent relations, similar to that described in Srinivas and Sarin (2014). Further, we have modified Eq. (9) to calculate MAE of EC at different wavelengths, as we have only MAE value of EC (678 nm) from EC OC analyzer.

$$(\text{MAE or } \sigma)_{\lambda 1} \; \alpha \; \lambda_1^{-\alpha} \qquad (10)$$

$$(\text{MAE or } \sigma)_{\lambda 2} \; \alpha \; \lambda_2^{-\alpha} \qquad (11)$$

Here we have MAE of λ_1 (678 nm) for EC, therefore to calculate λ_2, we used in the following formula.

$$(\text{MAE or } \sigma)_{\lambda 2} = (\text{MAE or } \sigma)_{\lambda 1} * (\lambda_1/ \lambda_2)^{\alpha} \qquad (12)$$

However, unlike BrC the angstrom exponent of EC has been suggested as ~ "1" by earlier studies (Cheng et al., 2011; Hecobian et al., 2010; Kirchstetter and Thatcher, 2012; Kirchstetter et al., 2004). Therefore, Eq. (12) can be rewritten as follows.

$$(\text{MAE or } \sigma)_{\lambda 2} = (\text{MAE or } \sigma)_{\lambda 1} * (\lambda_1/ \lambda_2)^{\alpha} \qquad (13)$$

To calculate BrC MAE at different wavelengths, we have used the measured absorbance signal and α observed values. The relative absorption of BrC (Water and Methanol) over EC calculated at 370, 410, 450, 490, 530 and 678 nm.

CHAPTER 3

Spatial and Temporal Characteristics of BrC Using Filter Based Techniques

This chapter discusses the filter-based BrC spectral characteristics over different regions of India with the major focus on the spatial and temporal variability of $PM_{2.5}$ mass, chemical compositions, and BrC optical properties.

3.1 Patiala, Punjab (a case study during BB period)

3.1.1 Temporal variability of measured species:

Figure 3.1 depicts the large temporal and day/night variability in the mass concentration of $PM_{2.5}$ and its chemical species over Patiala during the study period. This variability is attributable to different factors such as the dominance of specific sources (BB, FFB), atmospheric processes such as long-range transport, transformation, secondary organic aerosol (SOA) formation, boundary layer dynamics and meteorological conditions over the study region. The $PM_{2.5}$ mass concentration ranged from ~90 to 500 μg m^{-3} (average ± 1$\boldsymbol{\sigma}$ standard deviation: 230±114) with the average values of 154 ± 57, 271 ± 122, 156 ± 18 μg m^{-3} during pre-burning (T1), burning (T2) and post-burning (T3) periods, respectively (Figure 3.1a). Higher aerosol loading during T2 reflects the effect of crop-residue burning on ambient air quality. Observation period was also affected by emissions from firecrackers during Diwali festival (23 and 24 October-2014) that caused the highest mass concentration of T1 period. Minimum concentrations were recorded on October 14 and November 8 (Fig. 3.1a) due to washout of aerosol by considerable rainfall (~20 mm) on these days. Atmosphere was recharged quickly after the rain event during T2 which further highlights the impact of BB on ambient aerosol loading. Similarly, OC, EC, WSOC, levoglucosan, $b_{abs\_365\_Water}$ and $b_{abs\_365\_Methanol}$ ranged from ~7.0 to 178 μg m^{-3} (avg: 58 ± 42), ~1.8 to 19 μg m^{-3} (avg: 9.2 ± 3.5), ~4.9 to 85 μg m^{-3} (avg: 31 ± 20), ~0.2 to 10.8 μg m^{-3} (avg: 2.3 ± 2.4), ~2 to 112 Mm^{-1} (avg: 37 ± 27) and ~3 to 457 Mm^{-1} (avg: 121 ± 108), respectively. Detailed discussion on these species are provided in the subsequent sections. The samples associated with T2 (belongs to intense BB) period showed the highest day/night variability in all species

than those associated with T1 and T2 (Fig. 3.1). Paddy residues burning in open fields were forbidden by the local government, which is why burning activities usually occurred at night to evade supervision and penalties (Singh et al., 2016a; 2016b). This fact together with the shallow boundary layer contributed to higher night time concentrations than daytime concentrations.

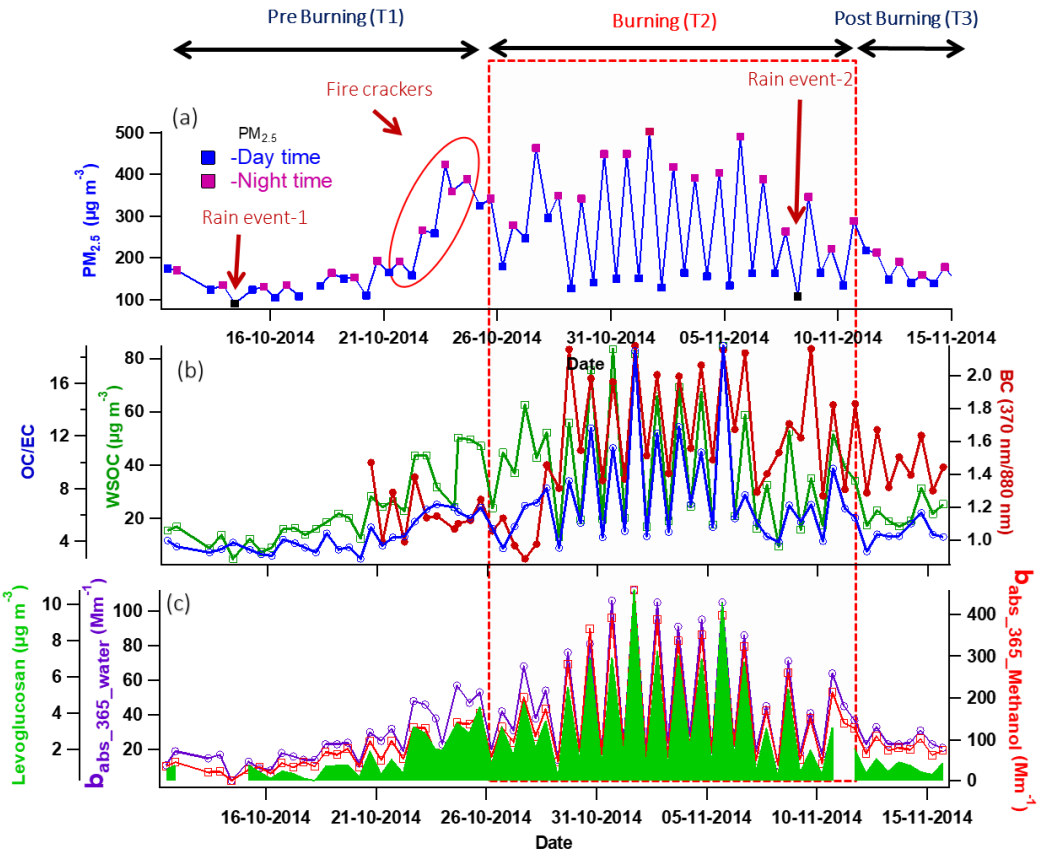

Figure 3.1: Temporal variability of (a) $PM_{2.5}$, (b) WSOC, OC/EC and BC (370/880) ratios, and (c) $b_{abs\_365\_water}$, $b_{abs\_365\_methanol}$, and Levoglucosan

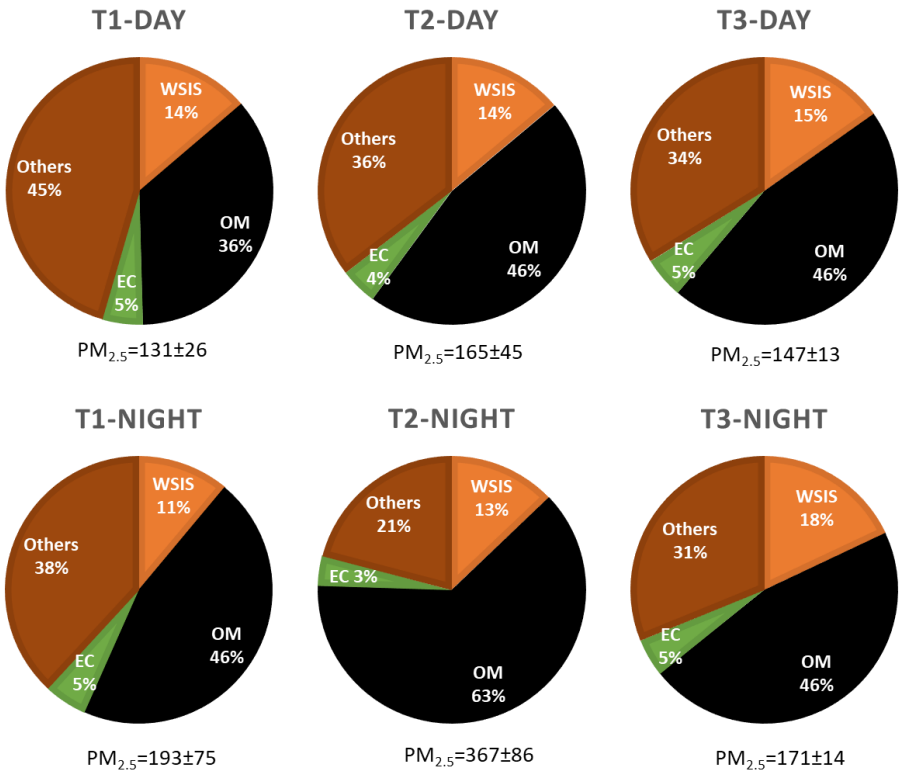

Figure 3.2: Chemical composition along with average $PM_{2.5}$ mass concentrations during days and nights each period. Here, WSIS is water-soluble inorganic species, EC is elemental carbon, OM is organic matter, and 'Others' is an unidentified fraction.

To the total daytime $PM_{2.5}$, the contributions of OM (2.1 times the measured concentration of OC, Rajput and Sarin, 2014) were 36%, 46%, and 46%, WSIS (sum of NH_4^++ Na^++ K^+ + Mg^{2+} + Ca^{2+}+ Cl^- + NO_3^- + SO_4^{2-}) were 14%, 41%, and 15%, and EC were 5%, 4%, and 5%, during T1, T2, and T3, respectively. Similarly, for night time samples, the contributions of OM were 46%, 63%, and 46%, WSIS were 11%, 13%, and 18%, and EC were 5%, 3%, and 5% during T1, T2 and T3, respectively. The observation suggests that OM was dominating during all the three periods, and nighttime OM concentrations were always higher than those observed during the daytime. Similar observations were reported by Rastogi et al. (2014) from

the same sampling site. During night time of T2 period, samples showed the highest OM concentrations (OM ~63%).

3.1.2. Carbonaceous aerosols and BB tracers:

Carbonaceous aerosol are consisting of OC and EC, where EC is the primary particle predominantly coming from combustion sources such as BB and FFB. On the contrary, OC can be of both primary as well as secondary origin. The OC/EC ratios are often used to assess the relative dominance of biomass vis-à-vis FFB sources with the understanding that higher OC/EC ratio suggest the significant source of carbonaceous aerosol is BB whereas lower OC/EC ratio indicates that they are predominantly from FFB (Feng et al., 2012; Rastogi et al., 2014). The OC/EC ratio varied from 2.7 to 19 (5.9 ± 3.2) during the study period with almost double OC/EC ratio during T2 (7.3 ± 3.7) in comparison to that during T1 (3.7 ± 0.6) and T3 (4.6 ± 0.8). This observation suggests that BB emissions were the dominant source of ambient carbonaceous aerosol over the study region. Many studies had also reported that the ratio of BC at 370 nm to BC at 880 nm could be used as a tracer to identify whether emissions from BB or FFB dominate aerosol over a given region. The ratio of BC (370/880) < 1.0 represents the dominance of emissions from FFB, whereas BC (370/880) > 1.0 depicts the dominance of BB emissions (Herich et al., 2011; Singh et al., 2014). In this study, the BC (370/880) ratios were 1.20 ± 0.20, 1.54 ± 0.40, and 1.40 ± 0.10 during T1, T2, and T3, respectively. The BC (370/880) ratios were high during the T2 period (Day: 1.31 ± 0.20 and Night: 1.50 ± 0.44), which further suggests that BB emits a large amount of BC, which has a substantial fraction of BrC (Figure 3.1b).

Another important primary fine particle is K^+, which is often used as a tracer for emissions from BB in many previously reported studies (Ram and Sarin, 2011; Rastogi et al., 2014). However, the K^+ is a questionable tracer for BB emissions because it may also come from other sources such as mineral dust, sea-salts, fertilizers, etc. In this study, statistical parameters (r^2 = 0.86, slope = 15.9, intercept =

-8.8) for an observed linear correlation between OC and K^+ for both daytime and night-time samples suggest that the K^+ was predominantly derived from BB. The observed slope is similar to that reported in Rastogi et al., 2014. Further, high K^+/EC ratio (>0.20) reflects the dominance of BB emissions whereas a low ratio (<0.10) would indicate the prevalence of fossil-fuel emissions (Andreae, 1983; Wang et al., 2005; Ram and Sarin, 2011; Rastogi et al., 2015). The study region shows very high K^+/EC ratios though with significant variability (0.2-2.8; avg: 0.51±0.41) during the sampling period, suggesting emissions from BB is dominant over those from FF burning.

Further, levoglucosan (1, 6-anhydro-b-D-glucopyranose) is considered an excellent molecular marker for BB (Simoneit et al., 1999). It is formed by the pyrolysis of cellulose, the primary building material of wood and agricultural crop residues, at temperatures higher than 300^{o}C (Wang et al., 2009). Although levoglucosan can be degraded in the atmosphere as reported in some simulation experiments and model studies, it is still considered as an ideal tracer for BB due to its high emission factors (Hu et al., 2013 and references are therein). In the present study, Levoglucosan and K^+ showed a strong correlation with a slope (0.94 ± 0.04, r^2 = 0.87, n = 62) different than those reported for domestic wood burning (Levo/ K^+<0.2), savanna fires (Levo/ K^+~20), and biofuel (Levo/ K^+ = 0.37 ± 0.1) in literature. This ratio (slope) can be used as a fingerprint for the paddy-residue burning over the IGP. The observed slope is similar to earlier studies over Amazon (Levo/ K^+ slope = 1.01, Schkolnik et al., 2005) when flaming combustion prevailed, and over Austria during wintertime (0.9-1.7) but higher (0.22-0.5) than that observed over Austria during summer (Caseiro et al., 2009). The highest K^+ values were obtained during the firework episode (Diwali festival). Previous studies have shown that aerosol from firework are rich in K^+ (Drewnick et al., 2006; Wang et al., 2007; Cheng et al., 2013). Comparison of levoglucosan and K^+ levels from fireworks can significantly bias their role as a BB tracer.

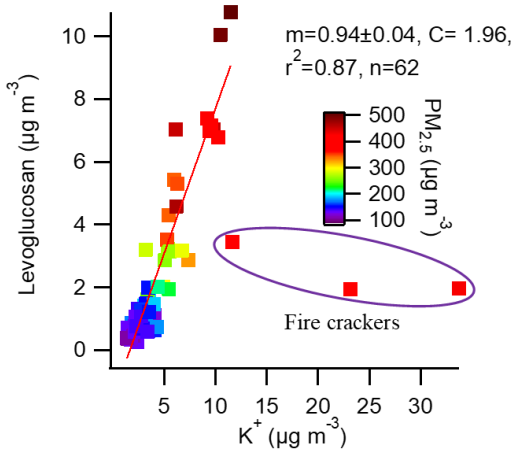

Figure 3.3: Scatter plot between levoglucosan and K^+ with the colored axis as $PM_{2.5}$

3.1.3 Optical properties of BrC and EC:

A statistical description of the chemical constituents and optical properties of BrC (***b_{abs} and σ***) for the samples collected during the three periods are given in Table 3.1 along with their day/night variability. During the T2 period, all the chemical species showed high concentrations with high night/day ratios. The b_{abs} and ***σ*** of BrC were assessed at 365 nm relative to 700 nm for both water and methanol extracts (Liu et al., 2015). The b_{abs} of methanol extracts can be, to some extent, used as a measure of light absorption by total organic aerosol (Cheng et al., 2016). The $b_{abs\_365\_Water}$ and $b_{abs\_365\_Methanol}$ showed a similar temporal variability as depicted by Levoglucosan, and BC (370/880) ratios, attesting that BB was the major source of BrC. The average $b_{abs\_365\_water}$ during the day (22 ± 10 M m^{-1}) and night (51 ± 30 M m^{-1}) were smaller than $b_{abs\_365\_Methanol}$ during the day (64 ± 31 M m^{-1}) and night (177 ± 124 M m^{-1}) respectively indicating that the $b_{abs\_365\_Methanol}$ was always higher than $b_{abs\_365\_Water}$ during both day and night, a result similar to earlier studies (Liu et al., 2013; Zhang et al., 2013; Cheng et al., 2016). These results also suggest that total BrC can absorb more incoming solar radiation than that can be absorbed by water-soluble BrC, and this could cause large underestimation of the forcing estimated using only water-

soluble BrC as a surrogate (Bosch et al., 2014; Kirillova et al., 2014a, 2014b). Hence it is crucial to estimate the forcing due to total BrC over different emission regions. This can help in better assessing the BrC effect on radiative forcing.

The $b_{abs\_365\_Water}$ and $b_{abs\_365\_Methanol}$ both showed much higher concentrations during the T2 period than that during T1 and T3 periods (Table 3.1). A very high BrC concentrations in the night samples of T2 period also suggest that BB derived fresh BrC absorbs more at 365 nm. The observed $b_{abs\_365\_water}$ values are similar to that reported earlier in Srinivas et al., (2016) for the day (40 ± 18) and night (52 ± 27) samples. Further, a linear regression analysis between WSOC and $b_{abs\_365\_water}$, and OC and $b_{abs\_365\_Methanol}$ was performed for the day and night samples. The observed slopes for water and methanol extracts for the day (Water: m = 0.94 ± 0.05, Methanol: m = 1.64 ± 0.06) and night (Water: m = 1.33 ± 0.06, Methanol: m = 2.52 ± 0.12) samples were significantly different. The observed slope for WSOC vs. $b_{abs\_365\_water}$ correlation is higher in the current study compared to that reported by Srinivas et al. (2016) from the same sampling site. The sampling frequency was also much higher in this study compared to Srinivas et al. (2016). Further, the observed slopes for the earlier reported studies over different regions are: Water: m = 2.0, Methanol: m = 1.8 over Jefferson Street and Yorkville (Liu et al., 2013), Water: m = 0.48, 0.39 and 0.80 over Bay of Bengal (BoB) IGP outflow, BoB sea outflow, (Srinivas and Sarin, 2013), Water: m = 0.70 over Kharagpur (Srinivas and Sarin, 2014), Water: m = 0.75 and 1.13 over Patiala (Srinivas et al., 2016), Water: m = 1.25, Methanol: m = 1.50 over Beijing (Cheng et al., 2016), and Water: m = 1.22 over Kanpur (Satish et al., 2017). In addition, a strong correlation was also observed between levoglucosan and $b_{abs\_365\_water}$ (r^2 = 0.94, slope = 10.9 ± 0.34, figure not shown), and levoglucosan and $b_{abs\_365\_Methanol}$ (r^2 = 0.95, slope = 43.5 ± 1.25, figure not shown) further indicating that BB is a strong source for BrC, which is consistent with earlier reported studies (Lack et al., 2012; Cheng et al., 2016).

A statistical description of the optical properties of BrC ($\sigma_{abs\_365\_Water}$, $\sigma_{abs\_365\_Methanol}$, and σ_{EC}) in the day and night samples are given in Table 3.2. The average b_{abs_365}

$_{Methanol}$ (121 ± 108) is about 3.3 times higher than the $b_{abs\_365\ \_water}$ (37±27), reflecting the absorbing capacity of water-insoluble vis-à-vis water-soluble BrC. The σ values were calculated for both water- and methanol-soluble extracts using Eq.4 & 5. The observed $\sigma_{abs\_365\_Methanol}$ was about 1.6, 1.9 and 2.0 times higher than $\sigma_{abs\_365\_Water}$ during T1, T2, and T3, respectively. However, all these values were assessed at 365 nm, which is mainly associated with HULIS, and BB can emit complex mixture chromophores which can show variable absorption at different wavelengths. Further, the $\sigma_{abs\_365\_Methanol}$ was about 0.62, 0.54 and 0.52 times lower than σ_{EC} during T1, T2, and T3, respectively. This suggests that the estimation of radiative forcing due to BrC is important.

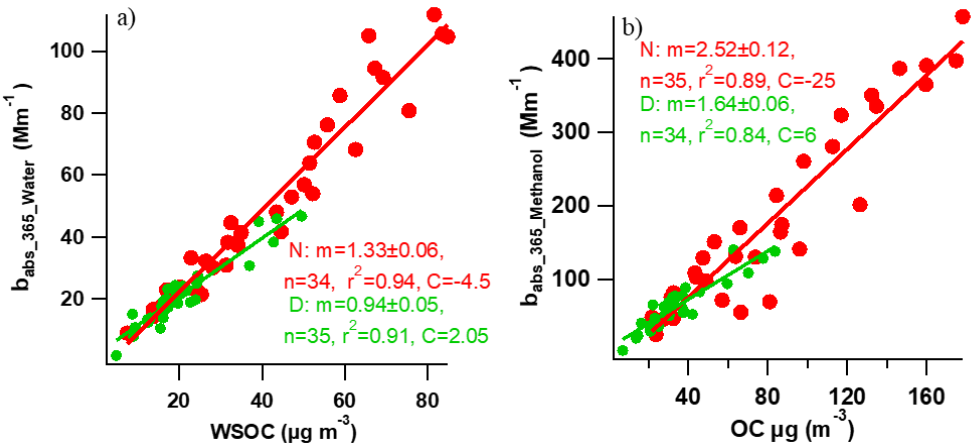

Figure 3.4: Linear regression plots of (a) WSOC vs $b_{abs\ \_365\_Water}$, and (b) OC vs $b_{abs\_365\_Methanol}$

Table 3.1: Statistical description (avg ± sd) of the concentrations of chemical constituents (µg m^{-3}) together with the absorption coefficient (Mm^{-1}) of light absorbing carbonaceous species and their Night/Day ratios in $PM_{2.5}$ samples

Chemical Species	Concentration (All) (Avg±Stdv)	Ratio (N/D)	Concentration T1	Ratio T1 (N/D)	Concentration T2	Ratio T2 (N/D)	Concentration T3	Ratio T3 (N/D)	Concentration (Diwali)	Ratio Diwali (N/D)
$PM_{2.5}$	228 ± 114	1.88 ± 0.87	154 ± 57	1.38 ± 0.87	270 ± 122	2.34 ± 0.71	156 ± 18	1.18 ± 0.17	339 ± 66	1.29 ± 0.09
K^+	5 ± 5.0	2.14 ± 1.44	2.0 ± 1.0	1.11 ± 0.43	5.0 ± 3.0	2.72 ± 1.22	3.0 ± 1.0	1.29 ± 0.2	16 ± 11	3.59 ± 3.08
WSOC	31 ± 20	2.20 ± 1.33	10 ± 6	1.26 ± 0.5	41 ± 23	2.99 ± 1.35	22 ± 5	1.26 ± 0.27	39 ± 9	1.40 ± 0.67
OC	58 ± 42	2.46 ± 1.55	28 ± 13	1.58 ± 0.51	76 ± 49	3.34 ± 1.65	35 ± 5	1.21 ± 0.18	79 ± 10	1.24 ± 0.20
EC	9.0 ± 3.0	1.54 ± 0.56	8.0 ± 2.0	1.31 ± 0.22	10.0 ± 4.0	1.79 ± 0.65	8 ± 1	1.07 ± 0.05	13 ± 2	1.26±0.27
Levoglucosan	2.37 ± 2.44	4.27 ± 3.67	0.84 ± 0.40	2.06 ± 1.40	3.43 ± 2.90	6.25 ± 3.94	0.97 ± 0.31	1.66 ± 0.60	2.68 ± 0.63	1.24 ± 0.55
WSOC/OC	0.58 ± 0.10	0.92 ± 0.18	0.60 ± 0.13	0.80 ± 0.20	0.56 ± 0.07	0.93 ± 0.12	0.63 ± 0.10	1.04 ± 0.15	0.49 ± 0.1	1.06 ± 0.36
OC/EC	5.88 ± 3.20	1.56 ± 0.80	3.69 ± 3.6	1.20 ± 0.32	7.72 ± 3.80	1.92 ± 0.93	4.62 ± 0.79	1.13 ± 0.17	6.30 ± 0.45	1.00 ± 0.06
K^+/EC	0.51± 0.41	1.44 ± 1.14	034 ± 0.10	0.85 ± 0.30	0.52 ± 0.23	1.59 ± 0.71	0.43 ± 0.1	1.21 ± 0.15	1.34 ± 1.02	3.55 ± 3.22
$b_{abs\_365\_water}$	37 ± 27	2.58 ± 1.66	17 ± 7	1.45 ± 0.58	49 ± 31	3.57 ± 1.68	25 ± 4	1.17 ± 0.19	42 ± 11	1.67 ± 0.84
$b_{abs\_365\text{-}Methanol}$	121 ± 108	2.95 ± 1.87	47 ± 24	1.90 ± 0.55	173 ± 125	4.06 ± 1.92	82 ± 15	1.23 ± 0.16	104 ± 35	2.04 ± 0.94

Table 3.2: The $\sigma_{abs\_365\_Water}$, $\sigma_{abs\_365\_Methanol}$, σ_{EC}, AAE_{Water}, and $AAE_{Methanol}$ during different periods

	Overall period	*Pre-burning(T1)*	*Burning (T2)*	*Post-burning(T3)*	*Fire crackers*
$\sigma_{abs\_365\_Water}$	0.4 - 1.7 (1.1 ± 0.2)	0.4 - 1.7 (1.0 ± 0.3)	0.8 - 1.6 (1.2 ± 0.2)	0.8-1.5 (1.2 ± 0.2)	0.9 - 1.2 (1.1 ± 0.1)
$\sigma_{abs\_365\_Methanol}$	0.5 - 2.9 (2.0 ± 0.5)	0.5 - 2.9 (1.6 ± 0.5)	1.5 - 2.8 (2.2 ± 0.4)	2.1-2.5 (2.3 ± 0.1)	0.8 - 1.8 (1.3 ± 0.4)
σ_{EC}	1.2 - 5.2 (2.2 ± 0.6)	1.5 - 5.2 (2.5 ± 0.7)	1.2 - 3.5 (2.0 ± 0.5)	1.6 - 3.0 (2.5 ± 0.4)	1.4 - 1.8 (1.6 ± 0.1)
AAE_{Water}	6.4 - 7.5 (6.8 ± 0.3)	6.4 - 7.2 (6.7 ± 0.2)	6.4 - 7.5 (6.9 ± 0.3)	6.5 - 6.7 (6.6 ± 0.1)	6.5 - 7.5 (6.7 ± 0.4)
$AAE_{Methanol}$	5.2 - 6.6 (5.8 ± 0.3)	5.5 - 6.6 (6.0 ± 0.2)	5.2 - 6.1 (5.7 ± 0.2)	5.4 - 5.7 (5.6 ± 0.1)	5.7 - 6.5 (6.1 ± 0.3)

The fractional contribution of mass absorption efficiency of BrC (Water and Methanol), relative to that of EC is calculated for the T1, T2 and T3 periods. This approach was obtained from previously reported studies (Srinivas and Sarin, 2014; Chakraborty et al., 2015; Srinivas et al., 2016). The MAE values for EC and BrC (Water and Methanol) were calculated (Eqs 6 to 13). The mean fractional relative contribution of MAE of BrC (Water and Methanol) over EC at different wavelengths (370, 410, 450, 490, 530 and 678 nm) is shown in Fig. 3.5. From this figure, it is noteworthy that the ratio of MAE of BrC to that of EC in water extracted samples are low compared to methanol extracted BrC for all three periods. During the T2 period, both water and methanol extracted BrC shows more fraction than the other two periods. The contribution from MAE of BrC (Water) at 370 nm is ~16-46% and MAE of BrC (Methanol) at 370 nm is~30-88% relative that of EC.

The observed values for water-soluble BrC is similar to that previously reported Srinivas et al. (2016).

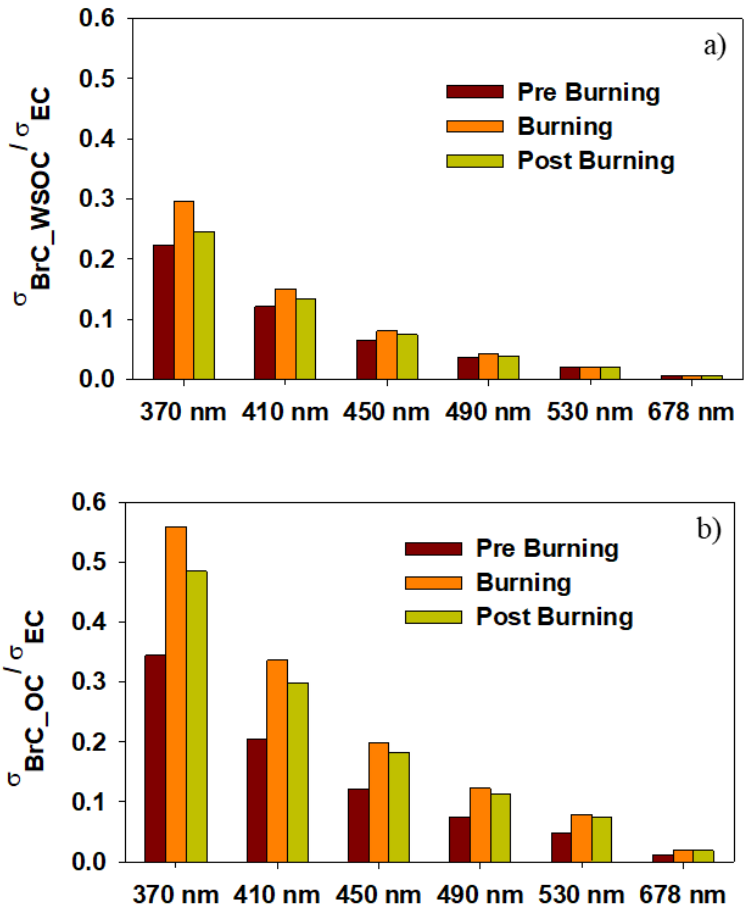

Figure 3.5: Fractional contribution of mass absorption efficiency of BrC (a) Water and (b) Methanol, relative to that of EC, in $PM_{2.5}$ samples before, during and after paddy-residue burning emissions

Our results are also consistent with that documented for water-soluble BrC emissions from biomass and biofuel burning (Chakrabarty et al., 2014; Srinivas et al., 2016) emissions of BrC relative that of EC. The average fractional values of BrC_370 nm (Water) relative that of EC is 22%, 30% and 24% during the T1, T2 and T3 periods

respectively (Fig. 3.5a). Similarly, the average fractional values of BrC_370 (Methanol) relative to that of EC is 34%, 56%, and 48% respectively (Fig. 3.5b). It is clearly seen that the fractional absorption decreases at higher wavelengths for all three periods. The BrC (Methanol) suggests that the BB emits highly light absorbing organics which absorb light at both shorter and longer wavelengths. This result further indicates that the study region consists of a significant fraction of light absorbing organics.

3.1.4 Proposed concept of using BrC spectra to assess their broad composition and characteristics:

BrC species may consist of a variety of organic chromophores with variable concentrations and different absorbing characteristics. Absorption coefficient (b_{abs}) spectra of water-extracts or methanol-extracts of aerosol represent the bulk optical property of water-soluble or methanol-soluble (assumed to be total) BrC, respectively, as a function of wavelength. If the BrC composition is uniform from sample to sample, then the ratio of b_{abs} spectra for different samples shall be uniform (constant) as a function of wavelength. The magnitude of this constant would suggest the relative abundance of BrC chromophores in different samples. However, if the BrC composition is not uniform from sample to sample, then one would expect variable ratio at different wavelengths depending upon the change in composition and concentrations of different chromophores.

It is known that different types of chromophores absorb strongly at different wavelengths e.g., HULIS type BrC (usually primary BrC) absorb strongly at around 365 nm whereas, nitro-aromatics types of BrC (usually secondary BrC) absorb strongly at relatively higher wavelength (>400 nm) (Graber and Rudich, 2006; Hoffer et al., 2006; Chen and Bond, 2009; Zhang et al., 2013; Lin et al., 2015; Zhao et al., 2015; Xie et al., 2017; Hems and Abbatt, 2018). The wavelength at which non-uniformity in b_{abs} spectra ratio is observed would indicate the change in the type of BrC in a given sample.

Further, the same concept can be applied to water-extracts and methanol-extracts of the same sample. One can calculate the ratio of b_{abs} at different wavelengths for water-extract to that for methanol extract, and use it to quantify the relative contribution of water-soluble and water-insoluble chromophores to total BrC as a function of wavelength in a given sample, presuming methanol-soluble BrC represents total BrC. It is a valid assumption as per literature (Sun et al., 2007; Chen and Bond, 2009; Cheng et al., 2016). These concepts are used in the subsequent sections on the samples collected from Patiala as a case study.

3.1.5 BrC composition and characteristics through b_{abs} spectra

Figure 3.6 shows a comparison of the b_{abs} spectra for BrC extracted with water (b_{abs_Water}), and methanol ($b_{abs\_Methanol}$). They exhibit very different light absorption properties during the T2 period compared to those observed during T1 and T3 periods. Variability in the night/day (N/D) ratio of b_{abs_Water} spectra during the T2 period was large compared to those observed during the T1 and T2 periods (Figures. 3.6a, 3.6b, 3.6c). The observation during T2 suggests that BB emits a variety of BrC chromophores with the highest concentrations of chromophores absorbing in 310 to 400 nm range. Magnitudes of N/D ratio were always >1, with highest values during T2 (1.8 to 3) followed by T3 (1.3 to 1.5) and T1 (1 to 1.3) over 310 to 600 nm range, reflecting the changes in composition and concentrations of BrC chromophores which absorb at different wavelengths. Here the absolute magnitude of ratio reflects the N/D change in chromophore concentrations, and the variability in magnitude of ratio indicates the N/D change

in composition, as proposed in section 3.1. During T1 and T3, slightly lower N/D ratio with noticeable variability in 450 to 600 nm range is suggestive of the presence of daytime secondary BrC in water-extracts. The b_{abs_Water} showed a sharp increase in absorption at 310-400 nm range during nights of the T2 period, which is likely due to HULIS from BB. (Hoffer et al., 2006; Lukács et al., 2007; Hecobian et al., 2010) In the same set of samples, a low absorption at >500 nm was also noticed, which was not observed during the T1 and T3 periods. Similar spectra were observed by Xie et al. (2017) for the laboratory generated secondary BrC formed by the reaction between benzene and m-cresol under high NO_X conditions.

Further, a spectral enhancement was observed in 410-490 nm range of b_{abs_Water} during the T2 period (as reflected in the N/D ratio, Figure 3.6b). This observation suggests that the observed spectral band was likely associated with the presence of a variety of nitro–aromatics, which were generated through SOA in the presence of NO_X (Xie et al., 2017). High NOx was observed in this study also during the T2 period.

A recent study, Cheng et al. (2016), suggested that the majority (~85%) of the organic compounds in the ambient PM could be methanol-soluble. In the present study, the average WSOC/OC ratio is about 0.60, i.e., ~40% of OC is water-insoluble. Figs. 3.6d, 3.6e, and 3.6f show the b_{abs} spectra and their N/D ratio for methanol-extracts during T1, T2, and T3, respectively. The $b_{abs\_Methanol}$ were much higher than b_{abs_Water}, suggesting water-insoluble BrC species are relatively more absorbing during all the three periods. During T2, both b_{abs_Water} and $b_{abs\_Methanol}$ shows higher values in the shorter wavelength range (310-400 nm); however, $b_{abs\_Methanol}$ showed the higher value in the visible region too (Fig. 3.6e). This observation suggests that $b_{abs\_Methanol}$ contains a significant fraction of water-insoluble chromophores which can absorb radiation in the visible region. This can be ascribed to the differences in solubility of the chromophores in water and methanol (Chen and Bond, 2009; Zhang et al., 2011, 2013).

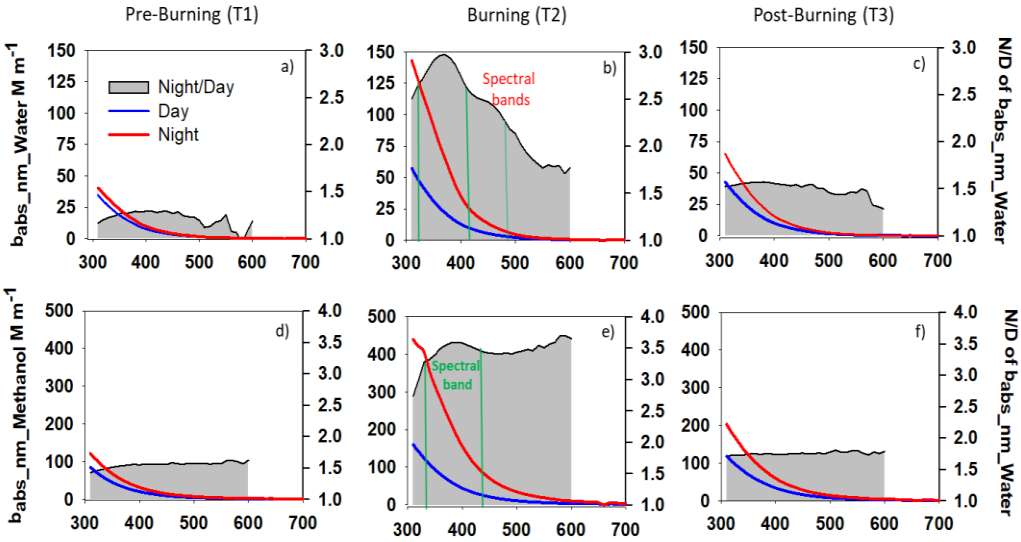

Figure 3.6: The b_{abs} spectra during the day and night and their Night/Day ratio for water-soluble BrC during (a) pre-burning (T1), (b) during burning (T2), and (c) during post-burning (T3) periods, and for methanol-soluble BrC during (d) pre-burning (T1), (e) during burning (T2), and (f) during post-burning (T3) periods. Note that Y-axes range are different for the figures (a,b,c) and (d,e,f).

Some studies suggest that the molecules comprised of more aromatic rings (i.e., a higher degree of conjugation) have a higher absorption that extends to longer wavelengths (Zhang et al., 2013). Further, Zhang et al. (2013) had documented BrC chemical speciation, which showed that a larger molecular weight polycyclic aromatic hydrocarbons (PAHs) absorbed more toward the visible range and had a lower solubility in water. Sun et al. (2007) suggested two kinds of organic carbon: a water-soluble organic mixture with some UV-visible absorption, and water-insoluble organic carbon with higher absorption (Hoffer et al., 2006; Sun et al., 2007; Chen and Bond, 2009).

Further, Quinoid compounds are strong candidates for such absorption (Sun et al., 2007). This type of absorption spectra was present in the nights of the T2 period; however, it disappeared in a day samples (Figure 3.6b, 3.6e). This could be due to

various reasons such as the evaporation of higher-volatility compounds (e.g., nitro-phenols) and/or photo-bleaching, etc. The similar observation is reported by Lin et al. (2016) which suggests that the decrease in absorbance does not follow a single exponential decay because different chromophores decompose at different rates. It is important to state here these statements are postulations from the measured absorption spectra of water-soluble and methanol-soluble extracts, and reported maximum absorption by different chromophores at different wavelengths in literature. To make firm conclusions, more work such as comparison of the measured molecular speciation and absorbance spectra is needed.

In general, the absorption in the visible range is more important to the energy balance than the absorption in the ultraviolet (UV) range as nearly 40% of solar energy is found at wavelengths between 400–600 nm. UV absorption affects photolysis, but wavelengths below 400 nm provide only about 4% to solar energy (Sun et al., 2007).

3.1.6 Relative contribution of the water-soluble and water-insoluble fraction of BrC to the total BrC

To investigate the contribution of the water-soluble and water-insoluble fraction of BrC to the total BrC during different periods, the ratio of b_{abs} (water/methanol) were calculated (Figure 3.7). The $b_{abs\_Methanol}$ represent total BrC, b_{abs_Water} denotes water-soluble BrC, and their difference reflects water-insoluble BrC. This approach helps in assessing the fraction of the water-soluble BrC in the total BrC. It is observed that on average (integrated over 310 to 600 nm) the water-soluble BrC contribute ~33, 27 and 26% in daytime samples whereas, 26, 19 and 23% in nighttime samples to total BrC in the samples collected during T1, T2 and T3 periods, respectively. Observations suggest that contributions of water-soluble BrC are relatively more in daytime samples compare to that in nighttime samples, and its fraction was minimum during T3, maximum during T1 and in between during T2. These observations also suggest that water-insoluble BrC dominates total BrC over the study regions during the study period. However, this water-soluble fraction of BrC was not uniform at all wavelengths. It decreases with

increasing wavelength and goes to as low as ~10% at 600 nm. Further, % water-insoluble BrC in both day-and-night samples was also estimated using equation 2.

$$\% \text{ Water-insoluble BrC} = \frac{b_{abs\_Methanol} - b_{abs\_Water}}{b_{abs\_Methanol}} * 100 \qquad (14)$$

The b_{abs} (water/methanol) ratios for the shorter (310-400 nm) and longer wavelength region (400-600 nm) were averaged. At the shorter wavelength region, water-insoluble fractions during the day (59%, 67%, and 67%) and night (67%, 72%, and 70%) samples were significant during T1, T2 and T3 periods, respectively. Similarly, at the longer wavelength region, water-insoluble fractions during the day (72%, 77%, and 79%) and nights (79%, 86% and 81%) were dominant during T1, T2 and T3 periods, respectively. During T2 period, night samples influenced by BB emissions showed highest fraction (~86%) of water-insoluble BrC and day/night differences at the shorter wavelength region were less than those observed at, the longer wavelength region (Fig. 3.3b). Lee et al. (2014) reported that chemical composition and optical properties of BrC could not be viewed as static, as they may change with time. Light-absorbing compounds (responsible for the color of BrC) can be potentially photo-bleached in sunlight and lose their ability to absorb visible radiation (Lee et al., 2014). Our observations suggest that BrC absorbing at higher wavelengths is predominantly water-insoluble, and they are affected by daytime atmospheric processes such as photolysis/oxidation of BrC chromophores and other transformation reactions (Lin et al., 2015; Liu et al., 2016; Lin et al., 2017; Satish et al., 2017).

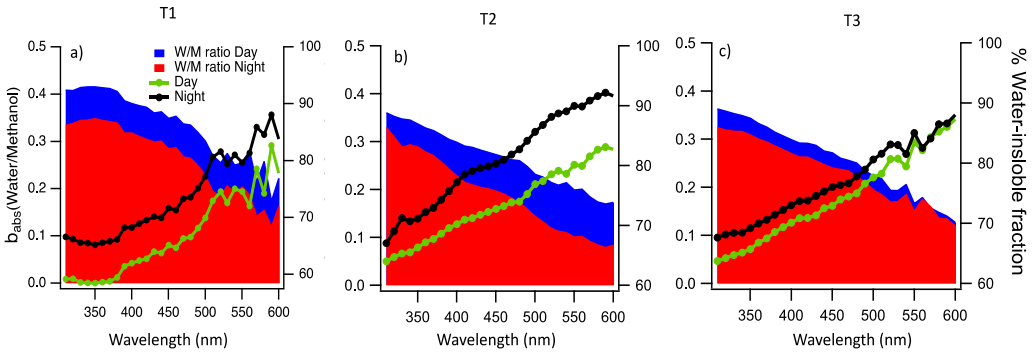

Figure 3.7: The b_{abs} (Water/Methanol) ratio vs. wavelength, and % of water-insoluble fraction vs. wavelength during a) T1 period, b) T2 period, and c) T3 period respectively. Note that shaded area is overlapped, i.e., daytime W/M (blue) was always higher than during night time (red); however, the absolute value of ratio varied as a function of wavelength. Green and black lines exhibit %water-insoluble BrC fraction as a function of wavelength.

3.1.7 Temporal variability in BrC composition through absorption spectra

In order to understand the day-to-day variability in BrC composition through absorption spectra, the absorptions at 400, 405, 420, 450, 500 and 550 nm wavelength (representing absorption by different nitro-aromatics) were normalized to the absorption at 365 nm (representing absorption by HULIS compounds) (Hoffer et al., 2006; Lukács et al., 2007; Hecobian et al., 2010; Zhang et al., 2013; Lin et al., 2015; 2016; 2017). WSON is comprised of different nitrogen-containing WSOC generated through SOA and NOx (Lin et al., 2015; Liu et al., 2016). Linear regression analysis between WSON and NOx showed good correlation (r^2 = 0.64) during the T2 period, suggesting the possibility of the presence of water-soluble nitrogen-bearing BrC compounds. Recent laboratory studies have documented that anthropogenic VOCs (Benzene, Toluene, Phenols) and PAHs react with nitrogen oxides and produce light absorbing nitro-aromatics (Zhang et al., 2011; Lin et al., 2015; Zhao et al., 2015; Wang et al., 2017; Xie et al., 2017; Hems & Abbatt, 2018). These classes of nitro-aromatics absorb in the visible region such as 400, 405, 420, 450, 500 and 550 nm (Lin et al., 2015; Wang et al., 2017; Xie et al., 2017).

Figure 3.8 shows the temporal variability in b_{abs_400}, b_{abs_405}, b_{abs_420}, b_{abs_450}, b_{abs_500}, b_{abs_550} normalized to b_{abs_365} for both water-soluble and methanol-soluble BrC. The observed ratios were higher at shorter wavelengths and decreased towards the visible region. It is interesting to note that methanol-soluble BrC showed relatively less variability during all the three periods. However, water-soluble samples showed higher day-night variability during the T2 period, and lesser variability in T1 and T3 periods. This further suggests that BB emits a noticeable fraction of water-soluble chromophore, which absorbs at the visible region. At 405 and 420 nm, the variability was very high during the T2 period. It could be the presence of nitro-aromatics BrC chromophores. At 405 and 420 nm during the T2 period, enhanced absorbance (>20%) was observed in the night the samples compared to day samples. Nitro-phenolic compounds like 2, 4-Dinitrophenol, 3-Nitrophenol, 2, 5-Dinitrophenol compounds absorb at 405, 420 nm, respectively (Lin et al., 2015). These compounds could be an important fraction of BrC in the urban atmosphere. Further, the overall normalized ratios for $b_{abs\_Methanol}$ were higher compared to those for b_{abs_Water}, further suggesting that there was always a significant insoluble fraction of BrC. However, this insoluble fraction was not uniform and showed maximum contribution during the burning period.

3.1.8 Air mass back trajectories:

The 7-day isentropic AMBTs were computed at an arrival height of 500 m using HYSPLIT, and GDAS reanalysis dataset. Fig. 3.9 depicts the AMBT cluster at 500 m over Patiala during October- November 2014. In this study, AMBTs show a regional pattern, thereby, indicating a major contribution from sources within northern India.

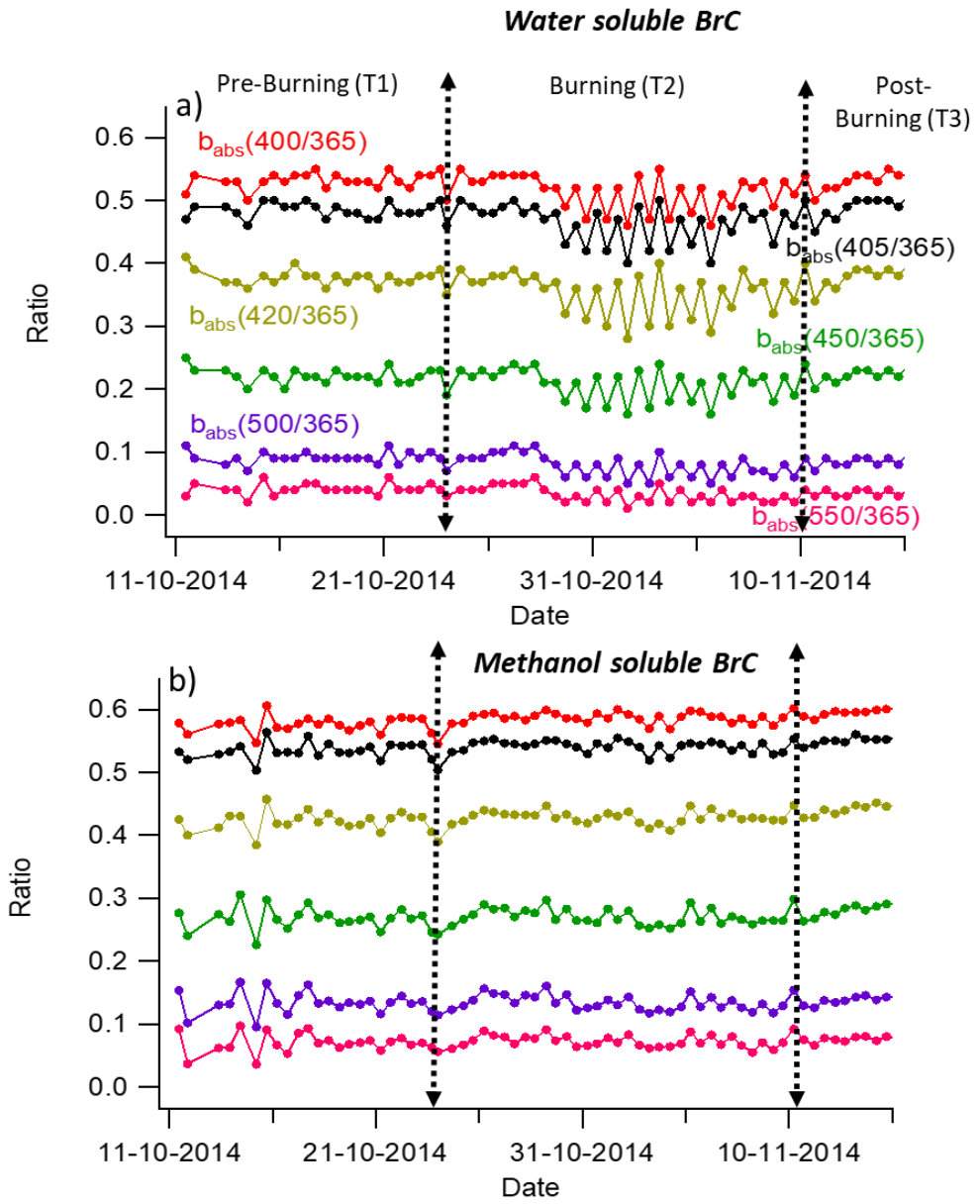

Figure 3.8: Temporal variability in the b_{abs_400}, b_{abs_405}, b_{abs_420}, b_{abs_450}, b_{abs_500}, b_{abs_550} normalized to b_{abs_365} for both (a) water-soluble and (b) methanol-soluble BrC

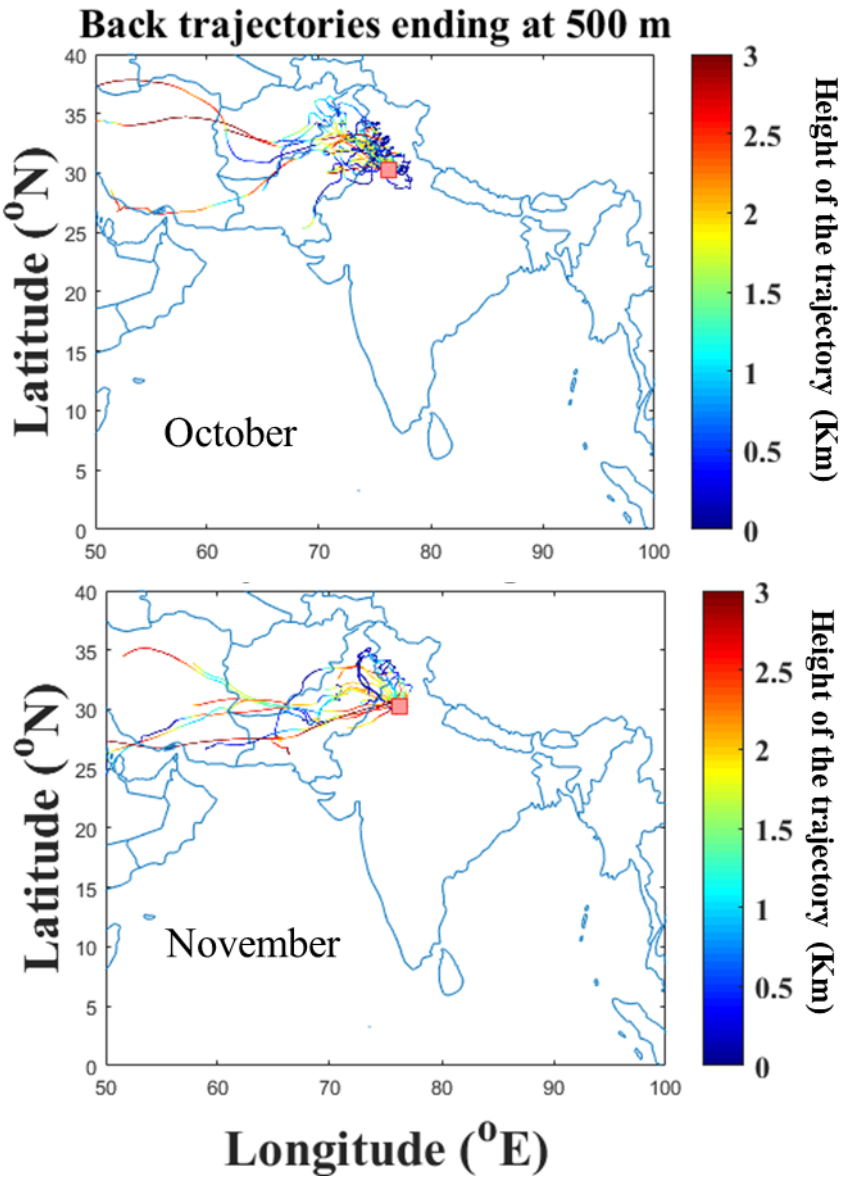

Figure 3.9 Air-mass back trajectories during October and November months

3.2 Parallel measurements over Patiala and Kanpur during winter period

3.2.1 Chemical Composition of $PM_{2.5}$ over Patiala and Kanpur:

The $PM_{2.5}$ concentration ranged from ~58 to 251 μg m^{-3} (131 ± 50) and 79 to 336 (167 ± 53) over Patiala and Kanpur, respectively, during the winter period. The average $PM_{2.5}$ mass over Patiala was less compared to the downwind Kanpur region. Further, the variability in $PM_{2.5}$ is attributable to different factors such as the dominance of specific sources (BB, FFB), atmospheric processes such as long-range transport, transformation, secondary organic aerosol (SOA) formation, boundary layer dynamics and meteorological conditions over the study regions. The $b_{abs\_365\_Water}$, $b_{abs\_365\_Methanol}$ ranged from ~4 to 44 Mm^{-1} (avg: 20 ± 9), ~13 to 76 Mm^{-1} (avg: 30 ± 16) over Patiala, and ~12 to 60 Mm^{-1} (avg: 27 ± 10) and ~20 to 107 Mm^{-1} (avg: 48 ± 21) over Kanpur, respectively. It is observed that b_{abs} values of both water-soluble and methanol-soluble OC were higher over Kanpur than that over Patiala during the study period. During the winter period, especially in December and January, the $b_{abs\_365\_Water}$ and $b_{abs\_365\_Methanol}$ was high, and the values are reduced in February month. The similar trends were observed in $PM_{2.5}$ concentrations as well.

Further, $b_{abs\_365\_Water}$ and $b_{abs\_365\_Methanol}$ showed similar temporal variability with water-soluble K^+ in Patiala and Kanpur samples (Figure 3.10). The water-soluble K^+ is often is used as a tracer for BB. Figure 3.11 depicts the chemical composition of $PM_{2.5}$ over Patiala and Kanpur during the winter period. The mass of organic matter (OM) was estimated using measured OC and approach suggested by Rajput et al. (2013). The mass of water-soluble inorganic species (WSIS = NH_4^++ Na^++ K^+ + Mg^{2+} + Ca^{2+}+ Cl^- + NO_3^- + SO_4^{2-}) was estimated by adding the concentrations of all measured inorganic species.

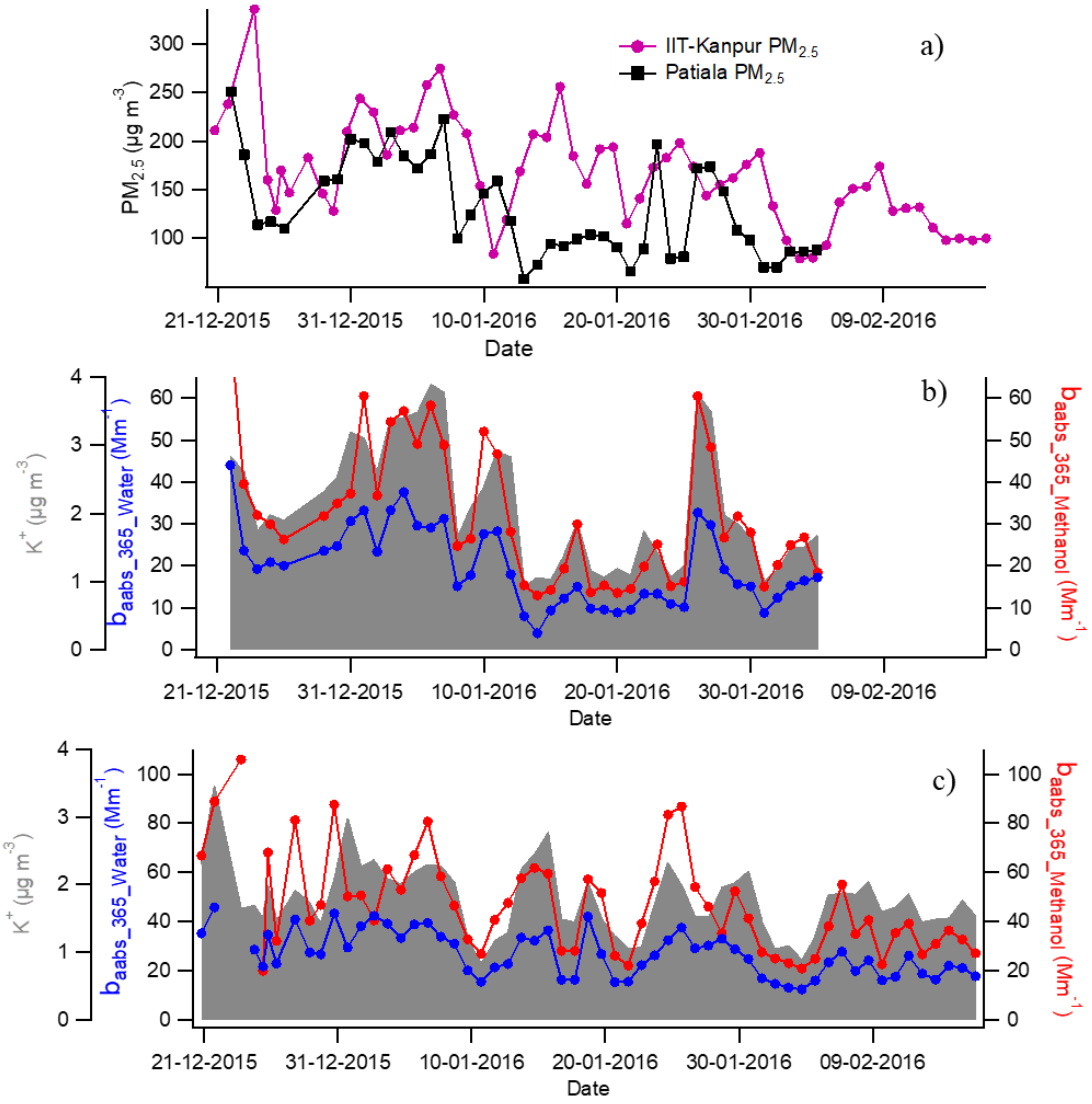

Figure 3.10: Temporal variability of (a) $PM_{2.5}$, (b) Patiala: $b_{abs\_365\_water}$, $b_{abs\_365\_methanol}$, and K^+, (c) Kanpur: $b_{abs\_365\_water}$, $b_{abs\_365\_methanol}$, and K^+

Further, the term 'others' denotes unaccounted $PM_{2.5}$ mass fraction. The contributions of OM were 48% and 42%, WSIS was 35% and 25% and EC was 2% and 5% to $PM_{2.5}$ over Patiala and Kanpur respectively, and the leftover portion was unknown. The observation suggests that OM was slightly higher in Patiala. High fraction of WSIS was also observed over Patiala.

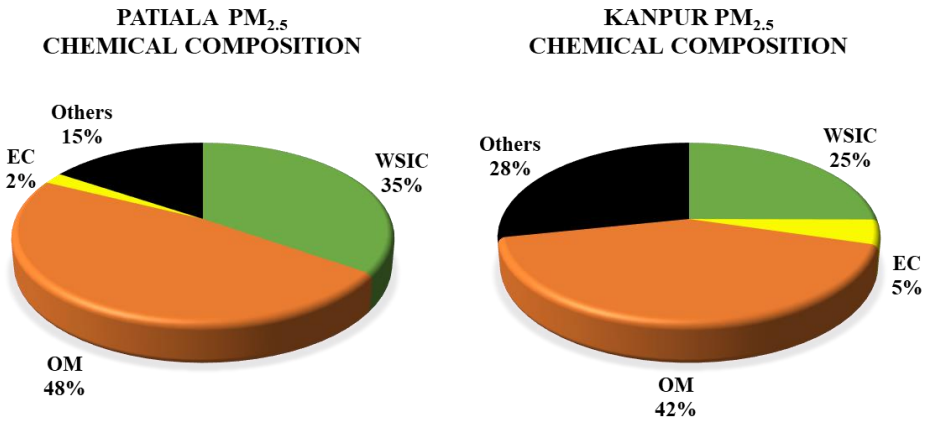

Figure 3.11: $PM_{2.5}$ Chemical compositions over Kanpur and Patiala

3.2.2 BrC optical properties:

The b_{abs} was calculated for both water and methanol extracts at UV (365 nm) and visible regions (450 nm and 510 nm). Light absorption by organic carbon extracted with water was always smaller than that extracted with methanol, although the value varied with wavelength and site. It is expected since methanol can dissolve a greater range of compounds than water which dissolves polar compounds only, as documented in the literature (Chen and Bond, 2010; Liu et al., 2013; Zhang et al., 2013). In the present study, the average WSOC/OC ratio was about 0.53 and 0.56 over Patiala and Kanpur, i.e., ~47% and ~44% of OC was water-insoluble.

In the literature, it is well reported that different types of chromophores absorb strongly at different wavelengths e.g., HULIS type BrC (usually primary BrC) absorb strongly at around 365 nm whereas, nitro-aromatics type of BrC (typically secondary BrC) absorb strongly at relatively higher wavelength (>400 nm) (Graber and Rudich, 2006; Hoffer et al., 2006; Chen and Bond, 2009; Zhang et al., 2013; Lin et al., 2015; Zhao et al., 2015; Xie et al., 2017; Hems and Abbatt, 2018). To understand the BrC chemical composition we have performed regression analysis between b_{abs_Water} vs. WSOC and $b_{abs\_Methanol}$ vs. OC (at 365 nm, 450 nm, and 510 nm) for Patiala and Kanpur sites. The regression analysis

shows nearly same slope both water and methanol soluble BrC over Patiala region (Fig 3.12). This infers that a significant fraction of BrC was water soluble over Patiala region. However, over Kanpur region, a significant difference was observed in slopes for water and methanol extracted OC (Fig. 3.13). The $b_{abs\_Methanol}$ was higher by ~61% at 365 nm, 54% at 450 nm and 43% at 510 nm compared to $b_{abs\_Water.}$ It suggests that methanol-soluble BrC chromophores significantly absorb light at both UV and visible regions. To investigate the contribution of the water-soluble and water-insoluble fraction to the total BrC during different periods, the ratio of b_{abs} (water/methanol) were calculated (Figure 3.14). The $b_{abs\_Methanol}$ represent total BrC, b_{abs_Water} denotes water-soluble BrC, and their difference reflects water-insoluble BrC. This approach helps in assessing the fraction of the water-soluble BrC in the total BrC. Further, % water-insoluble fraction was calculated over there different wavelength ranges (R1: 360-400 nm, R2: 410-500 nm, and R3: 510-600 nm). The observed % water-insoluble fraction was 40%, 43% and 45% over Patiala at R1, R2, and R2 respectively. Similarly, the observed % water-insoluble fraction was 45%, 51% and 60% over Kanpur at R1, R2, and R2 respectively. Over Patiala, there was not much difference in a %-water-insoluble fraction in UV and Visible regions. Observations suggest that contributions of water-insoluble BrC were more in Kanpur samples compare to that in Patiala samples.

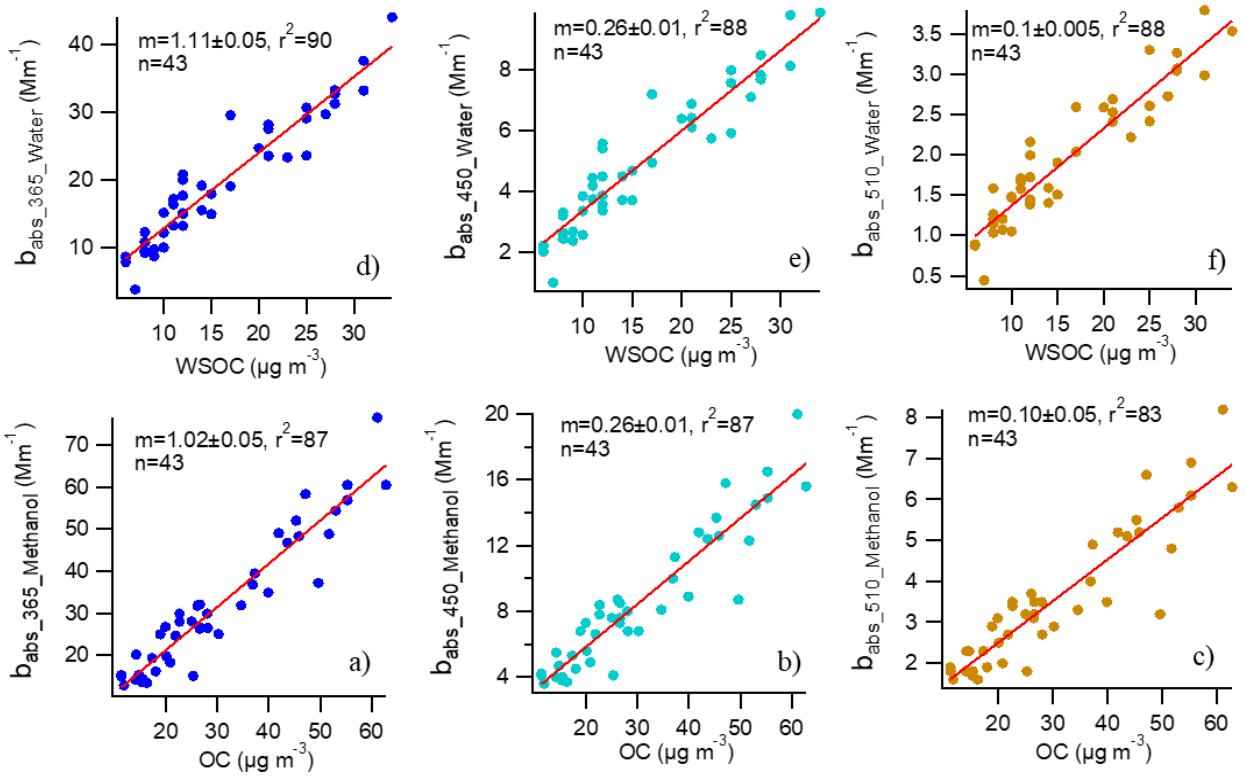

Figure 3.12: Linear regression plots of a) OC vs $b_{abs\_365\_Methanol}$, b) OC vs $b_{abs\_405\_Methanol}$, c) OC vs $b_{abs\_510\_Methanol}$, d) WSOC vs $b_{abs\_365\_Water}$, e) WSOC vs $b_{abs\_405\_Water}$, f) WSOC vs $b_{abs\_510\_Water}$ over Patiala region

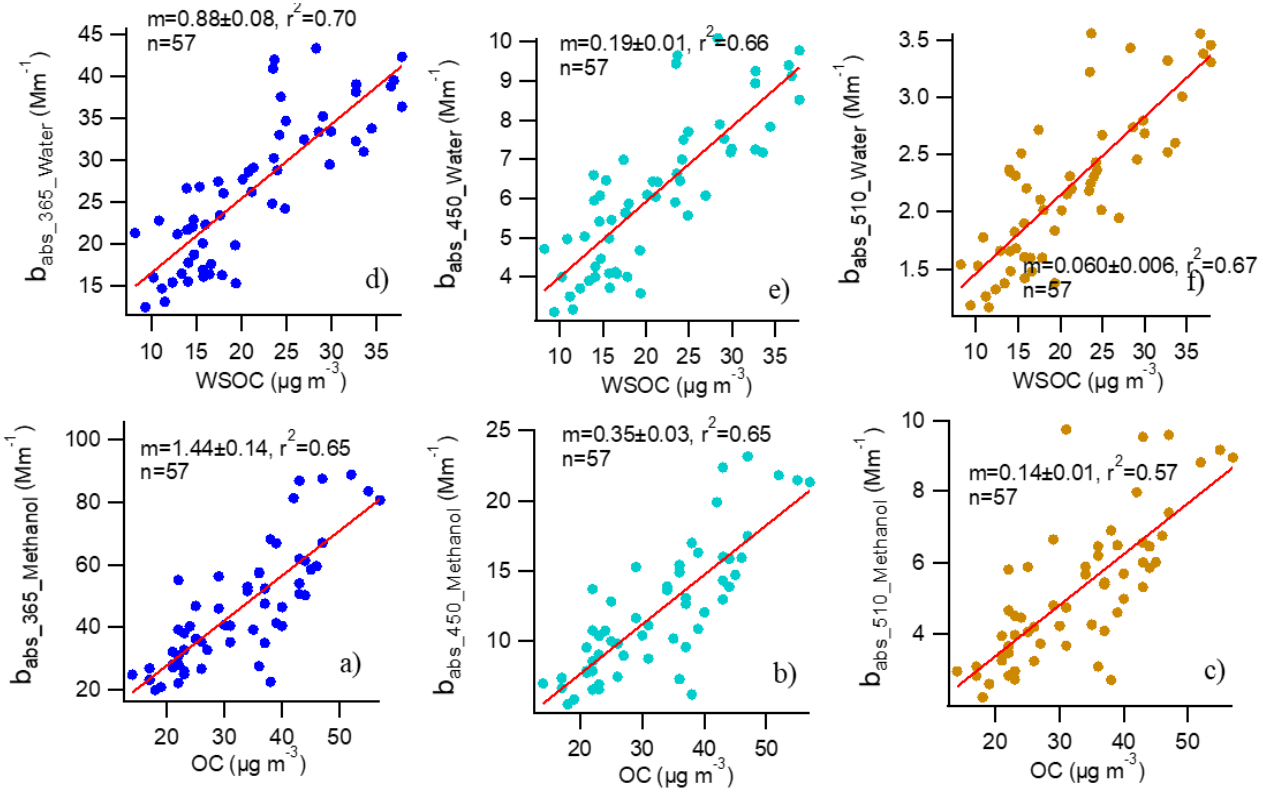

Figure 3.13: Linear regression plots of a) OC vs $b_{abs\_365\_Methanol}$, b) OC vs $b_{abs\_405\_Methanol}$, c) OC vs $b_{abs\_510\_Methanol}$, d) WSOC vs $b_{abs\_365\_Water}$, e) WSOC vs $b_{abs\_405\_Water}$, f) WSOC vs $b_{abs\_510\_Water}$ over Kanpur region

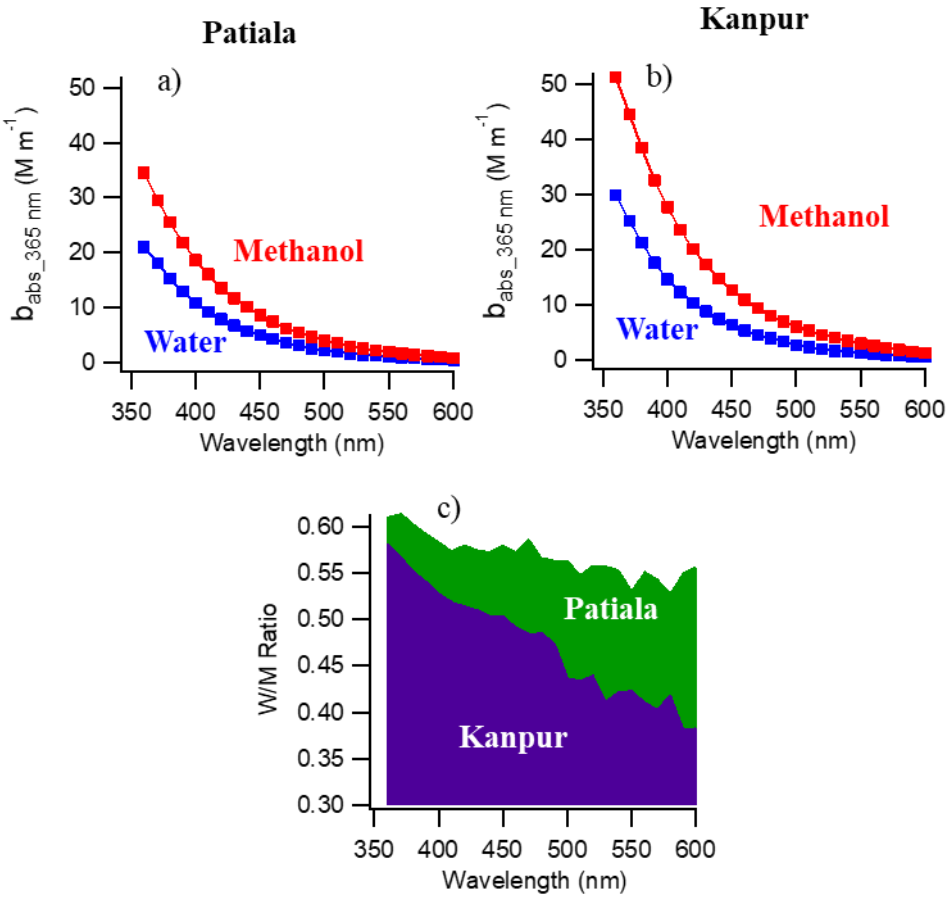

Figure 3.14: Averaged absorption spectra of water and methanol extracted BrC from a) Patiala, b) Kanpur and c) $b_{abs\_365\_Water}/b_{abs\_365\_Methanol}$ ratio (W/M ratio) over Patiala and Kanpur

The fractional contribution of MAE of BrC (Water and Methanol), relative to that of EC is calculated over Patiala and Kanpur regions. The mean fractional relative contributions of MAE of BrC (Water and Methanol) over EC at different wavelengths (370, 410, 450, 490, 530 and 678 nm) are shown in Figure 3.15. From this figure, it is stated that the ratio of MAE of BrC to that of EC in water extracted samples are low compared to methanol extracted BrC over Patiala and Kanpur. However, the ratio values over Kanpur are significantly higher at both UV and Visible regions compared to Patiala. At 365 nm, the ratios were ~ 6 times higher at Kanpur than that at Patiala, suggesting BrC over Kanpur is more absorbing.

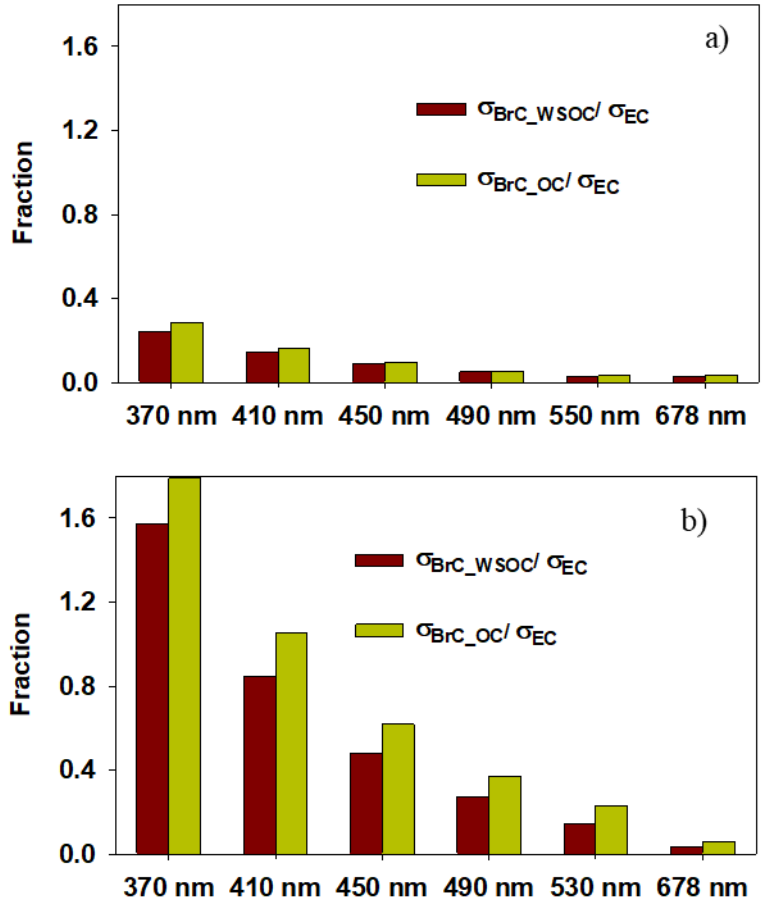

Figure 3.15: Fractional contribution of mass absorption efficiency of BrC (Water and Methanol), relative to that of EC at different wavelengths in $PM_{2.5}$ samples collected from a) Patiala and b) Kanpur

Table 3.3: Chemical and optical parameters over Patiala, Kanpur, Shillong and Port Blair regions in this study

Parameter	Patiala (Dec-Feb)	Kanpur (Dec-Feb)	Shillong (Jan-Apr)	Port Blair (Feb-Apr)
No of Samples	N=49	N=59	N = 35	N = 50
$b_{abs\_365\_Water}$ (M m^{-1})	4-44 (20 ± 9)	12-60 (27 ± 10)	5-31 (14 ± 6)	0.4-4.2 (1.4 ± 0.8)
$b_{abs\_365\_Methanol}$ (M m^{-1})	13-76 (30 ± 16)	20-107 (48 ± 21)	5-70 (27 ± 17)	0.8-11.3 (3.2 ± 1.9)
$\sigma_{abs\_365\_Water}$	0.6-1.7 (1.2 ± 0.2)	0.8-2.6 (1.3 ± 0.3)	0.4-2.3 (0.8 ± 0.4)	0.22-1.22 (0.46 ± 0.14)
$\sigma_{abs\_365\_Methanol}$	0.4-1.4 (1.1 ± 0.2)	0.6-3.4 (1.4 ± 0.4)	0.2-2.5 (1.1 ± 0.5)	0.24-0.91 (0.48 ± 0.13)
AAE_{Water}	5.7-7.2 (6.6 ± 0.3)	6.8-8.1 (7.1 ± 0.3)	5.9-8.3 (6.8 ± 0.5)	10.1-4.0 (7.3 ± 1.3)
$AAE_{Methanol}$	5.6-7.2 (6.4 ± 0.3)	5.9-7.1 (6.5 ± 0.3)	3.6-6.8 (5.6 ± 0.6)	7.0-5.3 (6.0 ± 0.3)
$PM_{2.5}$ (µg m^{-3})	58 -251 (131 ± 50)	79-336 (167 ± 53)	44-144 (88 ± 25)	23-65 (42 ± 11)
WSOC (µg m^{-3})	6-33 (16 ± 8)	8-45 (22 ± 9)	3.5-49.0 (17.4 ± 8.0)	1.6-5.3 (3.0 ± 1.0)
OC (µg m^{-3})	11-63(30 ± 15)	14-63 (33 ± 11)	5-73 (27 ± 14)	3.4-12.4 (6.3 ± 1.9)
EC (µg m^{-3})	1.0-5.2 (2.6 ± 1.3)	3.0-11.9 (7.3 ± 2.6)	0.6 - 10.5 (3.1 ± 1.6)	0.8-4.8 (0.9 ± 2.1)
K^+ (µg m^{-3})	0.9-3.9 (2.1 ± 0.9)	0.9-3.4 (1.8 ± 0.5)	0.2-2.4 (1.1 ± 0.5)	0.2-0.8 (0.5 ± 0.15)
OC/EC	5-25 (12 ± 4)	2.1-8.7 (4.7 ± 1.3)	4.2- 22.0 (9.4 ± 4.4)	1.8-5.8 (3.3 ± 0.9)
WSOC/OC	0.33-0.67 (0.53 ± 0.07)	0.28-0.94 (0.66 ± 0.15)	0.50 - 0.90 (0.66 ± 0.12)	0.34-0.70 (0.47 ± 0.09)
K^+/EC	0.36-1.95 (0.30 ± 0.87)	0.10-0.58 (0.27 ± 0.10)	0.11 - 1.02 (0.43 ± 0.24)	0.14-0.48 (0.26 ± 0.09)

3.2.3 BrC spectral characteristics:

AAE for water-soluble (AAE_{Water}) BrC from the filter samples ranged from 5.7-7.2 (6.6 ± 0.3) and 6.2-8.1 (7.1 ± 0.3) over Patiala and Kanpur region, respectively. Similarly, the AAE methanol-extracted ($AAE_{Methanol}$) BrC from filters ranged from 5.6-7.2 (6.4 ± 0.3) and 5.9-7.1 (6.5 ± 0.3), respectively. The AAE_{Water} and $AAE_{Methanol}$ showed daily variation over both sites (Figure 3.16), similar to results from the Beijing and Atlanta (Liu et al., 2013; Cheng et al., 2016). However, the monthly average of AAE_{Water} and $AAE_{Methanol}$ doesn't show any significant variability. The $AAE_{Methanol}$ values over Kanpur site are slightly lower than AAE_{Water}. This suggests that majority of water-soluble BrC chromophores absorb more light at UV region. Whereas methanol extracted BrC chromophores absorb light at both regions, so the dependency on wavelength is low. The average $AAE_{Methanol}$ values are lower compared to AAE_{Water}.

The 7-day isentropic AMBTs were computed at an arrival height of 500 m using HYSPLIT, and GDAS reanalysis dataset. Figs. 3.17 & 3.18 depict the AMBT cluster at 500 m over Patiala and Kanpur during December-2015 to February-2016. These air–masses transport aerosols from the north-west and increase the atmospheric particulate load over Patiala. Both Patiala and Kanpur shows regional transport indicating a significant contribution from sources within northern India.

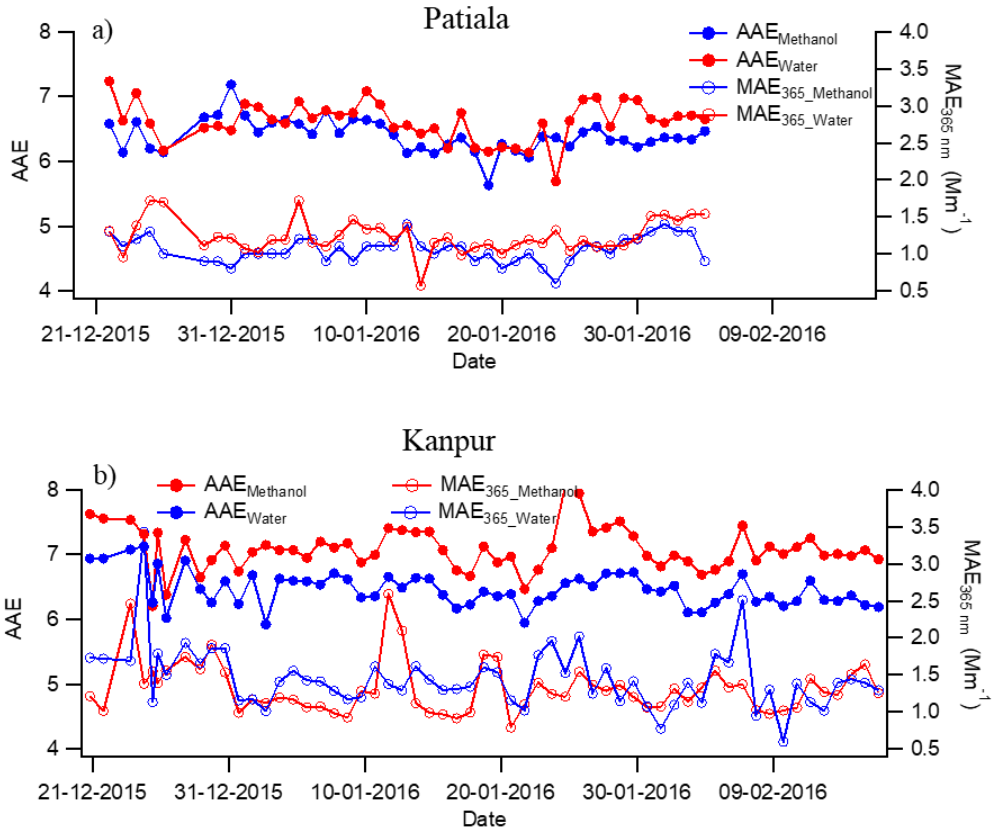

Figure 3.16: Daily variations of AAE and $MAE_{365\ nm}$ for water and methanol extracts over a) Patiala and b) Kanpur.

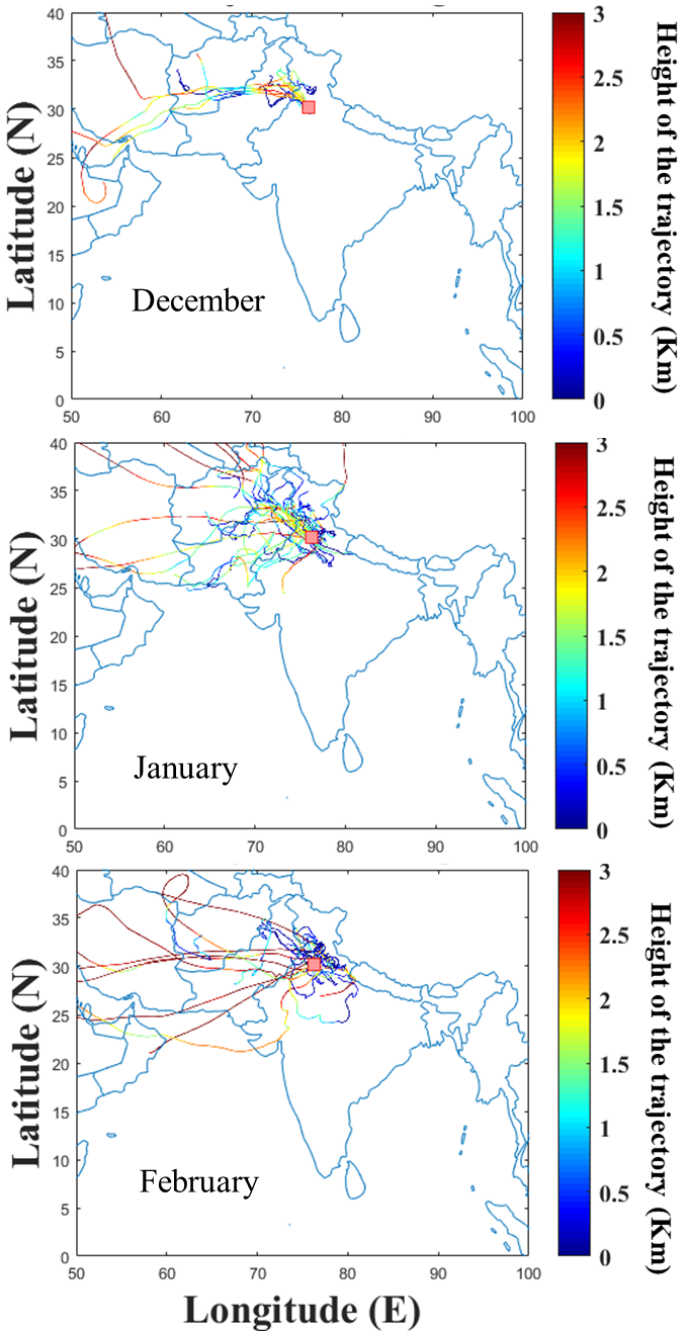

Figure 3.17: Air-mass back trajectories during December, January and February over Patiala

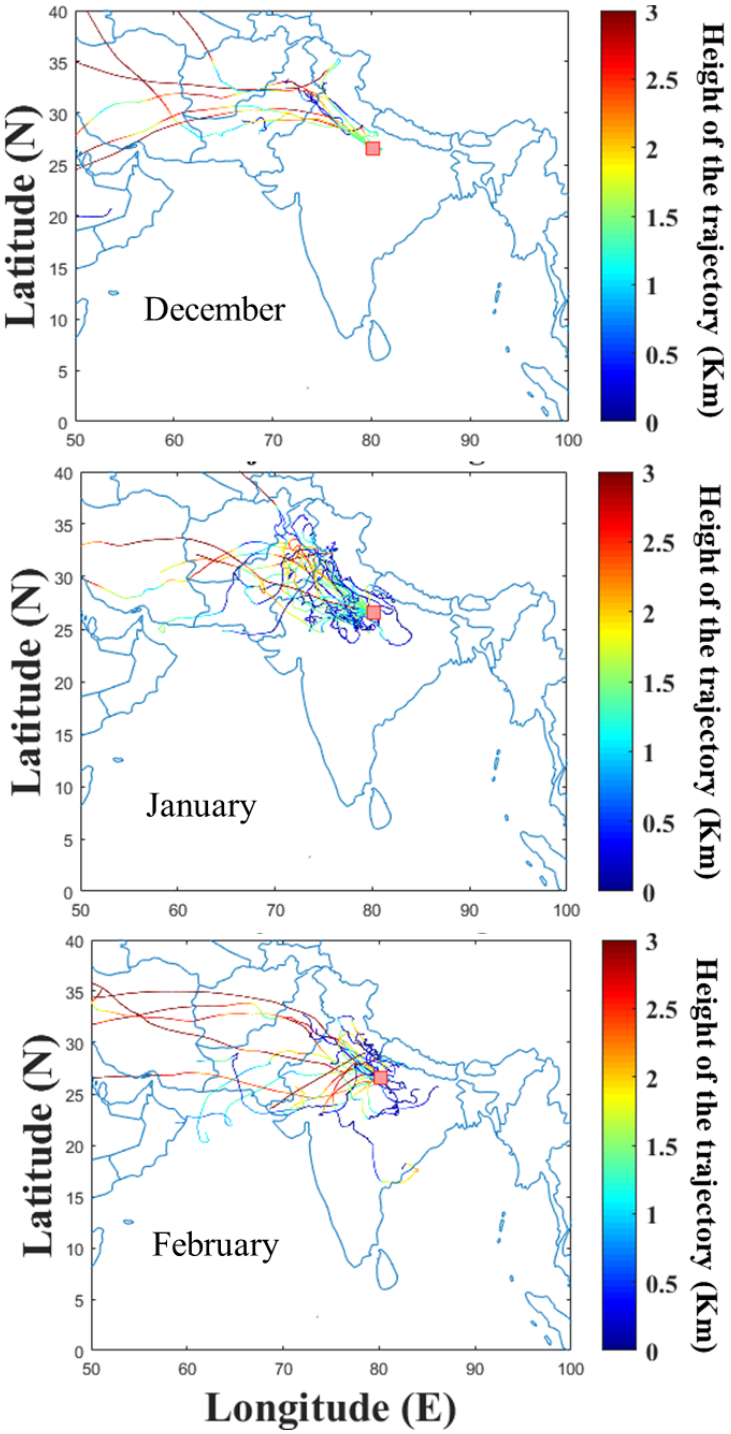

Figure 3.18: Air-mass back trajectories during December, January and February over Kanpur

3.3 Temporal variability and characteristics of light-absorbing organic aerosol from NE-Himalaya: Shillong region

3.3.1 Temporal variability of chemical species:

A statistical description of the range, mean and standard deviation for the optical properties of BrC ($b_{abs\_365\ nm}$, σ_{abs_365}, AAE) along with the concentrations of $PM_{2.5}$ and its chemical constituents are given in Table 3.3. Large temporal variability of PM and chemical species was observed during the study period (Figure 3.19). This variability is attributable to different factors such as the dominance of specific sources (BB, FFB), atmospheric processes such as long-range transport, transformation, secondary organic aerosol (SOA) formation, boundary layer dynamics and meteorological conditions over this region. Filter-based $PM_{2.5}$ mass concentration ranged from 44 - 144 (avg± sd: 88 ± 25) during the study period with the highest concentrations in January (100 ± 20) than the rest of the period. Low PM values observed in April were due to frequent rainfall. The b_{abs_365} of BrC for water and methanol extracts of $PM_{2.5}$ showed pronounced temporal variability. It varied from 5 to 31 M m^{-1} (14 ± 6 M m^{-1}) and 5 – 70 M m^{-1} (27 ± 17 M m^{-1}) for water-soluble and methanol-soluble BrC, respectively (Table 3.3). Furthermore, the temporal variability of $b_{abs\_365\_Water}$ and $b_{abs\_365\_Methanol}$ showed a similar trend as shown by WSOC, OC, water-soluble potassium (K^+, used as a proxy to assess the contribution from BB emissions) and K^+/EC, suggesting their common source and/or transport over the study region. Good correlations were observed between K^+ and WSOC ($r^2 = 0.50$), K^+ and OC ($r^2 = 0.66$), suggesting that their source could be associated with BB emissions. Further, the observed OC/EC ranged from 4.2 to 22.0 (9.4 ± 4.4), and K+/EC varied from 0.11 to 1.02 (0.43 ± 0.24), suggesting that their major contribution from BB. These ratios were higher compared to samples collected over Patiala during winter (Rastogi et al., 2015).

The $b_{abs\_365\_Water}$ of light absorbing water-soluble organics over Shillong (avg ± sd) is similar to that reported over Kharagpur (11.4 ± 4.8 Mm^{-1}; Srinivas and Sarin, 2014), BoB IGP outflow and BoB sea outflow (9.1 ± 2.5 and 6.9 ± 1.9 Mm^{-1}; Srinivas and Sarin, 2013) and lower compared to Patiala (day = 40 ± 18

Mm^{-1}, Night = 52 ± 27 Mm^{-1}; Srinivas et al., 2016), and Kanpur (24 ± 19 Mm^{-1}; Satish et al., 2017). However, $b_{abs\_365\_Water}$ (14 ± 6) and $b_{abs\_365\_Methanol}$ (27 ± 17) values in this study are comparable to BrC in Beijing winter $b_{abs\_365\_Water}$ (10 ± 7) and $b_{abs\_365\_Methanol}$ (26 ± 19) (Cheng et al., 2016). Methanol extracted organics also contains both primary and secondary organics. In the present study, the average WSOC/OC ratio is about 0.66, i.e., ~34% of OC is water-insoluble. The high WSOC/OC ratio suggests that the majority of the organic are water soluble (SOA) over the study region. The ratio of $b_{abs\_365\_Methanol}/b_{abs\_365\_Water}$ varied from 0.8-4.4 (1.9 ± 0.7), suggesting the presence of variable chromophores in the study region. The $b_{abs\_365\_Methanol}$ is ~2 times higher than $b_{abs\_365\_Water}$, indicating that an about half of the BrC was water-insoluble.

The slope of the linear regression plot between $b_{abs\_365\_Water}$ and WSOC, or $b_{abs\_365\_Methanol}$ and OC provides an estimate of MAE (σ_{abs_365}, in $m^2\,g^{-1}$) of water-soluble and methanol-soluble light absorbing organics over the sampling site. The WSOC vs. $b_{abs\_365\_Water}$ and OC and $b_{abs\_365\_Methanol}$ show a strong correlation, suggesting that they are coming from the same source. Temporal variation of $\sigma_{abs\_365\_Water}$ and $\sigma_{abs\_365\_Methanol}$ is shown in Figure 3.23. The MAE values for water and methanol extracts varied from 0.4 - 2.3 (0.8 ± 0.4) and 0.2 - 2.5 (1.1 ± 0.5), respectively. Throughout the study period, the $\sigma_{abs\_365\_Methanol}$ values were higher than $\sigma_{abs\_365\_Water}$, except in a few samples in the beginning and end of the sampling period. During this period, a high WSOC/OC (>0.80) ratio was observed. The $\sigma_{abs\_365\_Water}$ estimated over the BoB (Srinivas and Sarin, 2013) is relatively lower (0.45 ± 0.14 $m^2\,g^{-1}$) compared to study region (0.80 ± 0.40 $m^2\,g^{-1}$) and they are comparable to Kharagpur (Srinivas and Sarin, 2014). Both Shilong and Kharagpur receive a significant fraction of ambient aerosol through long-range transport from the IGP, which explains similar MAEs over both the sites. The average $\sigma_{abs\_365\_Methanol}$ was 75% higher than $\sigma_{abs\_365\_Water}$ over the study region.

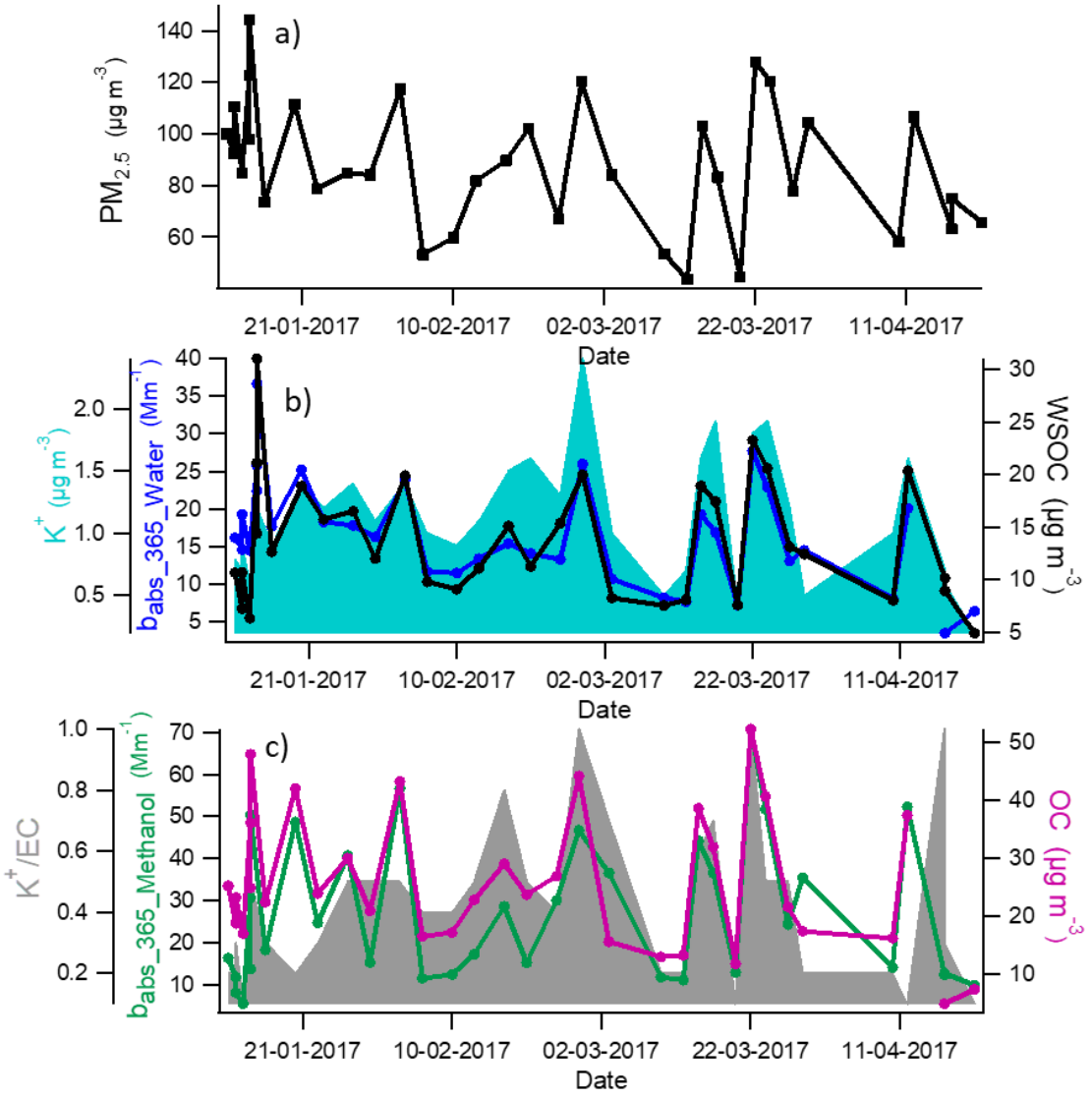

Figure 3.19: Temporal variability of different chemical species (a): $PM_{2.5}$; (b): WSOC, K^+ and $b_{abs\_365\_Water}$; and (c): OC, K+ /EC and $b_{abs\_365\_Methanol}$

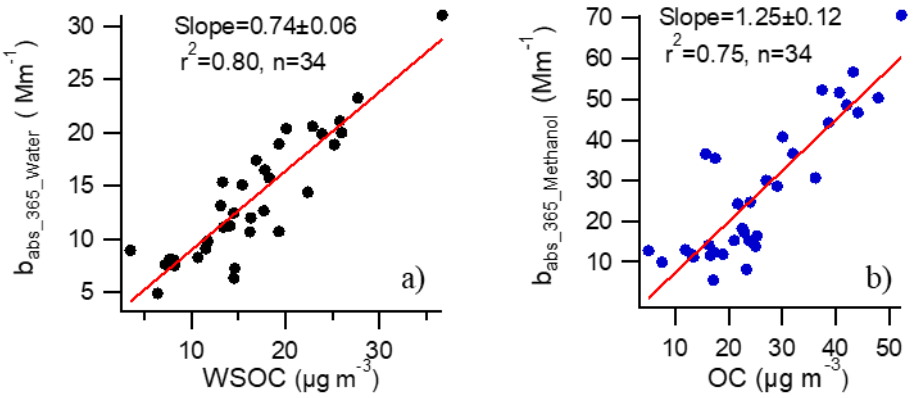

Figure 3.20: Regression plots of a) WSOC vs. $b_{abs\_365\_Water}$ and b) OC vs. $b_{abs\_365\_Methanol}$. The slope is given with standard error)

Further, we have estimated the % water-insoluble BrC fraction. The $b_{abs\_Methanol}$ represent total BrC, b_{abs_Water} denotes water-soluble BrC, and their difference reflects water-insoluble BrC. This approach helps in assessing the fraction of the water-soluble BrC in the total BrC. We have calculated % water-insoluble fraction over there different wavelength ranges (R1: 360-400 nm, R2: 410-500 nm, and R3: 510-600 nm). The observed % of the water-insoluble fractions were 52%, 60% and 64% over Shillong at R1, R2, and R2 respectively (Figure 3.21).

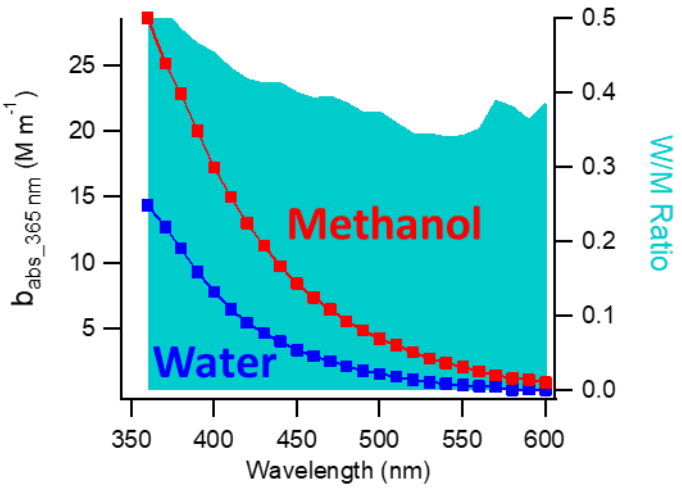

Figure 3.21: Averaged $b_{abs\_365\_Water}$ *and* $b_{abs\_365\_Methanol}$ *spectrum; and* $b_{abs\_365\_Wate}$ / $b_{abs\_365\_Methanol}$ *ratio (W/M ratio)*

The fractional contribution of MAE of BrC (Water and Methanol), relative to that of EC is calculated over NE-Himalayan region. This approach was obtained from previously reported studies (Chakrabarty et al., 2014; Srinivas and Sarin, 2014, Srinivas et al., 2016). The MAE values for EC and BrC (Water and Methanol) were calculated. The mean fractional relative contribution of MAE of BrC (Water and Methanol) over EC at different wavelengths (370, 410, 450, 490, 530 and 678 nm) are shown in Fig. 3.22. It is found that the ratio of MAE of BrC to that of EC in water extracted samples were low compared to methanol extracted BrC over the Shillong region. The overall fractional contribution of both water and methanol extracted BrC is relatively small compared to other sites.

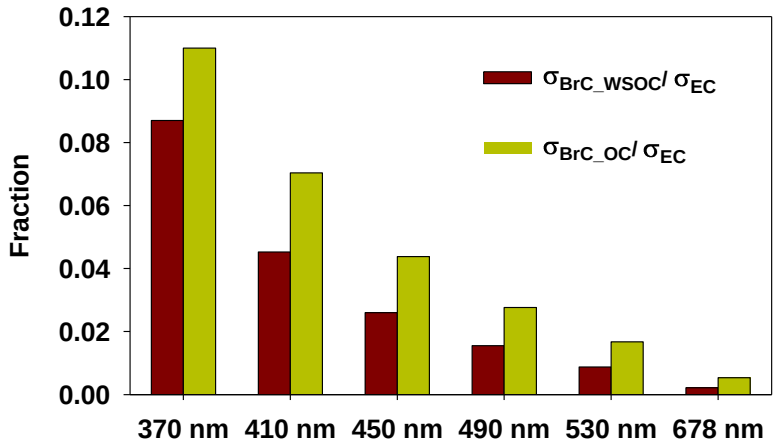

Figure 3.22: Fractional contribution of mass absorption efficiency of BrC (Water and Methanol), relative to that of EC, in $PM_{2.5}$ samples from NE-Himalaya, Shillong

3.3.2 Absorption Ångstrom Exponent (AAE):

The AAE for BrC (AAE_{BrC}) is determined from the slope of a linear regression fit of ln (b_{abs}) vs. ln (λ) for λ ranging from 360 and 480 nm (Liu et al., 2014; Cheng et al., 2016; Yan et al., 2018). Figure 3.23 shows the temporal trends of AAE of water and methanol extracted BrC. The water and methanol extracted AAE showed daily variation ranging from 5.9-8.3 (6.8 ± 0.5) and 3.6-6.8 (5.6 ± 0.6), respectively. Throughout the study period, AAE_{Water} values were higher than $AAE_{Methanol}$. The high wavelength dependency was observed at shorter wavelengths for AAE_{Water}. This suggests that the majority of water-soluble BrC chromophores absorb more light at UV region. Whereas methanol extracted BrC chromophores absorb light in both regions, so the wavelength dependency is low. The average $AAE_{Methanol}$ values were lower compared to $AAE_{Water.}$ It means that water extractable organic (mainly associated with secondary) is highly absorbing at shorter wavelengths than longer wavelengths. However, $AAE_{Methanol}$ which extracts the majority of primary and secondary organic shows less lambda

dependency. The observed AAE values are similar to previously reported studies (Table 3.3).

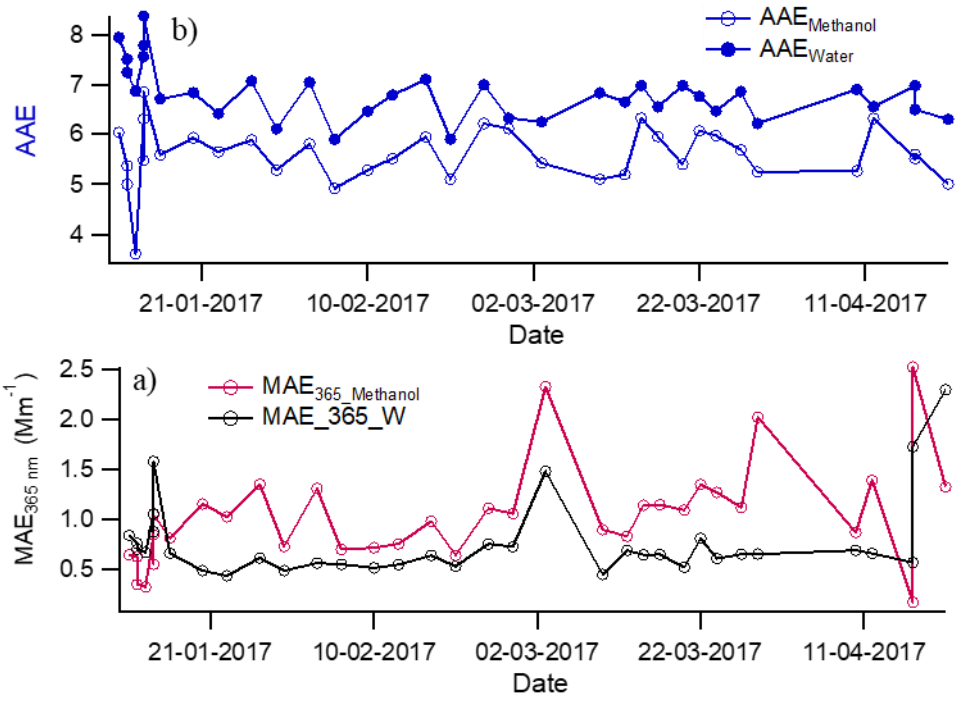

Figure 3.23: Temporal variability of (a) MAE_{365_Water}, $MAE_{365\_Methanol}$, and (b) AAE_{Water}, and $AAE_{Methanol}$

For the ease of understanding, seven-day AMBTs were plotted on a monthly basis, as shown in Figure 3.23. In January, February, and March, most of the air masses were coming from the IGP region. These air masses transport aerosol from the IGP is high during this period compared to the rest of the year (Rajput et al., 2013). However, in April the winds were from mostly from the east coast of the BoB and N-E region.

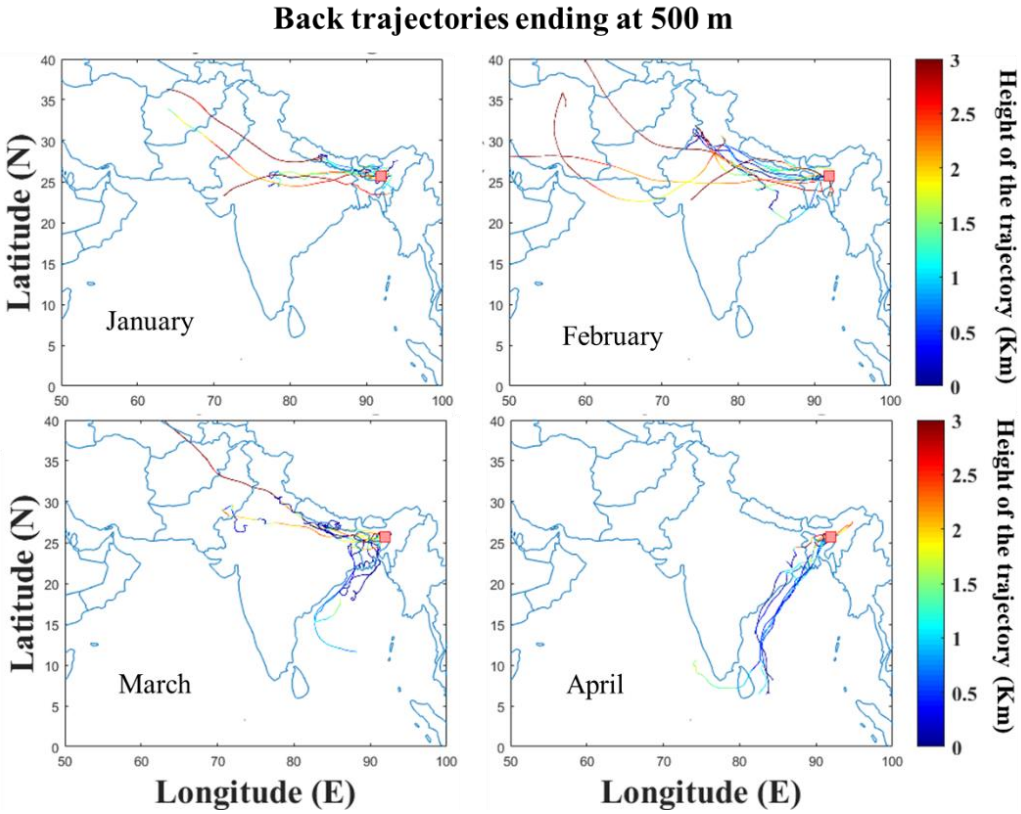

Figure 3.24 Air-mass back trajectories during January, February, March, and April over Shillong region

3.4Optical properties of light absorbing organic aerosol over an island station, Port Blair, in the Bay of Bengal

3.4.1 Temporal Variability of Chemical Species:

Figure 3.25 depicts the temporal variability in the mass concentrations of $PM_{2.5}$ and its chemical species over Port Blair during the study period. This variability is attributable to different factors such as major sources of species, their atmospheric processes such as long-range transport, transformation, secondary organic aerosol (SOA) formation, boundary layer dynamics and meteorological conditions over the study region. The $PM_{2.5}$ mass concentration ranged from 23 to 65 μg m^{-3} (average ± 1$\boldsymbol{\sigma}$ standard deviation: 42 ± 11) with the average values of 47 ± 5, 43 ± 12, and 38 ± 9 μg m^{-3} during February, March, and April, respectively (Figure 3.25 a). February and March months showed relatively high concentrations compared to April month. This variability was similar for all the other chemical species (Figure 3.25 b, c, d). Higher aerosol loading was observed in the second week of March due to the transport of aerosol mainly from southern states of India. Minimum concentrations were recorded on March 17th. The absorption signal at 365 nm measured on the aqueous and methanol extract of $PM_{2.5}$ showed a strong day to day temporal variability. Furthermore, this temporal variability of water-soluble potassium (K^+, a proxy for assessing the qualitative contribution from BB emissions) showed a similar trend as shown by $b_{abs\_365\_Water}$ and $b_{abs\_365\_Methanol}$. The $b_{abs\_365\ nm}$ for water and methanol extracted samples varied from 0.4 to 4.2 M m^{-1} (1.4 ± 0.8 M m^{-1}) and 0.8–11.3 M m^{-1} (3.2± 1.9 M m^{-1}), respectively. Further, the monthly variation of $b_{abs\_365\_Water}$ and $b_{abs\_365\_Methanol}$ during February (1.8 ± 0.6 M m^{-1}; 3.5 ± 0.9 M m^{-1}), March (1.6 ± 1.0 M m^{-1}; 3.7 ± 2.4 M m^{-1}), April (0.9 ± 0.3 M m^{-1}; 2.1 ± 0.8 M m^{-1}), respectively were very low compare to other sites. The $b_{abs\_365\_Water}$ values were similar in February and March, and reduced in April. The $b_{abs\_365\_Methanol}$ values in March were higher compared to February and April months. Water-insoluble BrC fraction was also high in March.

The OC/EC ratio varied from 1.8 to 5.8 (3.3 ± 0.9) during the study period with lower OC/EC ratio during February (2.8 ± 1.0) in comparison to that during March (3.4 ± 1.1) and April (3.5 ± 0.4). Many studies have also reported that the ratio of BC at 370 nm to BC at 880 nm can be used as a tracer to identify whether emissions from BB or FFB. Several studies had also reported that the ratio of BC at 370 nm to BC at 880 nm could be used as a tracer to identify whether emissions from BB or FFB dominate aerosol over a given region. The ratio of BC (370/880) < 1.0 represents the dominance of emissions from FFB, whereas BC (370/880) > 1.0 depicts the dominance of BB emissions (Herich et al., 2011; Raatingan et al., 2013; Singh et al., 2014). In this study, the BC (370/880) ratios were 0.88 ± 0.04, 0.94 ± 0.06, and 0.94 ± 0.06 during February, March, and April, respectively. The BC (370/880) ratios were similar throughout the sampling period. However, high ratio values observed during the second week of March and the third week of April which were >1. The detailed description of the range, mean and standard deviation for the optical properties of BrC along with chemical constituents is given in Table 3.3.

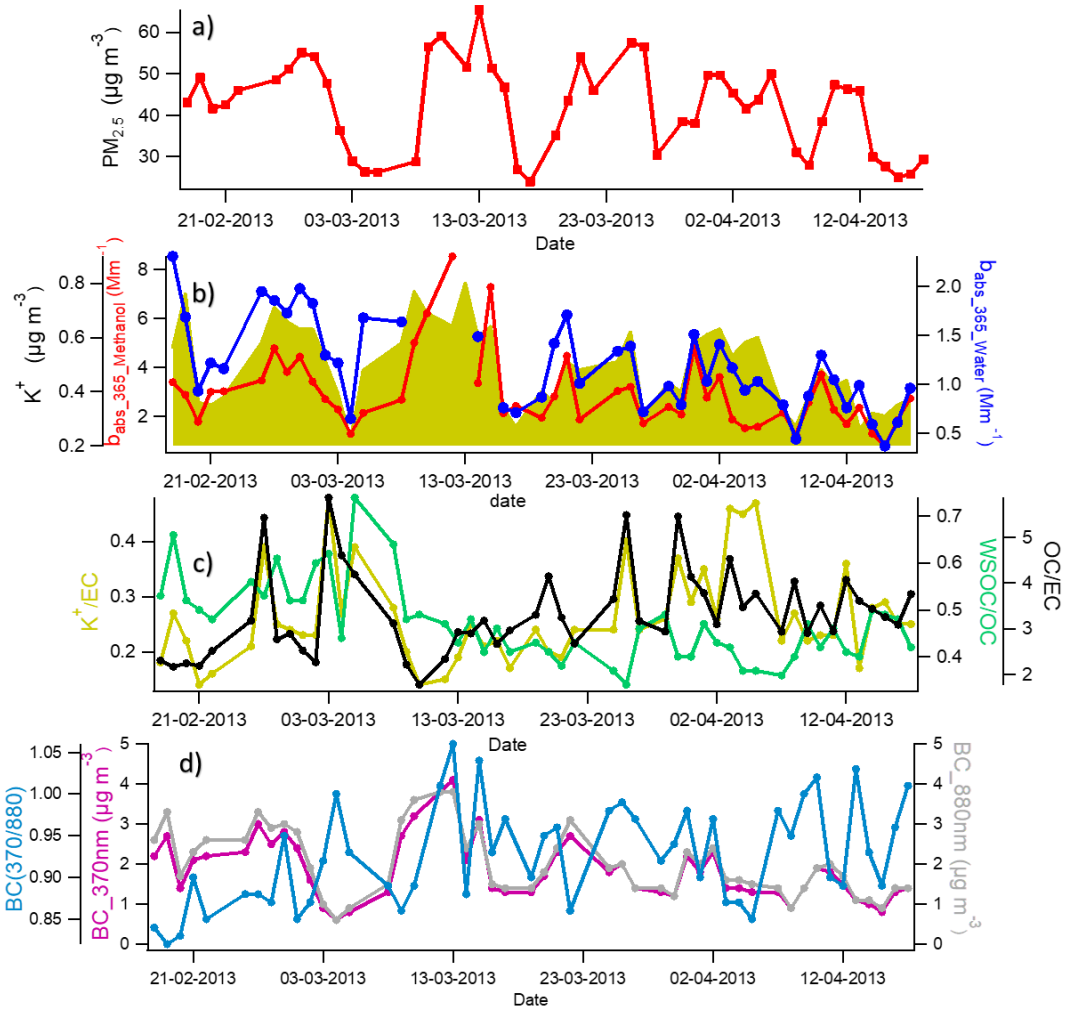

Figure 3.25: Temporal variability of different chemical species including (a) $PM_{2.5}$; (b) K^+, $b_{abs\_365\_Water}$ and $b_{abs\_365\_Methanol}$; (c) K^+/EC, WSOC/OC and OC/EC; and (d) BC_370 nm, BC_880 nm µg m^{-3}, BC (370/880)

3.4.2 BrC Absorption coefficient:

The b_{abs} of the water and methanol extracts were primarily investigated at a wavelength of 365 nm. A linear regression analysis for WSOC and $b_{abs\_365\_water}$, and OC and $b_{abs\_365\_Methanol}$ was performed for all samples. The observed slopes for water and methanol extracts were 0.64 ± 0.06 and 0.74 ± 0.06, respectively. The difference in these slopes suggests that water-soluble chromophores were significant.

The observed slopes for WSOC vs. $b_{abs\_365\_water}$ is similar to previously reported studies by Hecobian et al. (2010) at South Dekalb (0.60), a rural site in the southeast USA, by Zhang et al (2013) at Pasadena (0.73) and Riverside (0.74), California, Los Angeles (LA) Basin (~1.6; Zhang et al., 2013), BoB (IGP-outflow) (0.4; Srinivas et al., 2013), BoB (SEA-outflow) (0.5; Srinivas et al., 2013), Kharagpur (0.8; Srinivas et al., 2014) However, the observed slope was lower than that observed over Kanpur (1.22; Satish et al., 2017) and Patiala (1.3). Similarly, the observed slope for OC and $b_{abs\_365\_Methanol}$ was small compared to previous studies over different regions such as Jefferson Street and Yorkville (1.8; Liu et al., 2013), (1.5; Cheng et al., 2013). Also, a good correlation was also observed between water-soluble K^+ and $b_{abs\_365\_water}$ ($r^2 = 0.62$), and relatively poor correlation was observed for water-soluble K^+ and $b_{abs\_365\_Methanol}$ ($r^2 = 0.42$), further indicating that majority of the BrC could be water soluble.

To investigate BrC absorption at different wavelength, a regression analysis between WSOC vs. b_{abs_Water} (at 450 and 530 nm), and OC vs $b_{abs\_Methanol}$ (at 450 and 530 nm) was performed (Figure 3.26). The observed slopes suggest that methanol extracted BrC is slightly higher compared to water extracted BrC.

The $b_{abs\_Methanol}$ represent total BrC, b_{abs_Water} denotes water-soluble BrC, and their difference reflects water-insoluble BrC. This approach helps in assessing the fraction of the water-soluble BrC in the total BrC. Further, we have calculated % water-insoluble fraction over there different wavelength ranges (R1: 360-400 nm, R2: 410-500 nm, and R3: 510-600 nm). The observed % of the water-insoluble fraction was 57%, 62% and 65% over Port Blair at R1, R2, and R2 respectively. Further, Chen and Bond et al. (2010) suggested that these strongly light-absorbing

water-insoluble components are likely large molecular weight PAHs, such as quinones from BB and fossil fuel combustion (Sun et al., 2007). Zhang et al. (2013) showed estimated that the water-insoluble BrC, calculated as the difference between methanol- and water-extracted BrC, exhibited a tighter correlation with ambient EC concentrations (r^2 = 0.81,) than water-soluble BrC (r^2 = 0.40), suggesting that the water-insoluble BrC components and EC have similar sources (e.g., incomplete combustion from vehicle emissions and wood burning). However, in this study ambient EC concentrations showed poor correlation with water-insoluble BrC (r^2 = 0.29). A good correlation was observed for EC mass concentration with $b_{abs\_365\_water}$ (r^2 = 0.75) and $b_{abs\_365\_Methanol}$ (r^2 = 0.70), suggesting that both water and methanol soluble chromospheres were coming from the same source.

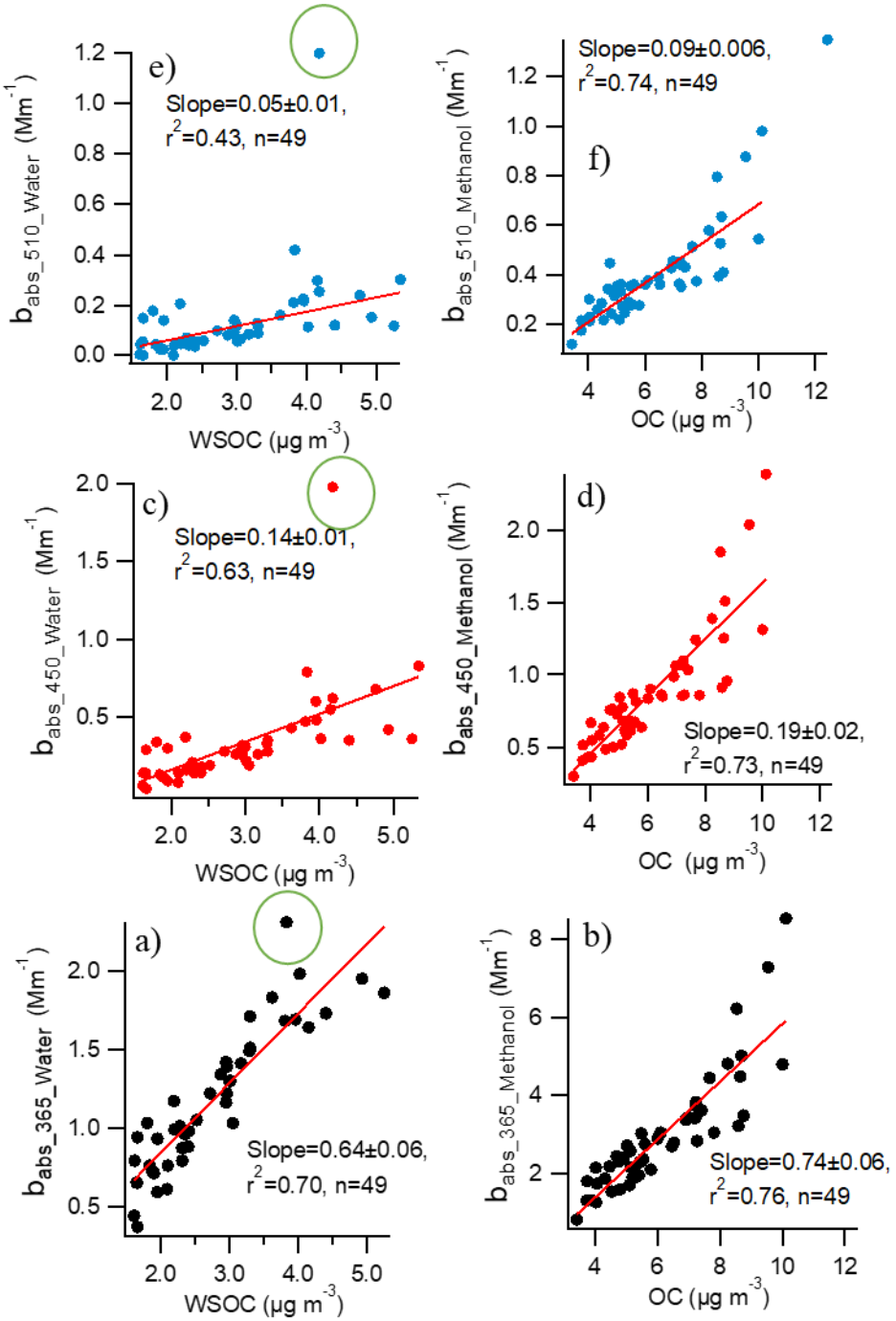

Figure 3.26: Linear regression plots of a) WSOC vs $b_{abs\_365\_Water}$, b) OC vs $b_{abs\_365\_Methanol}$, c) WSOC vs $b_{abs\_450\_Water}$, d) OC vs $b_{abs\_450\_Methanol}$ e) WSOC vs $b_{abs\_510\_Water}$ and e) OC vs $b_{abs\_510\_Methanol}$ over Port Blair region

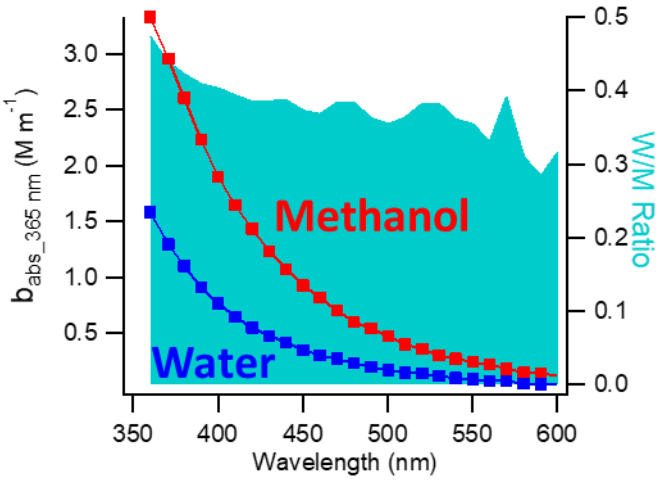

Figure 3.27: Averaged $b_{abs\_365\_Water}$ and $b_{abs\_365\_Methanol}$ spectrum and $b_{abs\_365\_Water}$ / $b_{abs\_365\_Methanol}$ ratio (W/M ratio)

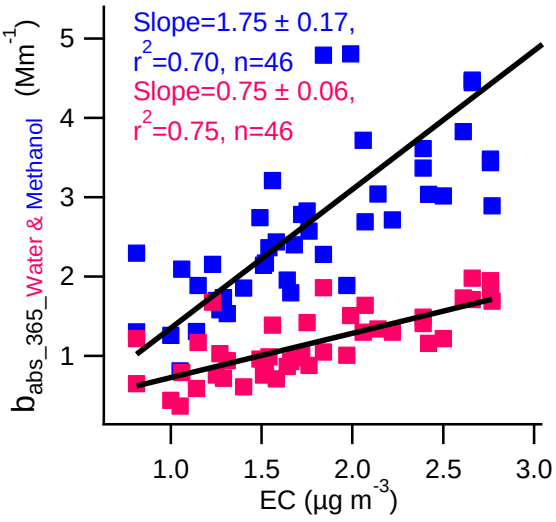

Figure 3.28: Scatter plot of EC vs $b_{abs\_365\_Water}$ and EC VS $b_{abs\_365\_Methanol}$

Further, the fractional contribution of MAE of BrC (Water and Methanol), relative to that of EC was calculated for the samples collected from Port Blair region. The mean fractional relative contribution of MAE of BrC (Water and Methanol) over EC at different wavelengths (370, 410, 450, 490, 530 and 678 nm) and their monthly variance are shown in Fig. 3.28. From this figure, it is noteworthy that the ratio of MAE of BrC to that of EC in water extracted samples are closer to the methanol extracted BrC for all three months. It is observed that both water and methanol extracted BrC showed a higher fraction in March. It means BrC chromophores in March were more absorbing at all the wavelengths. These results are similar to the previously reported study by Srinivas et al. (2014) over Kharagpur during winter period. Our results are also consistent with that documented for water-soluble BrC emissions from biomass and biofuel burning (Chakrabarty et al., 2014; Srinivas et al., 2016) emissions of BrC is relative that of EC. The average fractional values of BrC_370 (Water) relative to that of EC was 21%, 25% and 18% during the February, March, and April months respectively. Similarly, the average fractional values of BrC_370 (Methanol) relative to that of EC was 22%, 27%, and 15% during the February, March, and April months respectively. It is observed that the fractional absorption decreases at higher wavelengths for all the three months. A little higher absorption by BrC (Methanol) suggests that the study region consists of BrC chromophores which are water-insoluble, which can absorb light at both shorter and longer wavelengths.

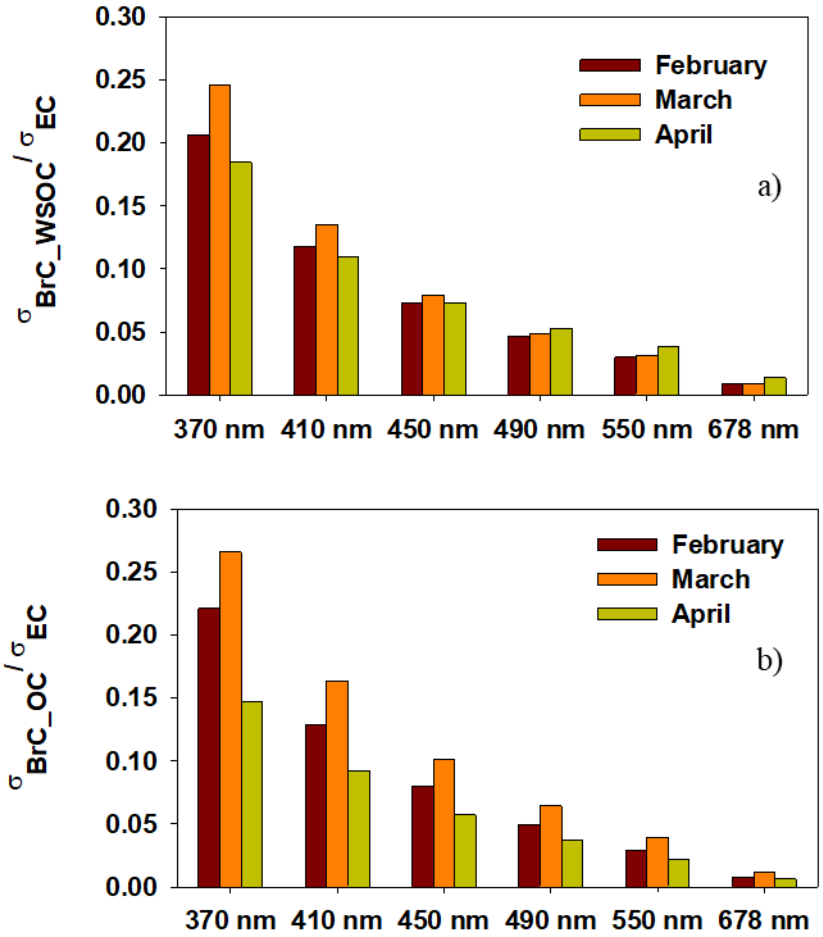

Figure 3.29: Fractional contribution of mass absorption efficiency of BrC ((a)Water and (b) Methanol) relative to that of EC in $PM_{2.5\ samples}$ from Port Blair region.

3.4.3 Absorption Ångstrom exponent (AAE) and Mass Absorption Efficiency at 365 nm (MAE):

The AAE for BrC (AAE_{BrC}) is determined from the slope of a linear regression fit of ln (b_{abs}) vs. ln (λ) for λ ranging from 360 and 480 nm (Liu et al., 2014; Cheng et al., 2016; Yan et al., 2018). The water and methanol extracted AAE showed daily variation ranging from 4.0-10.1 (7.3 ± 1.3) and 5.3-7.0 (6.0 ± 0.3). Throughout the period AAE_{Water} values were higher than $AAE_{methanol}$. The high

wavelength dependency observed at shorter wavelengths for AAE_{Water}. The lowest AAE_{Water} values were found on 9th March (3.95) and 3rd to 5th April (5.12 ± 0.09). During this period, less lambda dependency is attributed to fossil fuel emission sources. The observed AAE values are similar to previously reported studies. Reported AAE value over Los Angeles Basin AAE_{Water} is 7.58 and $AAE_{Methanol}$ is 4.82, over Beijing during winter period AAE_{Water} is 7.28 and $AAE_{Methanol}$ is 7.10, over Atlanta Jefferson Street AAE_{Water} is 6.79 and $AAE_{Methanol}$ is 4.98 etc. (Zhang et al., 2013).

The MAE or σ_{abs_365} values of both water and methanol extracts showed similar temporal variability. The $\sigma_{abs\_365\_Water}$ and $\sigma_{abs\_365\_Water}$ ranged from 0.22-1.22 (0.46 ± 0.14) and 0.24-0.91 (0.48 ± 0.13) during the study period. The monthly average $\sigma_{abs\_365\_Water}$ was 0.47 ± 0.11, 0.50 ± 0.16 and 0.40 ± 0.10, and $\sigma_{abs\_365\_Methanol}$ was 0.51 ± 0.07 0.48 ± 0.14 and 0.38 ± 0.07 during February, March and April, respectively. The highest $\sigma_{abs\_365\_Water}$ value was obtained on 9th March (1.12), and during this day high WSON mass concentration (2.01 µg m^{-3}) was also observed, possibly due to the presence of nitro-aromatics. Further, OC was comprised of 34−70% of WSOC for the filter samples. However, there are no significant differences in the $\sigma_{abs\_365\_Water}$ and $\sigma_{abs\_365\_Water}$ values during the study period. This implies that the study region consists of highly water soluble BrC chromophores.

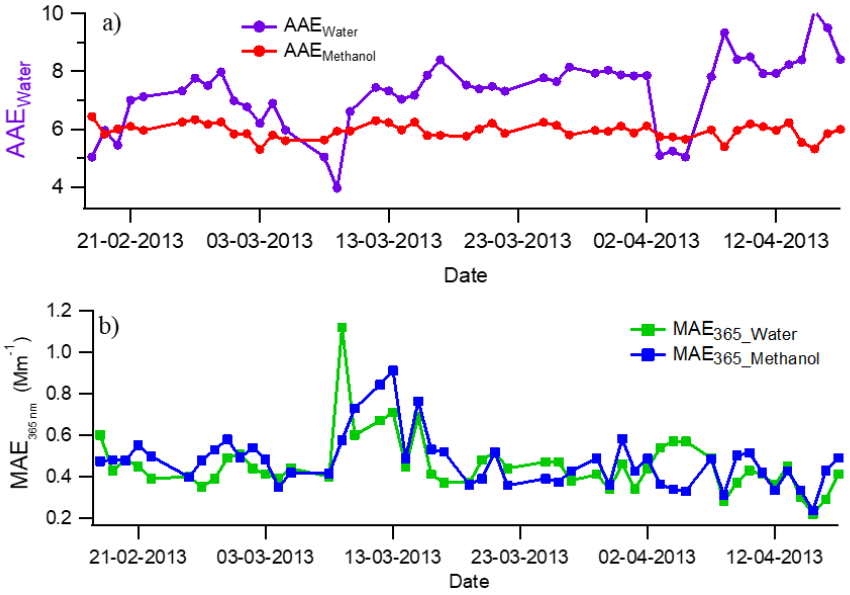

Figure 3.30: Daily variations of (a) AAE and (b) MAE or σ_{abs_365} for water and methanol extracts.

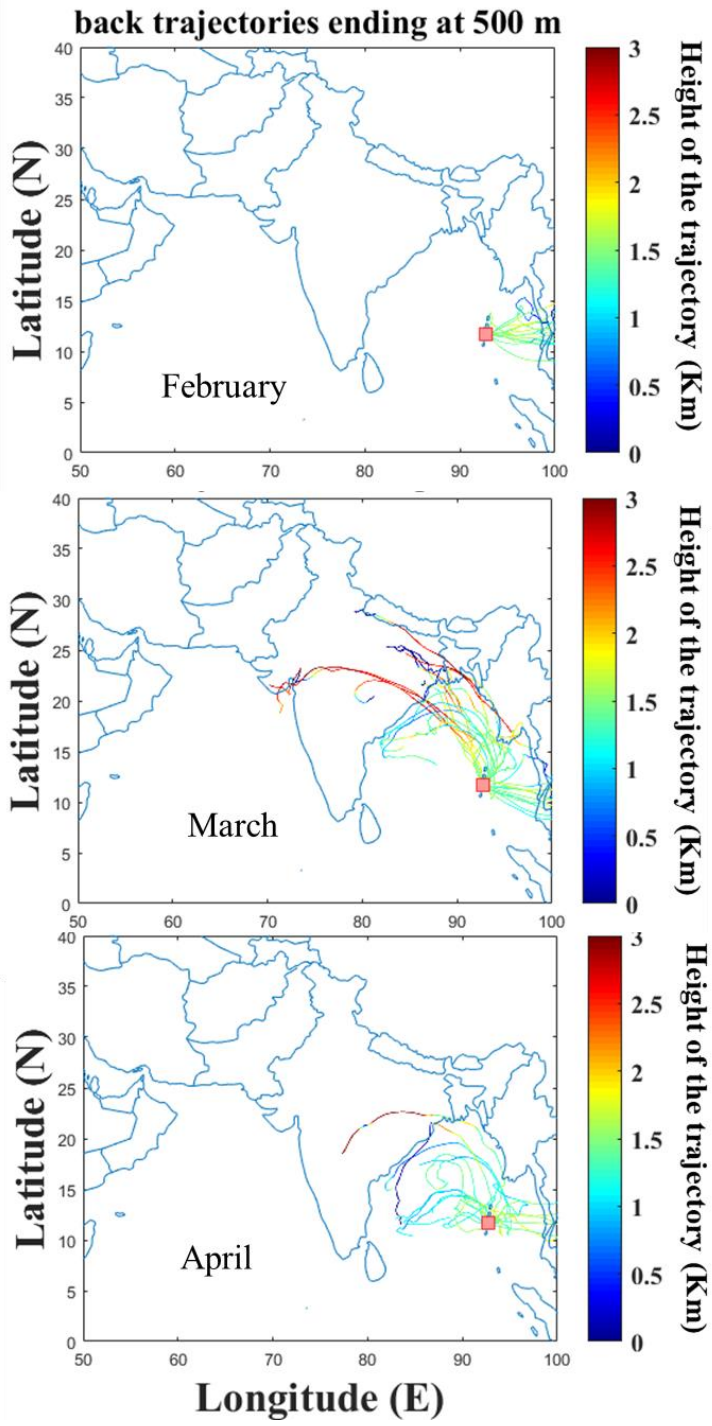

Figure 3.31 Air-mass back trajectories during February, March and April over Port Blair region

CHAPTER 4

Spatial and Temporal Characteristics of BrC Using Real-Time Measurements

In addition to filter based BrC measurements, we have also used real-time techniques to measure online-BrC. These real-time instruments provide highly time-resolved data sets which enable us to understand the changes and evolution of BrC in the atmosphere that is not observable in data sets provided by filters. Along with BrC measurements, the supporting species like light absorption of black carbon as well as trace gases like CO and NO_X were also measured. Real-time organic and inorganic species were also measured with High-Resolution Time-of-Flight Aerosol Mass Spectrometer (HR-ToF-AMS) at Kanpur site.

4.1 Kanpur Region

Semi-continuous measurements of water-soluble BrC were carried out at a site located in the campus of Indian Institute of Technology-Kanpur (IIT-K) (26.5 °N, 80.3 °E, and 142 m above mean sea level) during 20-December-2015 to 6-February-2016. Kanpur is located in the middle of the Indo-Gangetic Plain (IGP). A detailed description is given in chapter 2.2.

4.1.1 Temporal variability of WSOC and BrC:

Fig. 1 depicts a large diurnal and day-to-day variability in WSOC concentration and $b_{abs\_365\_Water}$ values. The WSOC varied from 1.0 to 72 μg m^{-3} (avg ± sd: 20 ± 13, 1σ) and $b_{abs\_365\_Water}$ ranged from 0.02 to 98 Mm^{-1} (24 ± 19) during the study period. This variability is attributable to various factors such as the dominance of specific sources (BB, FFB), atmospheric processes such as long-range transport, transformation, secondary organic aerosol (SOA) formation, and meteorological conditions over the central IGP. The possible roles of these factors are discussed in the subsequent text. Concentrations of gaseous species (CO, NO_X), inorganic ions (NH_4^+, NO_3^-, SO_4^{2-}, Cl^-), and AMS mass fragments of organic components (CH, CHO, CHO>1, CHO>1N, CHON) also exhibited a large variability during the study period, which were broadly similar to that of WSOC and $b_{abs\_365\_Water}$. Further, concentrations of all the measured species were relatively high with considerable fluctuations during December and January and subsequently subsided in February. Here, December and January months are characterized by

the lowest temperature, and subsequently, the temperature starts rising in February that also changes the boundary layer height. Winds also become stronger during February that enhances species removal from the study site (Rajput et al., 2016). Further, there was relatively high aerosol loading during nighttime, which is attributable to shallower boundary layer height. Lowest concentrations of all the species including WSOC and $b_{abs\_365\_Water}$ were observed during a rain event that occurred on January 19th (Fig. 4.1), which had cleaned the atmosphere. However, the atmosphere was loaded again quickly with significant concentrations of various chemical species within a few hours after the rain event, suggesting local sources were very active.

WSOC exhibited a strong correlation with $b_{abs\_365\_Water}$ (slope = 1.22 ± 0.007, r^2 = 0.70, n = 13265, intercept = -0.69 ± 0.17, Fig. 4.2 a), suggesting that a significant fraction of WSOC is BrC chromophores, which are absorbing at 365 nm. Here (and everywhere in the text), the slope is given with standard error. Further, MAE ranged from 0.003 to 5.26 m^2 g^{-1} (1.16 ± 0.60) during the study period. The average MAE value (1.16) is higher in comparison to those documented in literature such as 0.60 over South Deklab-USA, 0.73 over Pasadena-USA, 0.75 (daytime) and 1.13 (nighttime) over Patiala-India, and lower in comparison to values reported over Delhi (1.6) and Beijing (1.8) (Hecobian et al., 2010; Zhang et al., 2013; Kirillova et al., 2014; Srinivas et al., 2016). These observations suggest that the study region (including Patiala and Delhi) has higher abundances and/or higher absorbing capacity of BrC chromophores in comparison to those reported over different sites in the USA whereas, lower than that documented over Beijing, China.

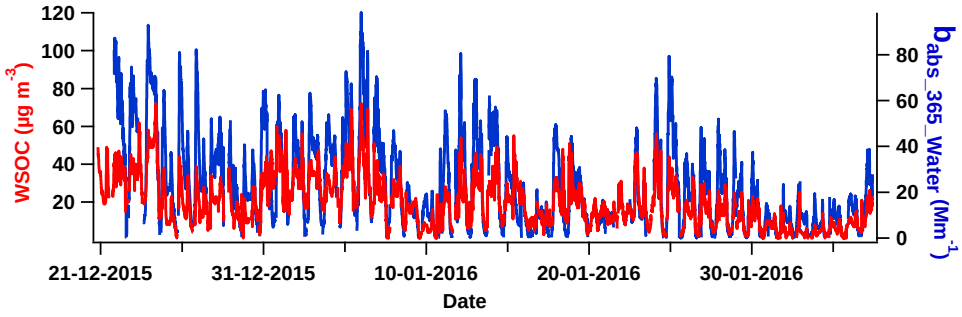

Figure 4.1: Temporal variability in WSOC concentration and BrC absorption coefficient ($b_{abs\_365\_Water}$) during the study period.

Significant variability in MAE (0.003 to 5.26 m^2 g^{-1}) could be due to various reasons such as different types of BrC species have different absorption properties, and their abundances are changing with time under different meteorological conditions. These chromophores could be primary and/or secondary BrC species from BB and/or FFB emissions with different absorption properties. Certain meteorological conditions may also reduce/enhance the absorption properties of BrC chromophores. To investigate and understand this variability, the data have been investigated in different ways.

Hours of the day are shown in colored scale in Fig. 4.2a. To understand the diurnal variability in the characteristics of BrC (Fig. 4.2b), the data have been split into three time periods, A: 18:00-06:00 hours (Evening + Night), B: 06:00-11:00 hours (Morning), and C: 11:00-18:00 hours (Middle of the day), respectively, as the $b_{abs\_365\_Water}$ data points corresponding to these time periods, appear to follow similar characteristics (Figs. 4.2a, b). A noticeable difference was observed in the MAE (m^2 g^{-1}) of WSOC for the periods A (slope=1.34 ± 0.01, r^2=0.76, n = 7181), B (slope=0.95 ± 0.01, r^2=0.72, n = 3223) and C (slope=0.58 ± 0.01, r^2=0.62, n = 2975) (Fig. 4.3), reflecting the change in absorbing properties of BrC at different time of the day. Here, the slopes are given with standard errors. The highest slope (representing MAE of WSOC) was observed for the data points corresponding to period A, and attributed to active primary sources, as corresponding H:C ratios (from HR-ToF-AMS) were relatively high during these

hours (discussed later). To understand the role of primary emissions on BrC characteristics, CO is also used as a tracer of emissions from primary sources (Hecobian et al., 2010). A reasonably good correlation (r^2 = 0.48, n = 12272) between $b_{abs\_365\_Water}$ and CO was observed (Fig. 4.4), suggesting primary emissions are a significant source of BrC (or its precursors) over the study region. Second highest MAE of WSOC was observed for the period B, possibly due to the influence of active primary sources and secondary formation of BrC. A substantial increase in WSOC/CO ratio was observed during period B, which is suggestive of SOA formation (Hecobian et al., 2010; Updyke et al., 2012). Both WSOC and $b_{abs\_365\_Water}$ increased rapidly during sunrise, which contrasts with that observed by Hecobian et al. (2010). When both WSOC and $b_{abs\_365\_Water}$ were high along with CO, the WSOC/CO and $b_{abs\_365\_Water}$/CO ratios are expected to be low; however, if these ratios were high, then it would indicate that there are multiple sources of these species (other than primary emissions) with different source strengths. The WSOC/CO and $b_{abs\_365\_Water}$ /CO ratios were low when local burning sources were present.

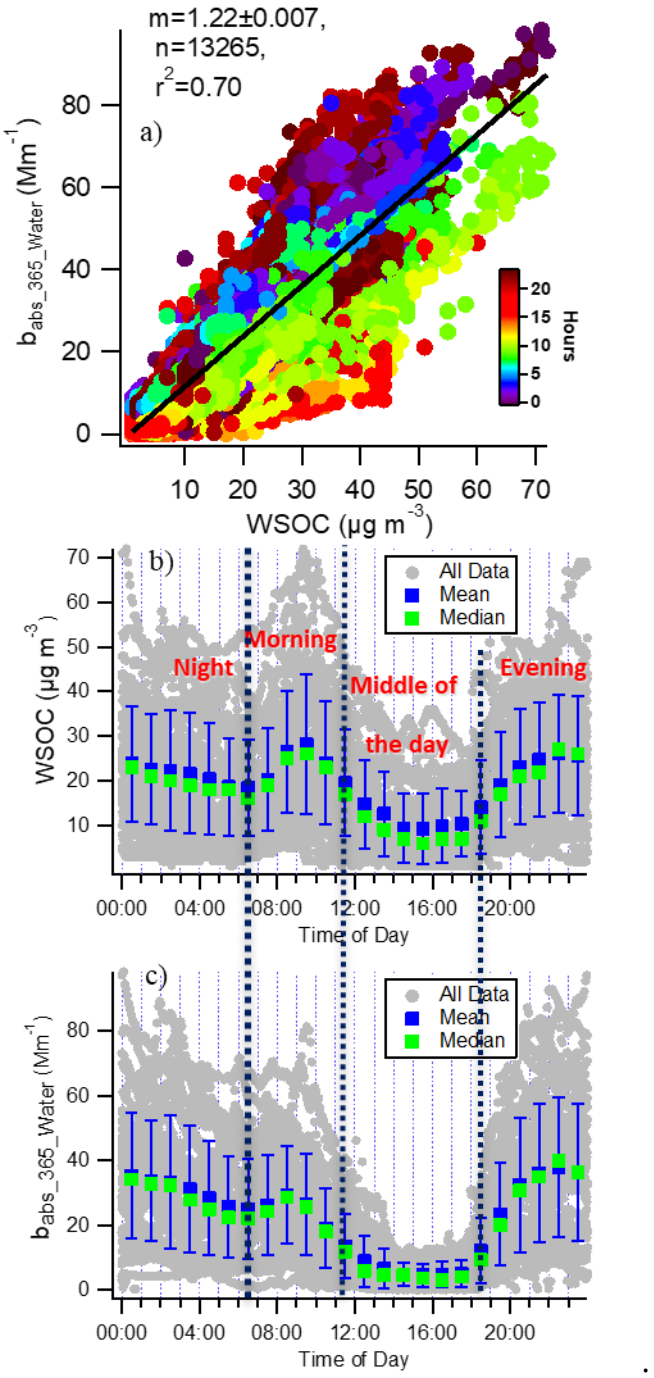

Figure 4.2: (a) Scatter plot between WSOC and $b_{abs\_365\_Water}$, (b) Diurnal trends of $b_{abs\_365\_Water}$ and (c) Diurnal trends of WSOC

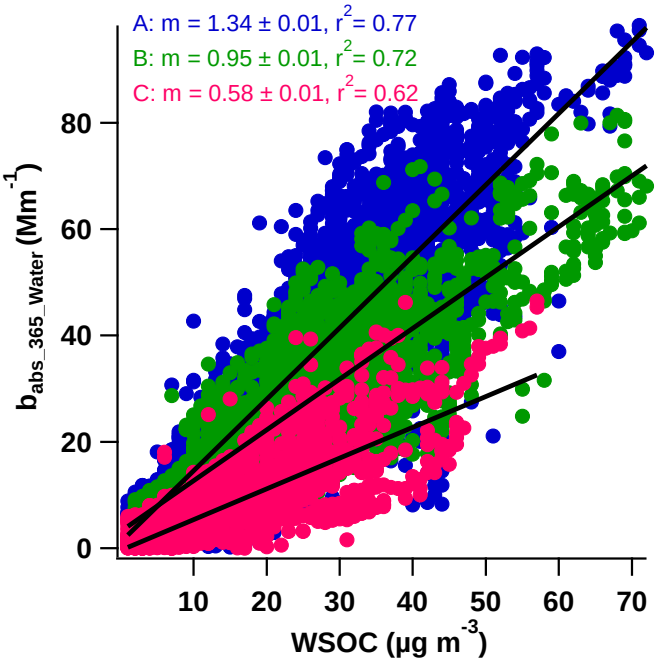

Figure 4.3: Scatter plot between the WSOC and $b_{abs\_365\_Water}$ at different periods of the day, where A: 18:00-06:00 hours (Evening + Night), B: 06:00-11:00 hours (Morning), and C: 11:00-18:00 hours (Middle of the day) respectively.

Lowest MAE of WSOC was observed during period C (slope = 0.58 ± 0.01, r^2 = 0.62, n = 2975) when BrC continued to decrease with increasing sunlight exposure. Middle of the day $b_{abs\_365\_Water}$ values (6 ± 5) was ~80-90% lower than those during nighttime 35 ± 21, (Fig. 4.2 b). This observation suggests that either daytime secondarily formed BrC is less absorbing, and/or ambient BrC goes through photobleaching during the daytime, or it is volatile and evaporates with increasing temperature during daytime (Fig. 4.6, discussed later) (Zhong and Jang, 2014; Liu et al., 2015; Zhao et al., 2015). Expanded boundary layer height during daytime would also reduce $b_{abs\_365\_Water}$ values. However, the exact reason (s) for the decrease in $b_{abs\_365\_Water}$ values during the day remains unclear, especially since chemical measurements for this potential degradation or dilution processes lack in this study.

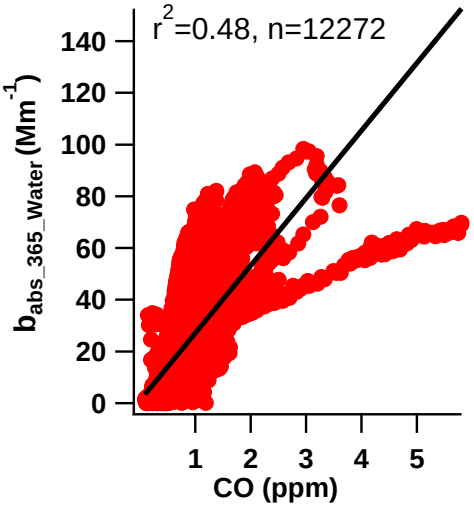

Figure 4.4: Scatter plot between the $b_{abs\_365\_Water}$ (Mm^{-1}) and CO (ppm) during the study period.

4.1.2 Diurnal variability in BrC chromophores:

BrC is characterized by an absorption spectrum that smoothly increases from the visible to UV wavelengths (Laskin et al., 2015). The BrC absorption at 365 nm has been shown to be mainly associated with HULIS compounds; however, other chromophores may peak at different wavelengths. The absorption observed at different wavelengths may or may not change uniformly throughout the day as the chromophore composition may or may not be constant all the time. Different types of chromophores can be emitted from various sources and/or formed in the atmosphere. Budisulistiorini et al. (2017) have shown that the direct burning of several types of biomass can produce primary BrC (Budisulistiorini et al., 2017). Recent laboratory studies have found that anthropogenic VOCs (benzene, toluene, phenols and polycyclic aromatic hydrocarbons (PAHs) react with nitrogen oxides and produce nitroaromatics (Graber and Rudich, 2006; Hoffer et al., 2006; Lukács et al., 2007; Chen and Bond, 2009; Zhang et al., 2013; Lin et al., 2015; Zhao et al., 2015; Xie et al., 2017; Hems and Abbatt, 2018). Nitrophenols and nitrocatechols have been identified as a dominant light absorbing compounds in

cloud water samples and in $PM_{2.5}$ particles impacted by BB and FFB (Desyaterik et al., 2013; Lin et al., 2015).

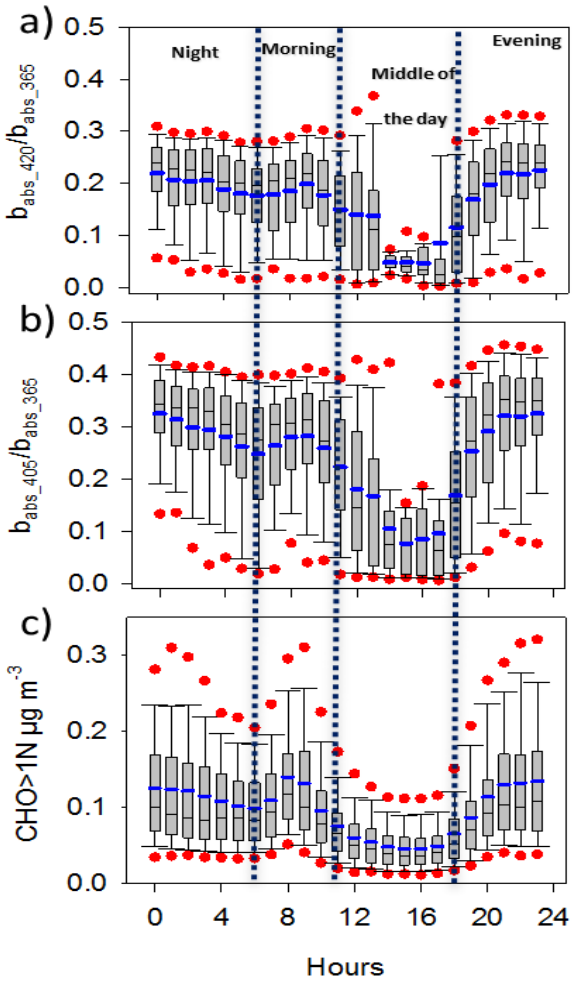

Figure 4.5: Box-whisker plots showing diurnal trends of (a) $b_{abs\_420\_Water}$/ $b_{abs\_365\_Water}$, (b) $b_{abs\_405\_Water}$/ $b_{abs\_365\_Water}$, and (c) CHO>1N. The boundary of the box closest to zero indicates the 25th percentile, black and blue lines within the box represent median and mean, respectively, and the boundary of the box farthest from zero indicates the 75th percentile. Error bars above and below the box indicate the 90th and 10th percentiles. Red circles are indicative of outliers.

In the present study, absorptions at 405 nm (representing 2,4-dinitrophenol) and 420 nm (representing 3-nitrophenol) were selected to compare with 365 nm (representing HULIS) (Lin et al., 2015). It is expected that spectral absorbance would be different at different times of the day if BrC composition is not uniform. Ratios of $b_{abs\_405\_Water}/b_{abs\_365\_Water}$ and $b_{abs\_420\_Water}/b_{abs\_365\_Water}$ were investigated to understand whether BrC composition was uniform during the study period and/or whether there was any diurnal variability in BrC composition over the study site. Absorption ratios of $b_{abs\_405\_Water}/b_{abs\_365\_Water}$ and $b_{abs\_420\_Water}/b_{abs\_365\_Water}$ exhibited considerable variability at different times of the day (Figs. 4.5a, b), suggesting BrC composition was not uniform. These ratios were minimum during the afternoon (14:00 to 17:00), more or less similar during the evening and night hours, and exhibit a small positive hump during morning rush hours (08:00 to 10:00) (Figs. 4.5 a, b). Interestingly, the diurnal trends in $b_{abs\_405\_Water}/b_{abs\_365\_Water}$ and $b_{abs\_420\_Water}/b_{abs\_365\_Water}$ during rush hours were similar to that exhibited by organic compounds of CHO>1N family (Fig. 4.5c). It implies that considerable fraction of BrC chromophores could be nitrogen-containing organic compounds over the study region, and likely they are volatile and/or affected by photo-bleaching (as ratios were minimum during afternoon hours, Fig. 4.5). These observations also suggest that BrC chromophores are a variable mixture of at least HULIS and nitrogen-containing organic compounds over the study region, and BrC absorption properties at a given time depend upon the type of chromophores and meteorological parameters.

4.1.3 Effect of meteorological conditions on BrC:

Atmospheric BrC species are susceptible to photochemical degradation, as their optical properties can be altered by aqueous-phase photochemical processing with both photo-enhancement and photo-bleaching processes (Zhong and Jang, 2014). In this study, the $b_{abs\_365\_Water}$ depicted photo-enhancement during early hours after sunrise, possibly due to aqueous-SOA formation as WSOC also increased at this time. BrC absorption diminished during the middle of the day (Fig. 4.2 b), likely due to photo-dissociation and/or due to volatile nature of BrC, as the temperature went to maximum during this time (Fig. 4.6). The lower BrC could also be because the planetary boundary layer (PBL) height was also highest during the middle of the day (Fig. 4.6). Zhao et al. (2015) had documented that the presence of oxidants like O_3 and OH radicals (abundant during daytime) may degrade BrC into smaller and more volatile organic compounds. Higher absorption during the evening to night is attributable to primary sources as well as shallow boundary layer height (Fig. 4.6), and the absence of volatilization and photo-bleaching processes.

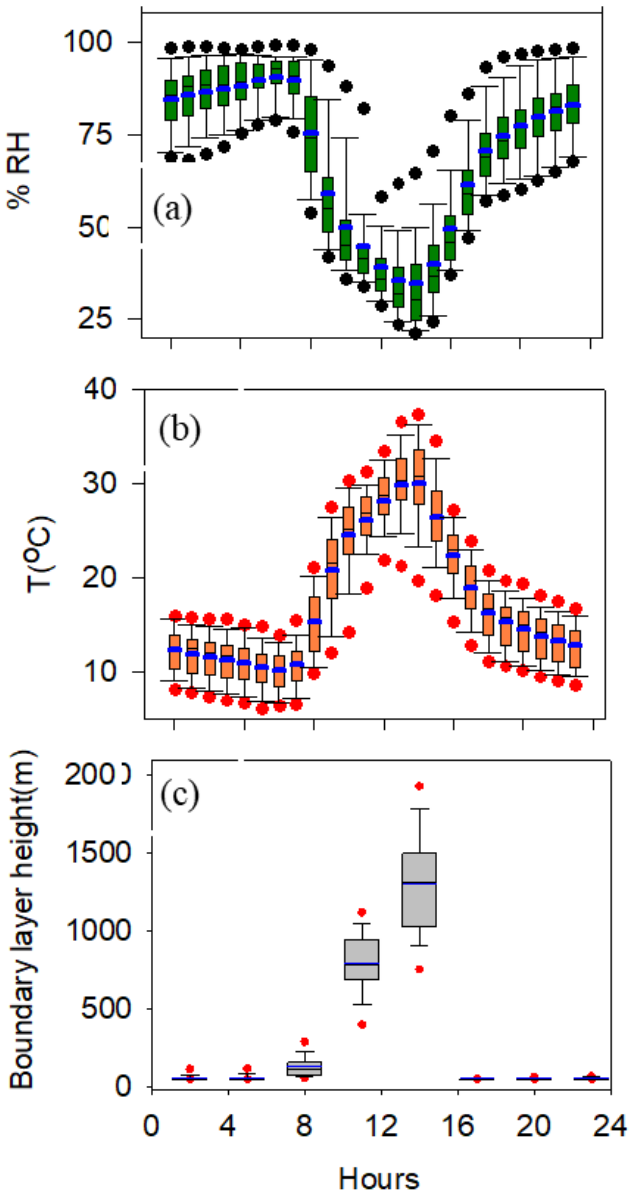

Figure 4.6: Box-whisker plot showing diurnal trends of (a) % Relative humidity (%RH,), (b) Temperature (T, °C) and (c) atmospheric boundary layer height (m). The boundary layer height (m) data (1 degree, 3 hourly, Global) was obtained from NOAA-Hysplit model.

4.1.4 Characteristics of BrC from different sources:

Positive matrix factorization (PMF) analysis was performed on the V-mode high-resolution data of AMS organic mass spectra, where the OA were further divided into several factors based on their characteristics (Figure 4.7). These factors include low-volatility oxygenated OA (LVOOA-1 and LVOOA-2), semi-volatile oxygenated OA with significant contribution from biomass burning organics (SVOOA-BBOA-1 and SVOOA-BBOA-2), hydrocarbon-like OA (HOA), and biomass burning OA (BBOA). Source profiles of these factors are presented in Fig. 4.7. To understand the relation and relative source contribution of different OA factors to BrC absorption, these factors are plotted against $b_{abs\_365\_Water}$ (Fig 4.8). In the same figure, the WSOC/OA ratio is also used as a colored axis to understand the effect of these factors on BrC as a function of their solubility in water. Here, WSOC data is from PILS-TOC and OA is from HR-ToF-AMS. It is noteworthy that WSOC/OA ratios are used rather than water-soluble organic matter (WSOM)/OA ratio to avoid uncertainty associated with WSOM, which requires an assumed constant factor to be multiplied to WSOC. On average, the WSOC/OA ratio was 0.14 ± 0.06 during the study period.

Total OA shows a very strong correlation with WSOC (slope = 0.17 ± 0.001, r^2 = 0.79, n = 7380, figure not shown). Total OA also exhibits a strong linear regression with $b_{abs\_365\_Water}$ (slope= 0.20 ± 0.002, r^2 = 0.64, n = 6470), and the slope of this regression is expected to be a weighted average of the slopes of $b_{abs\_365\_Water}$ with different PMF fractions of OA. The order of slopes was SVOOA-BBOA-2 (1.58 ± 0.019) > HOA (0.97 ± 0.014) > SVOOA-BBOA-1 (0.77 ± 0.017) > BBOA (0.64 ± 0.007) > LVOOA-1 (0.38 ± 0.004), which indicate the absorption capacity of BrC from respective source factors. One factor (LVOOA-2) had not shown a good correlation (r^2 = 0.05) with $b_{abs\_365\_Water}$. It infers that oxidized or aged OA does not absorb considerably, as LVOOA-2 consists of highly oxidized organic species (Fig. 4.7 f). The PMF factors of OA aerosol from BB origin are BBOA, SVOOA-BBOA-1, and SVOOA-BBOA-2. Here, $b_{abs\_365\_Water}$ showed a good correlation with BBOA (slope = 0.64 ± 0.007, r^2 = 0.55, n = 6442, O/C = 0.26) and SVOOA-BBOA-2 (slope= 1.58 ± 0.019, r^2 =

0.50, n = 6471, O/C = 0.43), but not with SVOOA-BBOA-1 (slope= 0.77 ± 0.017, r^2 = 0.22, n = 6471, O/C = 0.55); it further suggests that more oxidized OA are less absorbing in nature (Di Lorenzo et al., 2017). Such an observation also suggests that primary BB emissions produce strongly absorbing BrC, which include a large contribution from semi-volatile species (SVOOA-BBOA-2) (Budisulistiorini et al., 2017). Further, SVOOA-BBOA-2 also consists of the highest N/C (0.07) ratio among all OA factors (Fig 4.7 d), suggesting that nitrogenous compounds enhance the absorbing capacity of the OA.

However, an abundance of both $b_{abs\_365\_Water}$ and SVOOA-BBOA-2 reduces during the daytime when temperature increases, suggesting photochemical oxidation and/or volatilization of SVOOA-BBOA-2 in the atmosphere reduces BrC absorbing capacity, as discussed in the previous section. Further, the hydrocarbon types primary OA (or HOA) exhibited considerable linearity with BrC absorption (slope = 0.97 ± 0.014, r^2 = 0.40, n = 6447), suggesting primary sources are a significant contributor to light-absorbing OA over the study region. The lowest slope was observed with LVOOA-1 (slope = 0.38 ± 0.004, r^2 = 0.54, n = 6471), further indicating that aging or oxidation of organics reduces their light absorption capability. This result has important implications in predicting the light absorbing capability of OA based on its PMF derived factors. Further, higher $b_{abs\_365\_Water}$ value for data points with higher WSOC/OA ratios suggests that water-soluble chromophores from respective sources are relatively more absorbing (Fig. 4.8).

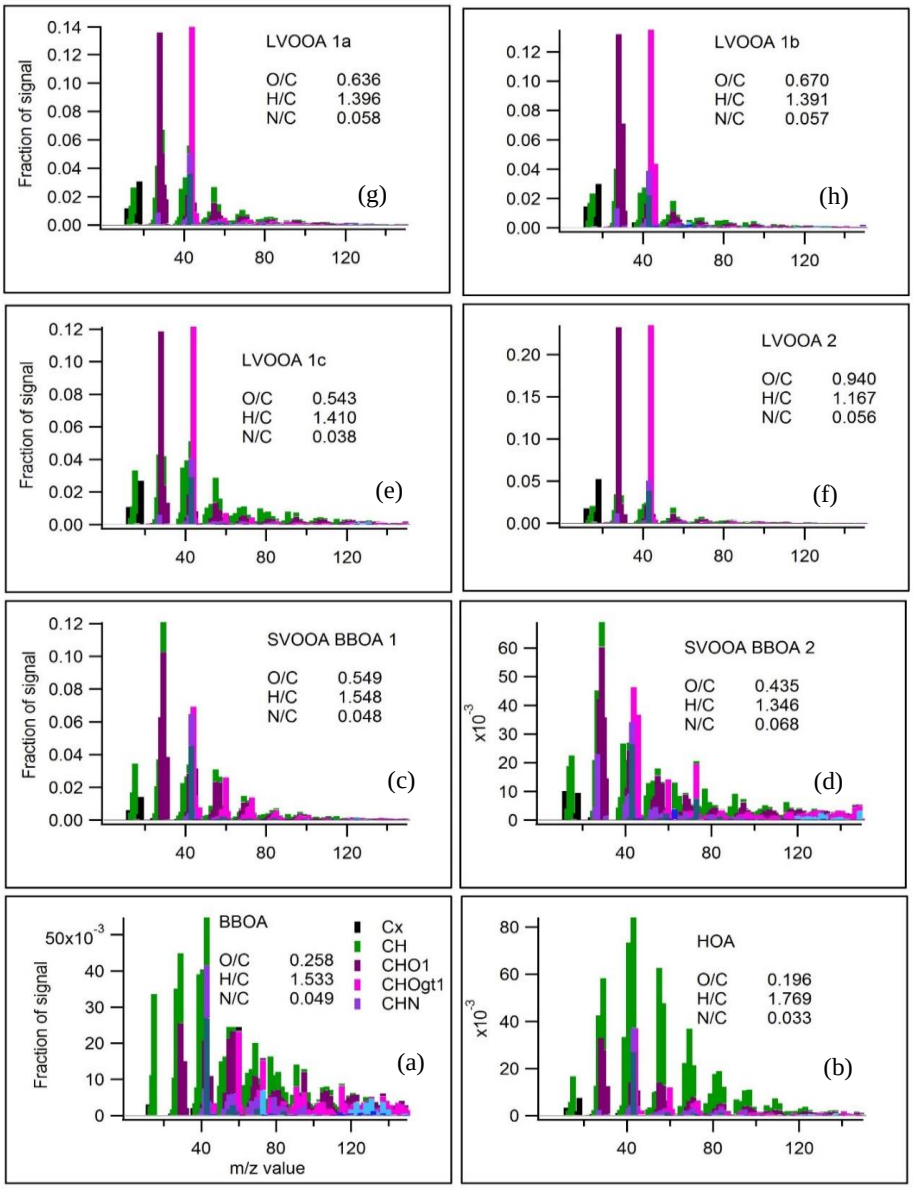

Figure 4.7: Combined HR-PMF factor profiles. (a) biomass burning OA (BBOA), (b) hydrocarbon-like OA (HOA), (c) semi volatile oxygenated OA biomass burning OA 1 (SVOOA BOOA 1), (d) semi volatile oxygenated OA biomass burning OA 2 (SVOOA BOOA 2), (e) low volatile oxidized OA 1c (LVOOA 1c), (f) low volatile oxidized OA 2 (LVOOA 2), (g) low volatile oxidized OA 1a (LVOOA 1a), (h) low volatile oxidized OA 1b (LVOOA 1b).

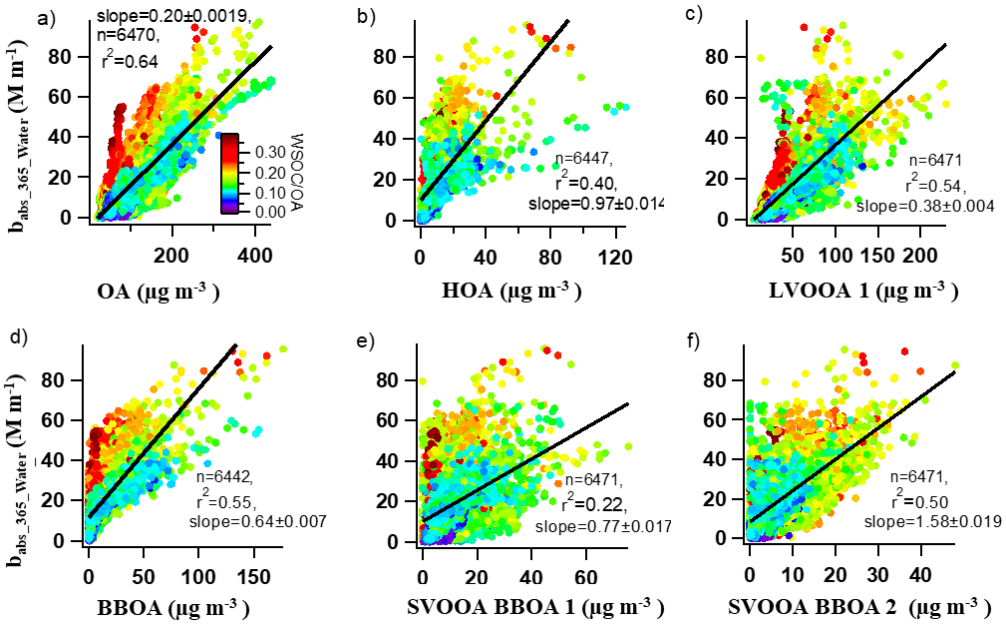

Figure 4.8: Linear regressions analysis of $b_{abs\_365\_Water}$ with PMF derived factors like (a) organic aerosol (OA), (b) hydrocarbon-like OA (HOA), (c) low volatile oxygenated OA (LVOOA1), (d) biomass burning OA (BBOA), (e) semi volatile oxygenated OA biomass burning oxygenated OA 1 (SVOOA BBOA 1) and semi-volatile oxygenated OA biomass burning oxygenated OA (SVOOA BBOA 2).

4.2 Measurements of atmospheric brown carbon over a big semi-arid urban city (Ahmedabad) of western India

The BrC absorption at 365 nm and WSOC mass concentration in ambient $PM_{2.5}$ were measured semi-continuously using an assembled system (PILS-LWCC-TOC) consisting of a particle-into-liquid sampler coupled to a liquid waveguide capillary cell (LWCC) and total organic carbon (TOC) analyzer over Ahmedabad during November 2015. Along with BrC measurements, the supporting data like trace gases like CO and NO_X were measured.

4.2.1 Temporal variability of WSOC and BrC:

Fig. 4.9 depicts a considerable day-to-day variability in WSOC concentration and $b_{abs\_365\_Water}$ values. The WSOC varied from 1.0 to 116 µg m^{-3} (avg ± sd: 11 ± 9, 1σ) and $b_{abs\_365\_Water}$ ranged from 1 to 126 Mm^{-1} (10 ± 12) during the study period. This variability is attributable to various factors such as the dominance of specific sources (BB, FFB), secondary organic aerosol (SOA) formation, and meteorological conditions, etc. Concentrations of gaseous species (CO, NOX), also exhibited large variability during the study period (Fig. 4.9), which were broadly similar to that of WSOC and $b_{abs\_365\_Water}$. On November 9th, the highest concentrations were observed for both WSOC and $b_{abs\_365\_Water.}$ These concentrations are attributed to emissions from combustion sources.

WSOC exhibited a moderate correlation with $b_{abs\_365\_Water}$ (slope = 0.79 ± 0.01, r^2 = 0.44, n = 3949, Fig. 4.10), suggesting that the WSOC is consist of BrC chromophores, which are absorbing at 365 nm. Further, MAE ranged from 0.03 to 3.90 m^2 g^{-1} (0.97 ± 0.78) during the study period. The average MAE value (0.97) was higher in comparison to those documented in literature such as 0.60 over South Deklab-USA, 0.73 over Pasadena- USA. This MAE value is close to Kharagpur (0.8), and lower in comparison to values reported over Delhi (1.6) and Beijing (1.8), and Kanpur (1.16) (Hecobian et al., 2010; Srinivas and Sarin, 2013; Zhang et al., 2013b; Kirillova et al., 2014; Srinivas and Sarin, 2014; Srinivas et al., 2016; Satish et al., 2017).

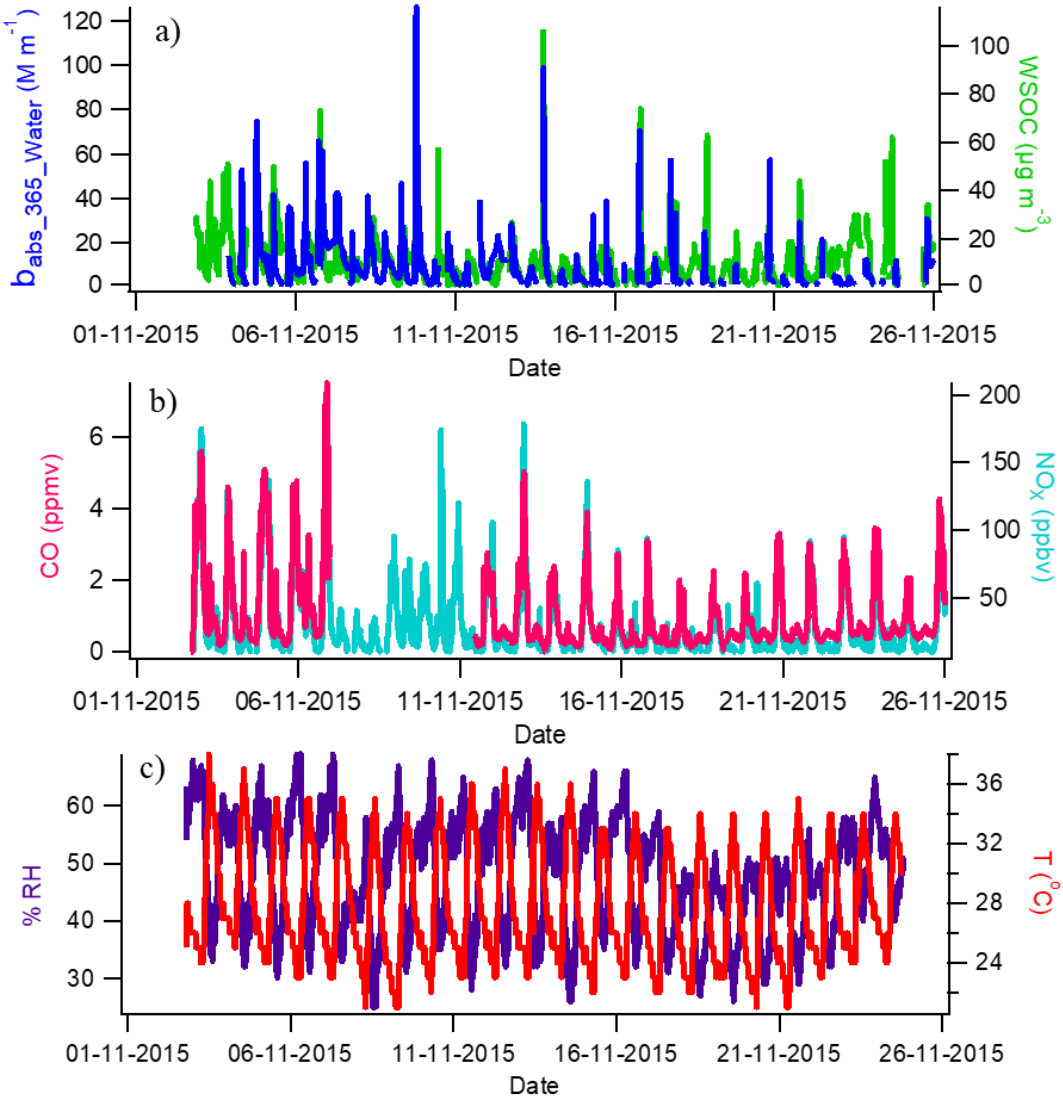

Figure 4.9: Temporal variability of (a) $b_{abs\_365nm\_Water}$ and WSOC; (b) CO and NO_X; and (c) % RH and T

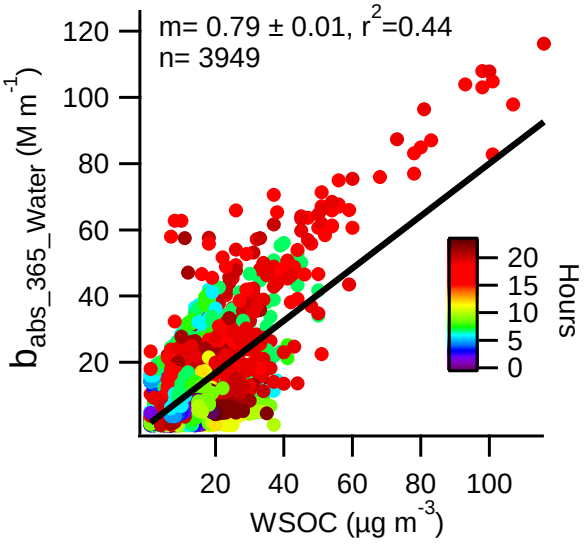

Figure 4.10: Scatter plot between WSOC and $b_{abs\_365\_Water}$ and hours of the day plotted as the colored axis

4.2.2 Diurnal variability of WSOC and BrC species:

Fig 4.11 depicts the diurnal variability of WSOC, $b_{abs\_365\_Water,}$ and MAE. The strong diurnal variability was observed in these species likely due to changes in emission sources, physico-chemical transformations, transport and deposition processes (Rastogi et al., 2015). The observed diurnal pattern was slightly different over Ahmedabad compared to those observed over Kanpur (Satish et al., 2017) and Delhi. The $b_{abs\_365\_Water}$ peaks were observed in the morning (06:00-09:00) and evening (17:00-22:00) hours. However, morning peak for WSOC showed a more extended period (07:00 to 12:00) compared to $b_{abs\_365\_Water.}$ A substantial increase in WSOC/CO ratio was also observed from morning to afternoon hours of the day (08:00-16:00), which is suggestive of SOA formation.

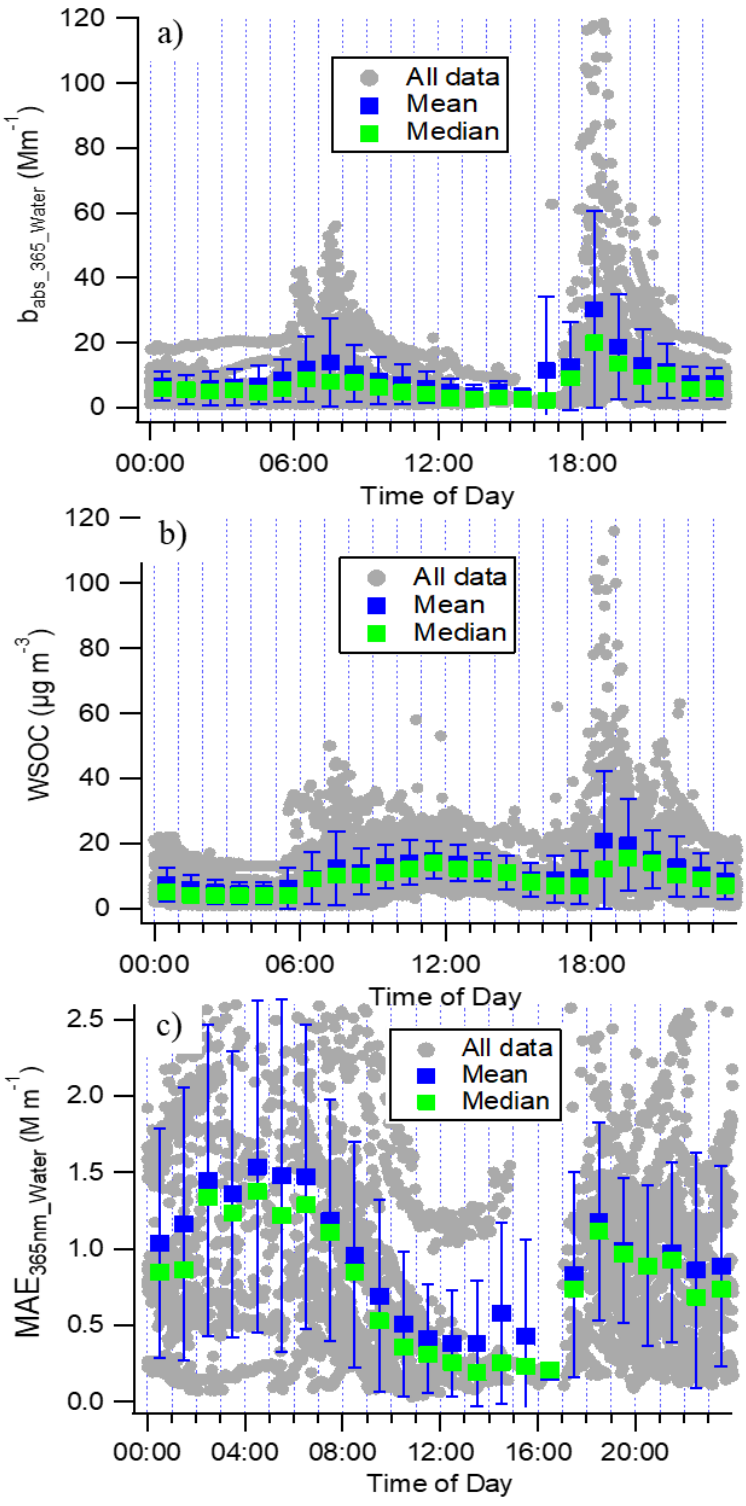

Figure: 4.11: Diurnal trends of a) $b_{abs\_365\_Water}$, b) WSOC and c) MAE_{365nm_Water}

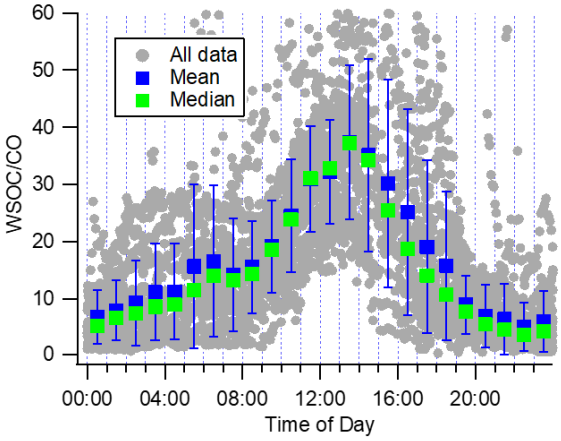

Figure 4.12: Diurnal variability of WSOC/CO over Ahmedabad

Further, MAE values also showed strong diurnal variability. High MAE values were observed during evening rush hours and night hours. During the night hours, high MAE values were observed, even though the absolute concentration of WSOC, $b_{abs\_365\_Water}$ were low. This suggests that during night hours, the majority of WSOC was BrC. The MAE values were reduced during day (11:00-17:00) hours, which can be ascribed to photo-bleaching/volatilization of BrC.

On a few days, unusually high concentrations of species were observed (Fig. 4.14). There were many events occurred during the study period. For example, Figure 4.13 shows the temporal trends of $b_{abs\_365nm\_Water}$, WSOC, MAE_{365nm_Water}, WSOC/CO, % RH and T during 5 to 6th November. On November 5th evening (5:30 PM), emissions from local combustion sources were observed. Both $b_{abs\_365nm\_Water}$ and WSOC concentrations were high from evening to night hours (6th 00:00 hours). During this period, WSOC/CO (tracer of secondary organic aerosol formation) values were low which suggests that primary emission was dominant. However, in the night after 00:00 hours both $b_{abs\_365nm\_Water}$ and WSOC values were low, but MAE values were high, suggesting the secondary formation of BrC during the night. The second peak observed in morning hours, and during this period both MAE and WSOC/CO values are high, suggesting both primary

and secondary sources contributing in the morning hours. Further, the absorbance decreases considerably as temperature increases, indicating BrC could be semi-volatile and/or undergoing through photo-dissociation.

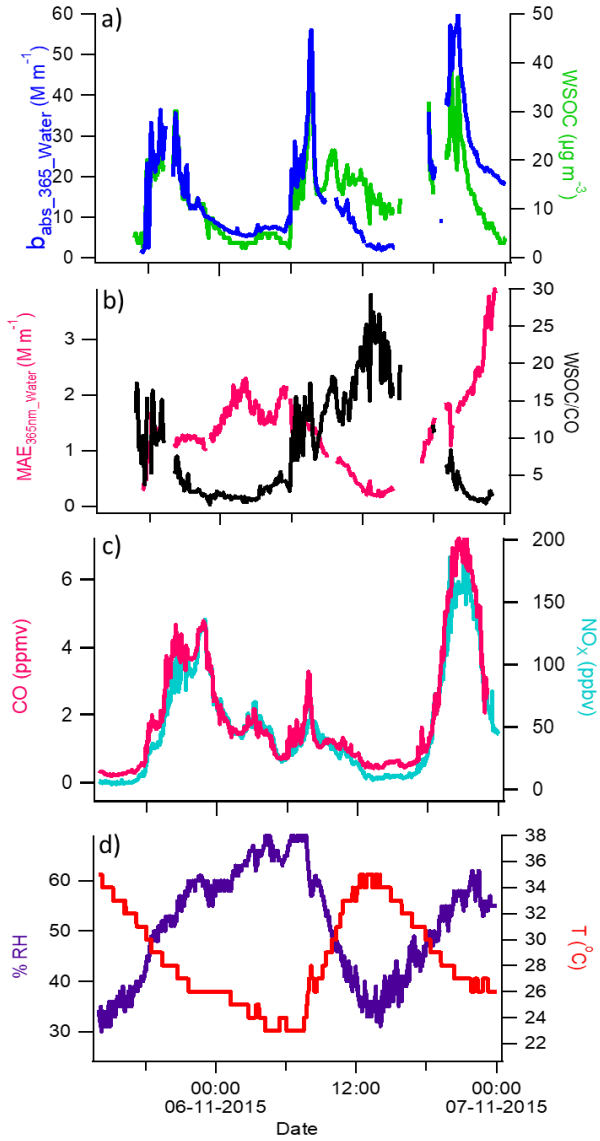

Figure 4.13: (a): $b_{abs\_365nm\_Water}$ and WSOC; b): MAE and WSOC/CO; c) CO and NO_X; d): % RH and T

4.3 Temporal variability of brown carbon spectral characteristics over Delhi

The BrC absorption spectra (300-700 nm) and WSOC mass concentration in ambient $PM_{2.5}$ have been measured semi-continuously using an assembled system (PILS-LWCC-TOC) consisting of a particle-into-liquid sampler coupled to a liquid waveguide capillary cell (LWCC) and total organic carbon (TOC) analyzer. Along with BrC measurements, the supporting data like BC, and trace gases like CO and NO_X were measured.

4.3.1 Temporal variability of BrC and WSOC:

Fig. 4.15 depicts a considerable diurnal and day-to-day variability in WSOC concentration and $b_{abs\_365nm\_Water}$ values. The WSOC varied from 1.0 to 62 µg m^{-3} (avg ± sd: 16 ± 9, 1σ) and b_{abs_365nm} ranged from 0.05 to 65 Mm^{-1} (18 ± 12) during the study period. This variability can be attributable to various factors such as the dominance of specific sources BB, FFB, and atmospheric processes, etc. Concentrations of gaseous species (CO, NO_X), and BC also exhibited large variability which was broadly similar to WSOC and $b_{abs\_365nm\_Water.}$ Further, concentrations of all the measured species were relatively high with considerable fluctuations during January and subsequently subsided in February and March (monthly average values are given in Fig. 4.14). Further, there was relatively high aerosol loading during night-time, which is attributable to shallower boundary layer height and heavy duty vehicular emissions in the night hours. The concentration of CO, $NO_{X,}$ and BC values were very high compared to Kanpur region. BC_370 nm values were high in January compared to BC_880 nm. This suggests that in January, Delhi was influenced by both BB and FFB emissions.

WSOC exhibited a strong correlation with $b_{abs\_365\_Water}$ (slope = 1.21 ± 0.007, r^2 = 0.72, n = 11635, intercept = −0.66 ± 0.12), suggesting the presence of a significant but variable fraction of water-soluble chromophores. Hours of the day are shown in colored scale in Fig. 4.15, which indicates the diurnal variability of MAE. Further, MAE ranged from 0.005 to 3.34 m^2 g^{-1} (1.12 ± 0.46) during the

study period. The average MAE value (1.12) is higher in comparison to those documented in literature such as 0.60 over South Deklab-USA, 0.73 over Pasadena- USA, Ahmedabad (0.79), 0.75 (daytime) and 1.13 (nighttime) over Patiala-India, and lower in comparison to values reported over Delhi (1.6) and Beijing (1.8) (Hecobian et al., 2010; Zhang et al., 2013; Kirillova et al., 2014; Srinivas et al., 2016; Satish et al., 2017). These observations suggest that the study region (including Patiala and Delhi) has either higher abundances and/or higher absorbing capacity of BrC chromophores in comparison to those reported over different sites in USA whereas, lower than that documented over Beijing, China. Further, MAE values were calculated at different wavelengths and they showed a decreasing trend with increasing wavelength (365 nm: m = 1.20, r^2 = 0.72; 405 nm: m = 0.60, r^2 = 0.72; 420 nm: m = 0.48, r^2 = 0.70; 450 nm: m = 0.371, r^2 = 0.64; 490 nm: m = 0.30, r^2 = 0.52; and 550 nm: m = 0.1, r^2 = 0.46).

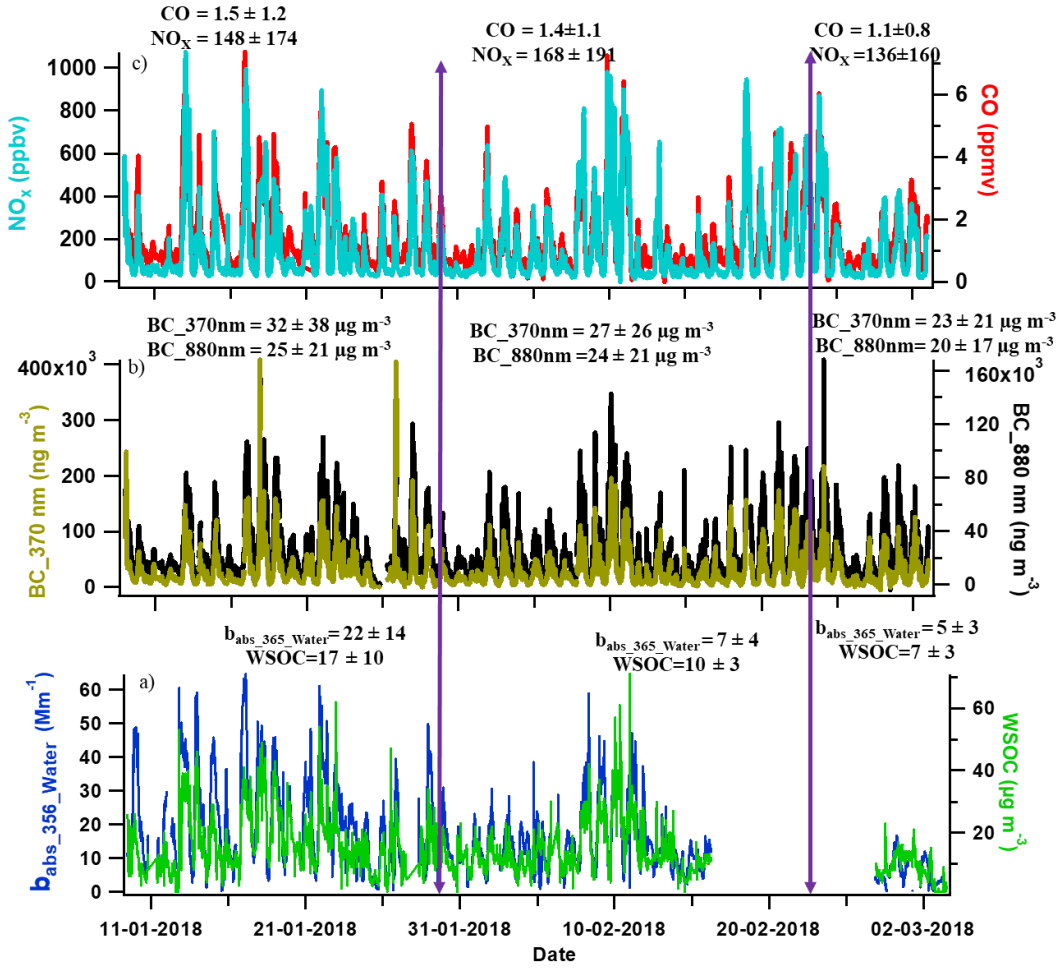

Figure 4.14: Temporal variability of different chemical species and monthly averaged values are also listed (a): $b_{abs\_365nm\_Water}$ and WSOC; (b): BC_370, BC_880; (c): CO and NO_X

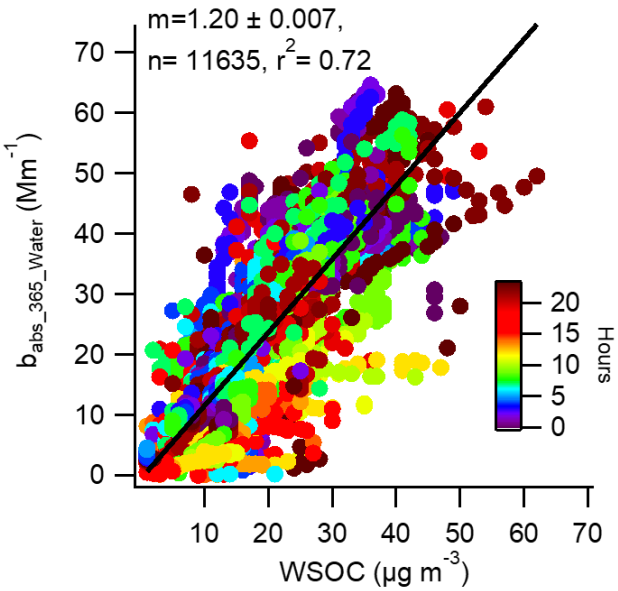

Figure 4.15: Scatter plot between WSOC (µg m^{-3}) and $b_{abs\_365\_Water}$ (Mm^{-1}) and hours of the day plotted as the colored axis

4.3.2 Diurnal variability of WSOC and BrC:

Fig. 4.16 depicts the diurnal variability of WSOC, $b_{abs\_365\_Water}$, and MAE. A strong diurnal variability was observed in these species due to emission sources, physico-chemical transformations, transport and deposition processes (Rastogi et al., 2015). There are only very few studies from India and limited studies in the world which have documented diurnal trends of WSOC species in ambient aerosol. The diurnal pattern of WSOC and $b_{abs\_365\_Water}$ were similar to previously reported study over Kanpur region (Satish et al., 2017). The photochemical SOA formation was evident during morning hours (08:00 to 10:00 hours) whereas variability during late evening/night hours (19:00 to 23:00 hours) is attributable to

both due to primary emission and secondary formation of WSOC and $b_{abs\_365\_Water}$. However, after the evening peak, $b_{abs\_365\_Water}$ showed high concentrations throughout the night (00:00 to 10:00), and this could be attributed to primary emission due to heavy-duty vehicles in the night hours. MAE is also following similar trends with WSOC and $b_{abs\_365\_Water,}$ and these trends are similar to Kanpur site.

A substantial increase in WSOC/CO ratio was observed from morning to afternoon hours of the day (10:00-16:00), which is suggestive of SOA formation (Fig. 4.17b). Further, $b_{abs\_365\_Water}$/CO is also suggesting that secondary BrC was dominant from 00:00 to 12:00 hours and it reduced during early evening rush hours (Hecobian et al., 2010; Zhang et al., 2013). Both $b_{abs\_365\_Water}$/CO and WSOC/CO values were reduced in the evening and morning rush hours due to the relative dominance of emissions from primary emissions. WSOC and $b_{abs\_365\_Water}$ increased rapidly during sunrise, which contrasts with that observed by Hecobian et al. (2010). When both WSOC and $b_{abs\_365\_Water}$ were high along with CO, the WSOC/CO and$b_{abs_365_Water}$/CO ratios are expected to be low; however, if these ratios are high then it would indicate that there are multiple sources of these species (other than primary emissions) with different source strengths. The WSOC/CO and $b_{abs\_365\_Water}$/CO ratios were low when local burning sources were present.

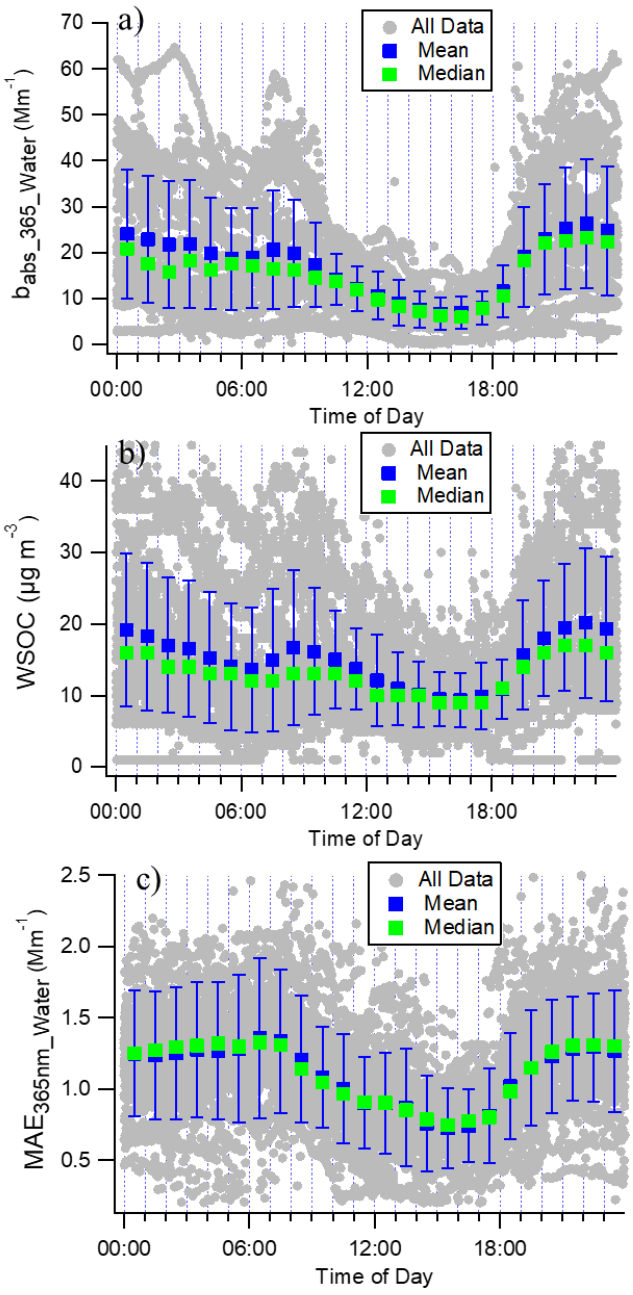

4.16: Diurnal trends of a) $b_{abs\_365\_Water}$, b) WSOC and c) MAE

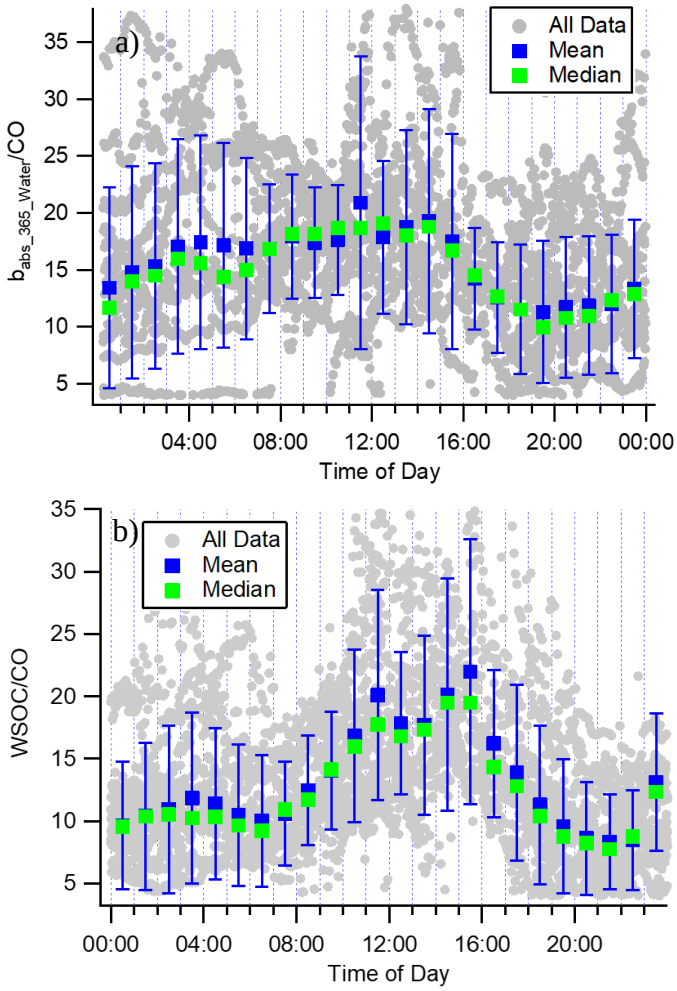

*Figure 4.17: D*iurnal trends of $b_{abs\_365\_Water}$/CO and WSOC/CO

4.3.3 Effect of meteorological conditions on BrC:

Most of the reported studies on BrC aging are focused on secondary BrC, which observed to undergo rapid photo-bleaching with atmospheric lifetimes on the order of minutes to several hours (Sareen et al., 2013; Lee et al., 2014; Zhao et al., 2015; Lin et al., 2017). In this study, we have observed the effect of photo-bleaching on BrC absorption spectra. In January, BrC spectra showed double hump with the first peak between 300 nm to 360 nm and a second peak between 450 nm to 550 nm. This type of absorption peak suggests the presence of

secondarily formed nitroaromatics in the atmosphere (Hems & Abbatt, 2018; Lin et al., 2015; Wang et al., 2017; Xie et al., 2017; Zhang et al., 2011; Zhao et al., 2015). Further, the second hump disappeared during day hours, and overall BrC absorption at shorter wavelengths also decreased, which can be ascribed to photo-bleaching/volatilization of BrC and/or rising boundary-layer height. Updyke et al. (2012) reported similar BrC absorption spectrum (secondary aged BrC) peaking at 500 nm, as observed in this study. Such type of BrC absorption spectra was also observed in different laboratory generated BrC studies (Sareen et al., 2013; Lee et al., 2014; Zhao et al., 2015; Lin et al., 2017). However, quantitative predictions of the BrC contribution to the light absorption is still a challenging task because of BrC composed of variable chromophores. Optical properties of organic compounds strongly depend on their molecular structures, so it is essential to understand BrC chromophores in molecular level. BrC absorption at the visible region is very important in regional climate studies.

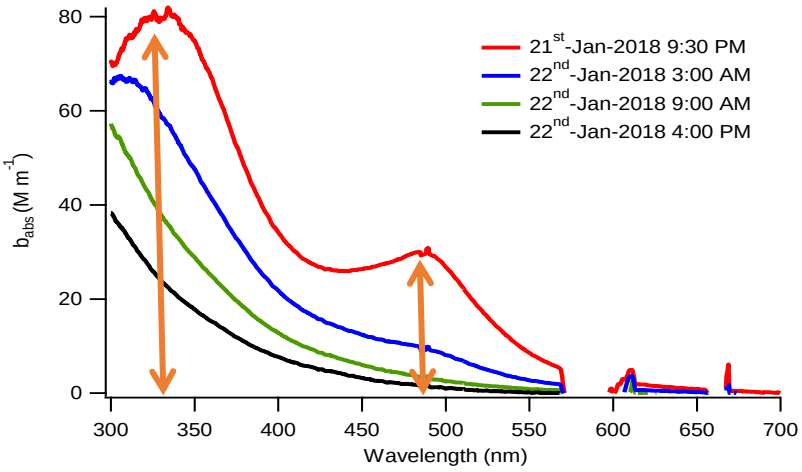

Figure 4.18: BrC absorption spectra at different periods of the day

CHAPTER 5

Summary and Future Scope

5.1 Summary

BrC immersed in cloud droplets can absorb light and facilitate evaporation/dispersion of clouds (Hansen et al., 1997, Laskin et al., 2015). It contributes ~35% of the direct radiative forcing warming by carbonaceous aerosols (Lin et al., 2014). However, to assess the effects of BrC on air quality and climate, a proper understanding of its sources and characteristics on temporal and spatial scales is very important (Satiah et al., 2017). In this study, we have characterized atmospheric brown carbon using both offline and online techniques. With an aim to understand the characteristics of BrC over different regions dominated by different emission sources and/or meteorological conditions, many sampling regions and periods for sampling were selected. Further, we have investigated the BrC variability concerning its sources, chemical composition, optical properties, and atmospheric evolution.

This study suggests that primary emissions from biomass burning (BB) and fossil fuel burning (FFB) are the major sources of highly absorbing BrC. Secondary BrC and aged/oxygenated OA are relatively less absorbing. Further, BrC absorption decreases as the day progresses achieving a minimum during afternoon hours. It is also shown that BrC composition is not uniform throughout the day. Our observations suggest that BrC chromophores are a variable mixture of at least HULIS and nitrogen-containing organic compounds over the study regions. These results have implications in regional radiation budget. This study qualitatively depicts the possible role of meteorological parameters on the abundances of BrC, which may be useful in assessing meteorological effects on similar atmospheric species.

Site specific summary of BrC characteristics are given below.

5.1.1 Patiala during Biomass Burning:

In this study, day/night (10-hour integration time) pair of ambient $PM_{2.5}$ samples (n = 69) were collected every day before (n = 21), during (n = 36) and after (n = 8) a large-scale paddy-residue burning during October-November 2014. BrC was

extracted using water and methanol, and subsequently, BrC absorption spectra were stored for 300-700 nm wavelength range for all the samples. Major observations/inferences/conclusions from this work are:

- The $PM_{2.5}$ mass concentration ranged from ~90 to 500 μg m^{-3} (average ± 1$\boldsymbol{\sigma}$ standard deviation: 230 ± 114) with the average values of 154 ± 57, 271 ± 122, 156 ± 18 μg m^{-3} during pre-burning (T1), burning (T2) and post-burning (T3) periods, respectively, reflecting the effect of BB emissions on ambient air quality.
- The $b_{abs\_365\_Water}$ and $b_{abs\_365\_Methanol}$ ranged ~2 to 112 Mm^{-1} (avg: 37±27) and ~3 to 457 Mm^{-1} (avg: 121±108), respectively, suggesting a considerable presence of water-insoluble BrC.
- In linear regression plots of WSOC vs $b_{abs\_365\_Water}$, and OC vs $b_{abs\_365\_Methanol}$, their slopes for day (Water: m = 0.94 ± 0.05, Methanol: m = 1.64 ± 0.06) and night (Water: m = 1.33 ± 0.06, Methanol: m = 2.52 ± 0.12) samples were significantly different. This observation suggests that a significant fraction of water-insoluble chromophores was emitted from BB emissions.
- In the present study, Levoglucosan and K^+ showed a strong correlation with a slope (0.94 ± 0.04, r^2 = 0.87, n = 62) different than those reported for domestic wood burning (Levo/ K^+<0.2), savanna fires (Levo/ K^+~20), and biofuel (Levo/ K^+ = 0.37 ± 0.1) in literature. This ratio (slope) can be used as a fingerprint for the paddy-residue burning over the IGP.
- We observed that BB emits a significant fraction of water-soluble fraction that absorb at the UV region, whereas the water-insoluble fraction absorbs at both UV and visible region. Further, the highest fraction (~86%) of water-insoluble BrC was observed during BB emissions (T2 period).
- At 370 nm, the contribution from MAE of BrC (Water) is ~16-46% and MAE of BrC (Methanol) is~30-88% relative that of EC, indicating the role of BrC in climate forcing.
- %-Water-insoluble fraction was calculated over their different wavelength ranges (R1: 360-400 nm, R2: 410-500 nm, and R3: 510-600 nm). Over Patiala

(BB period), the observed %-water-insoluble fraction during pre-burning (T1: R1 = 63%, R2 = 69%, and R3 = 79%), burning (T2: R1 = 72%, R2 = 77%, and R3 = 85%) and post-burning (T3: R1 = 70%, R2 = 75%, and R3 = 82%) periods were considerable.

5.1.2 Parallel measurements over Patiala and Kanpur during winter period:

In this study, ambient $PM_{2.5}$ samples (24-hour integration time) were collected over Patiala (n = 43) and Kanpur (n = 59) during winter Dec, 2015 to Feb, 2016 period. BrC was extracted using water and methanol and BrC absorption spectra was stored from 300-700 nm for all the samples. Major observations/inferences/conclusions from this study are:

- The $PM_{2.5}$ concentration ranged from ~58 to 251 μg m^{-3} (131 ± 50) and 79 to 336 (167 ± 53) over Patiala and Kanpur, respectively, during the winter period. Primary emission and secondary formation associated with BB and FFB were prominent during winter period over these regions.
- The $b_{abs\_365\_Water}$ and $b_{abs\_365\_Methanol}$ ranged from ~4 to 44 Mm^{-1} (avg: 20 ± 9) and ~13 to 76 Mm^{-1} (avg: 30 ± 16) over Patiala, and ~12 to 60 Mm^{-1} (avg: 27 ± 10) and ~20 to 107 Mm^{-1} (avg: 48 ± 21) over Kanpur, respectively. Both water and methanol soluble BrC concentrations were relatively high over Kanpur. This suggests that Kanpur is more influenced by different emission sources.
- In linear regression plots of WSOC vs $b_{abs\_365\_Water}$ and OC vs $b_{abs\_365\_Methanol}$, their slopes for water (m = 1.11 ± 0.05) and methanol (m= 1.02 ± 0.05) were similar over Patiala. Further, both water and methanol extracted BrC also showed similar spectral characteristics over Patiala. However, the water-soluble BrC is found to be more absorbing compared to methanol soluble BrC, which contradicts the observations made over other sampling sites. This suggests that BrC chromophores over Patiala were highly water soluble.
- In linear regression plots of WSOC vs $b_{abs\_365\_Water}$ and OC vs $b_{abs\_365\_Methanol}$ over Kanpur, slopes for water (m= 0.88 ± 0.06) and methanol (m= 1.44 ± 0.14) plots were significantly different. Methanol Extracted BrC shows higher

absorption compared to water extracted BrC. This observation suggests that water-insoluble BrC chromophores were dominant over Kanpur.

- Mass absorption efficiency (MAE) fraction of BrC over EC is estimated and found to be very high over Kanpur than that over Patiala. At 365 nm, the ratios were ~ 6 times higher at Kanpur than that at Patiala. It is important to note that over Kanpur region, the ambient BrC was also more absorbing.
- %-Water-insoluble fraction was calculated over their different wavelength ranges (R1: 360-400 nm, R2: 410-500 nm, and R3: 510-600 nm). The observed % water-insoluble fractions were 40%, 43% and 45% at R1, R2, and R2, respectively, over Patiala. Similarly, the observed % water-insoluble fractions were 45%, 51% and 60% at R1, R2, and R2, respectively, over Kanpur.

5.1.2.1 Kanpur (Online BrC measurements):

In this study, we conducted semi-continuous measurements of water-soluble organic carbon (WSOC) and BrC using particle-into-liquid sampler coupled with liquid waveguide capillary cell and total carbon analyzer (PILS-LWCC-TOC) over Kanpur during winter season (December 2015 to February 2016). Major observations/inferences/conclusions from this work are:

- Considerable diurnal and day-to-day variability in WSOC concentration and $b_{abs\_365\_Water}$ values were observed. The WSOC varied from 1.0 to 72 µg m^{-3} (avg ± sd: 20 ± 13, 1σ) and b_{abs_365} ranged from 0.02 to 98 Mm^{-1} (24 ± 19) during the study period. This suggests the BrC chromophores concentrations were highly variable during the study period.
- WSOC exhibited a strong correlation with b_{abs_365} (slope =1.22 ± 0.007, r^2 = 0.70, n = 13265, intercept= -0.69 ± 0.17), suggesting that a significant fraction of WSOC is BrC chromophores, which are absorbing at 365 nm.
- Diurnal variability in the absorption coefficient of BrC at 365 nm ($b_{abs\_365\_Water}$) showed higher values (35 ± 21 Mm^{-1}) during late evening to early morning hours and was attributed to primary emissions from biomass burning (BB) and fossil fuel burning (FFB). The b_{abs_365} reduced by more than 80% as the day progressed, which was ascribed to photobleaching/volatilization of BrC and/or due to raising planetary boundary layer (PBL) heights.

- In order to understand the day-to-day variability in BrC composition through absorption spectra, the absorptions at 405, and 420 nm wavelength (representing absorption by different nitro-aromatics) were normalized to the absorption at 365 nm (representing absorption by HULIS compounds). Strong diurnal variability was observed for the ratios of b_{abs_405}/b_{abs_365} and b_{abs_420}/b_{abs_365} which suggests that BrC composition was not uniform throughout the day.
- Mass absorption efficiency (MAE) values of WSOC ranged from 0.003 to 5.26 $m^2\ g^{-1}$ (1.16 ± 0.60) during the study period. This result suggests that the sampling region contains different types of BrC chromophores.
- A moderate correlation (r^2 = 0.50, slope = 1.58 ± 0.019, n = 6471) of $b_{abs\_365\_Water}$ was observed with the semi-volatile oxygenated organic aerosol (SV-OOA) fraction of BB resolved from positive matrix factorization (PMF) analysis of organic mass spectral data obtained from an HR-ToF-AMS. This result suggests that the majority of the BrC chromophores over study region were SV-OOA.
- The low-volatility OOA (LV-OOA) fraction of BB had a similar correlation to $b_{abs\_365\_Water}$ (r^2 = 0.54, slope 0.38 ± 0.004, n = 6442), but appears to have a smaller contribution to the absorption.
- In the scatter plot between WSOC µg $m^{-3}$and $b_{abs\_365\_Water}$, the color axis plotted using elemental ratios (H:C and O:C). We observed high H:C corresponds high $b_{abs\_365nm\_Water}$ and high O:C corresponds to lower $b_{abs\_365nm\_Water}$. It is inferred that over study region primary emitted BrC is more absorbing and absorption reduces as OA gets oxidized.
- Further, higher $b_{abs\_365\_Water}$ value for data points showed a positive relationship with higher WSOC/OA ratios suggests that water-soluble chromophores from respective sources are relatively more absorbing.

5.1.3 Delhi (Winter):

Semi-continuous measurements of water-soluble organic carbon (WSOC) and BrC were also performed using PILS-LWCC-TOC over Delhi during winter season

(December 2017 to February 2018). Major observations/inferences/conclusions from this work are:

- Considerable diurnal and day-to-day variability were observed in WSOC concentration and $b_{abs\_365nm\_Water}$ values. The WSOC varied from 1.0 to 62 µg m^{-3} (avg ± sd: 16 ± 9, 1σ) and b_{abs_365nm} ranged from 0.05 to 65 Mm^{-1} (18 ± 12) during the study period. This result suggests that BrC chromophores are highly variable over the study region.
- WSOC exhibited a strong correlation with an absorption coefficient ($b_{abs\_365\_Water}$) (slope = 1.21 ± 0.007, r^2 = 0.72, n = 11635, intercept = −0.66 ± 0.12), suggesting the presence of a significant but variable fraction of water-soluble chromophores.
- MAE ranged from 0.005 to 3.34 m^2 g^{-1} (1.12 ± 0.46) during the study period. Further, MAE value calculated at different wavelengths; it shows a decreasing trend with increasing wavelength (365 nm: m = 1.20, r^2 = 0.72; 405 nm: m = 0.60, r^2 = 0.72; 420 nm: m = 0.48, r^2 = 0.70; 450 nm: m = 0.371, r^2 = 0.64; 490 nm: m = 0.30, r^2 = 0.52; and 550 nm: m = 0.1, r^2 = 0.46).
- The photochemical secondary organic aerosol formation was evident during morning hours (08:00 to 10:00 hours) whereas variability during late evening/night hours (19:00 to 23:00 hours) is attributed to both due to primary emission and secondary formation of WSOC and $b_{abs\_365\_Water}$.
- Diurnal pattern of MAE also followed similar trends with WSOC and $b_{abs\_365\_Watter}$, and these trends are similar to those observed over Kanpur site.
- Further, diurnal pattern of $b_{abs\_365nm\_Water}$/CO suggests that secondary BrC was dominant throughout the day from 00:00 to 12:00 hours and it reduced during early evening rush hours.
- In January, BrC spectra showed a dual hump with the first peak at 300 nm (likely due to HULIS) and second at 500 nm (likely due to secondary nitroaromatics). The second hump disappeared during day hours, and overall BrC absorption at shorter wavelengths also decreased, which was ascribed to photo-bleaching/volatilization.

5.1.4 NE-Himalayan region (Shillong):

In this study, ambient $PM_{2.5}$ samples (24-hour integration time) were collected over Barapani, Shillong region (n = 35) during Jan-Apr, 2017. BrC was extracted using water and methanol and BrC absorption spectra stored from 300-700 nm for all the samples. Major observations/inferences/conclusions from this work are:

- $PM_{2.5}$ mass concentration ranged from 44 - 144 (avg ± sd: 88 ± 25) during the study period with the highest concentrations in January (100 ± 20) than the rest of the period. January month was influenced by local BB emissions.
- The $b_{abs\_365\_Water}$ and $b_{abs\_365\_Methanol}$ ranged from 5 to 31 M m^{-1} (14 ± 6 M m^{-1}) and 5 – 70 M m^{-1} (27 ± 17 M m^{-1}), respectively, over Shillong region, suggesting the dominance of water-insoluble BrC likely due to local BB emissions during the winter period.
- In linear regression plots of WSOC vs $b_{abs\_365\_Water}$ and OC vs $b_{abs\_365\_Methanol}$, their slopes for water (m = 0.74 ± 0.06) and methanol (m = 1.25 ± 0.12) were significantly different. The methanol-soluble BrC slope is two times higher than water-soluble BrC. The majority (~ 60%) BrC is found to be insoluble in water. The observed % of the water-insoluble fraction was 52%, 60% and 64% at R1, R2, and R2, respectively, over Shillong region.
- Fractional contribution MAE of BrC (Water and Methanol) over that of EC was low.

5.1.5 Port Blair region conclusion of the study:

In this study, ambient PM_{10} samples (24-hour integration time, n = 50) were collected over Port Blair region (Andaman Nicobar group of Islands) during Feb-Mar, 2013. BrC was extracted using water and methanol, and BrC absorption spectra was stored from 300-700 nm for all the samples. Major observations/inferences/conclusions from this work are:

- The $PM_{2.5}$ mass concentration ranged from 23 to 65 μg m^{-3} (42 ± 11) with the average values of 47 ± 5, 43 ± 12, and 38 ± 9 μg m^{-3} during February, March, and April, respectively.

- The $b_{abs\_365\_Water}$ and $b_{abs\_365\_Methanol}$ ranged from 0.4 to 4.2 M m^{-1} (1.4 ± 0.8 M m^{-1}) and 0.8–11.3 M m^{-1} (3.2 ± 1.9 M m^{-1}), respectively. The methanol-soluble BrC was more than two times higher than water-soluble BrC. However, linear regression plots of WSOC vs $b_{abs\_365\_Water}$, and OC vs $b_{abs\_365\_Methanol}$ showed similar slopes for water (0.64 ± 0.06) and methanol (0.74 ± 0.06) extracts. The difference in these slopes suggests that water-soluble chromophores were dominant.
- Further, the monthly variation of $b_{abs\_365\_Water}$ and $b_{abs\_365\_Methanol}$ during February (1.8 ± 0.6 M m^{-1}; 3.5 ± 0.9 M m^{-1}), March (1.6 ± 1.0 M m^{-1}; 3.7 ± 2.4 M m^{-1}), April (0.9 ± 0.3 M m^{-1}; 2.1 ± 0.8 M m^{-1}) showed a decreasing trend. From February to April, both water and methanol-soluble BrC values reduced significantly.
- Both water and methanol extracted BrC showed similar MAE values. Further, EC was found to be well correlated with $b_{abs\_365\_water}$ (r^2 = 0.75) and $b_{abs\_365\_Methanol}$ (r^2 = 0.70), suggesting both water and methanol soluble chromospheres came from the similar source and/or transport pathway. Similarly, BrC absorption relative to EC values also found to be similar for water and methanol extracted BrC.
- The observed %- water-insoluble fraction was 57%, 62% and 65% at R1, R2, and R2, respectively, over Port Blair.

5.1.6 Ahmedabad (November 2015):

Semi-continuous measurements of WSOC and BrC were also performed using PILS-LWCC-TOC over Delhi during November, 2014. Major observations/inferences/conclusions from this work are:

- A considerable day-to-day variability was observed in WSOC concentration and $b_{abs\_365\_Water}$ values. The WSOC varied from 1.0 to 116 µg m^{-3} (avg ± sd: 11 ± 9, 1σ) and $b_{abs\_365\_Water}$ ranged from 1 to 126 Mm^{-1} (10 ± 12) during the study period. This result suggests that BrC chromophores were highly variable during the study period.
- WSOC exhibited a moderate correlation with $b_{abs\_365\_Water}$ (slope = 0.79 ±

0.01, r^2 = 0.44, n = 3949), suggesting that a fraction of WSOC is BrC chromophores, which are absorbing at 365 nm.

- The observed diurnal pattern of $b_{abs\_365\_Water}$ and WSOC was slightly different over Ahmedabad compared to those observed over Kanpur and Delhi sites. During winter period, Kanpur and Delhi sites were largely influenced by BB and FFB emissionswith relatively high concentrations during night over these regionscompared to that over Ahmedabad.
- Diurnal pattern of $b_{abs\_365\_Water}$ peaked in the morning (06:00-09:00) and evening (17:00-22:00), which was attributed to rush hours. However, morning peak for WSOC lasted for more extended period (07:00 to 12:00) compared to $b_{abs\_365\_Water}$.
- Diurnal pattern of WSOC/CO ratio showed a substantial increase from morning to afternoon hours of the day (08:00-16:00), which suggests that SOA formation was dominant during day hours.
- MAE ranged from 0.03 to 3.90 $m^2\ g^{-1}$ (0.97 ± 0.78) during the study period with lower MAE values during day time (attributed to Photo bleaching/ expansion of boundary layer) and high values during night hours.

5.2 Future Scope

This study provides the BrC characteristics of ambient aerosols ($PM_{2.5}$) from urban, rural and high-altitude sites in India using online and offline techniques. However, there is still much work that needs to be done to understand the role of brown carbon in the atmosphere. Understanding photobleaching of BrC chromophores in the atmosphere is one the challenging research area. Also, the increase in the wavelength dependence of BrC absorption suggests that not all BrC molecules respond similarly to photobleaching. Further studies on the molecular speciation of BrC could yield valuable insights into both primary and secondary BrC. Vertical profiles of BrC composition and characteristics through aircraft measurements needs attention. It will allow one to assess the role of BrC on clouds and climate forcing. BrC properties from specific sources can also be assessed through chamber based experiments.

References

Abbatt, J.P.D., Thomas, J.L., Abrahamsson, K., Boxe, C., Granfors, A., Jones, A.E., King, M.D., Saiz-Lopez, A., Shepson, P.B., Sodeau, J., Toohey, D.W., Toubin, C., Glasow, R. Von, Wren, S.N., Yang, X., 2012. Halogen activation via interactions with environmental ice and snow in the polar lower troposphere and other regions. Atmospheric Chemistry and Physics 12, 6237–6271. doi:10.5194/acp-12-6237-2012

Ackerman, T., Toon, O., 1981. Absorption of visible radiation in atmosphere containing mixtures of absorbing and nonabsorbing particles. Applied Optics 20, 3661–3668. doi:10.1364/AO.20.003661

Andreae, M.O., Gelencsér, a., 2006. Black carbon or brown carbon? The nature of light-absorbing carbonaceous aerosols. Atmospheric Chemistry and Physics Discussions 6, 3419–3463. doi:10.5194/acpd-6-3419-2006

Birch, M.E., Cary, R.A., 1996. Elemental Carbon-Based Method for Monitoring Occupational Exposures to Particulate Diesel Exhaust. Aerosol Science and Technology 25, 221–241. doi:10.1080/02786829608965393

Bond, T. C., 2001. Spectral dependence of visible light absorption by carbonaceous particles emitted from coal combustion. Geophysical Research Letters 28(21), 4075-4078

Bond, T.C., Habib, G., Bergstrom, R.W., 2006. Limitations in the enhancement of visible light absorption due to mixing state. Journal of Geophysical Research Atmospheres 111, 1–13. doi:10.1029/2006JD007315

Bond, T.C., Doherty, S.J., Fahey, D.W., Forster, P.M., Berntsen, T., Deangelo, B.J., Flanner, M.G., Ghan, S., Kärcher, B., Koch, D., Kinne, S., Kondo, Y., Quinn, P.K., Sarofim, M.C., Schultz, M.G., Schulz, M., Venkataraman, C., Zhang, H., Zhang, S., Bellouin, N., Guttikunda, S.K., Hopke, P.K., Jacobson, M.Z., Kaiser, J.W., Klimont, Z., Lohmann, U., Schwarz, J.P., Shindell, D., Storelvmo, T., Warren, S.G., Zender, C.S., 2013. Bounding the role of black

carbon in the climate system: A scientific assessment. Journal of Geophysical Research Atmospheres 118, 5380–5552. doi:10.1002/jgrd.50171

Bosch, C., A. Andersson, E. N. Kirillova, K. Budhavant, S. Tiwari, P. S. Praveen, L. M. Russell, N. D. Beres, V. Ramanathan, and Ö. Gustafsson., 2014. Sourcediagnostic dual-isotope composition and optical properties of water-soluble organic carbon and elemental carbon in the South Asian outflow intercepted over the Indian Ocean. Journal of Geophysical Research: Atmospheres 119, 11,743–11,759. doi:10.1002/ 2014JD022127.

Budisulistiorini, S.H., Riva, M., Williams, M., Chen, J., Itoh, M., Surratt, J.D., Kuwata, M., 2017. Light-Absorbing Brown Carbon Aerosol Constituents from Combustion of Indonesian Peat and Biomass. Environmental Science and Technology 51, 4415−4423. https://doi.org/10.1021/acs.est.7b00397

Carbon, S., 1983. Soot Carbon and Excess Fine Potassium: Long-Range Transport of Combustion-Derived Aerosols Abstract. Science 220, 10–13.

Caseiro, A., Bauer, H., Schmidl, C., Pio, C.A., Puxbaum, H., 2009. Wood burning impact on PM10in three Austrian regions. Atmospheric Environment 43, 2186–2195. https://doi.org/10.1016/j.atmosenv.2009.01.012

Chakraborty, A., Bhattu, D., Gupta, T., Tripathi, S.N., Canagaratna, M.R., 2015. Real-time measurements of ambient aerosols in a polluted Indian city: Sources, characteristics, and processing of organic aerosols during foggy and nonfoggy periods. Journal of Geophysical Research 120, 9006–9019. https://doi.org/10.1002/2015JD023419

Chanpimol, S., Seamon, B., Hernandez, H., Harris-love, M., Blackman, M.R., 2017. HHS Public Access 527. doi: 10.1186/s40945-017-0033-9.Using

Chen, Y., Bond, T.C., 2009. Light absorption by organic carbon from wood combustion. Atmospheric Chemistry Physics Discussions. 9, 20471–20513. https://doi.org/10.5194/acpd-9-20471-2009

Cheng, Y., Engling, G., He, K.B., Duan, F.K., Ma, Y.L., Du, Z.Y., Liu, J.M., Zheng, M., Weber, R.J., 2013. Biomass burning contribution to Beijing aerosol. Atmospheric Chemistry Physics 13, 7765–7781. https://doi.org/10.5194/acp-13-7765-2013

Cheng, Y., He, K. bin, Du, Z. yu, Engling, G., Liu, J. meng, Ma, Y. liang, Zheng, M., Weber, R.J., 2016. The characteristics of brown carbon aerosol during winter in Beijing. Atmospheric Environment 127, 355–364. https://doi.org/10.1016/j.atmosenv.2015.12.035

Chowdhury, S., Dey, S., Tripathi, S.N., Beig, G., Mishra, A.K., Sharma, S., 2017. "Traffic intervention" policy fails to mitigate air pollution in megacity Delhi. Environmental Science and Policy 74, 8–13. doi: 10.1016/j.envsci.2017.04.018

Desyaterik, Y., Sun, Y., Shen, X., Lee, T., Wang, X., Wang, T., Collett, J.L., 2013. Speciation of "brown" carbon in cloud water impacted by agricultural biomass burning in eastern China. Journal of Geophysical Research: Atmospheres 118, 7389–7399. https://doi.org/10.1002/jgrd.50561

Doney, S. C., Mahowald, N., Lima, I., Feely, R. A., Mackenzie, F. T., Lamarque, J. F., & Rasch, P. J., 2007. Impact of anthropogenic atmospheric nitrogen and sulfur deposition on ocean acidification and the inorganic carbon system. Proceedings of the National Academy of Sciences, 104 (37), 14580-14585

Di Lorenzo, R.A., Washenfelder, R.A., Attwood, A.R., Guo, H., Xu, L., Ng, N.L., Weber, R.J., Baumann, K., Edgerton, E., Young, C.J., 2017. Molecular-Size-Separated Brown Carbon Absorption for Biomass-Burning Aerosol at Multiple Field Sites. Environmental Science and Technology 51, 3128−3137. https://doi.org/10.1021/acs.est.6b06160

Drewnick, F., Hings, S.S., Curtius, J., Eerdekens, G., Williams, J., 2006. Measurement of fine particulate and gas-phase species during the New Year's

fireworks 2005 in Mainz, Germany. Atmospheric Environment 40, 4316–4327. https://doi.org/10.1016/j.atmosenv.2006.03.040

Drozd, G.T., McNeill, V.F., 2014. Organic matrix effects on the formation of light-absorbing compounds from α-dicarbonyls in aqueous salt solution. Environmental Sciences: Processes and Impacts 16, 741–747. doi:10.1039/c3em00579h

Dusek, U., Andreae, M.O., Curtius, J., Schneider, J., Frank, G.P., Hildebrandt, L., Walter, S., Chand, D., Drewnick, F., Hings, S., Jung, D., Borrmann, S., 2006. Size Matters More Than Chemistry for Cloud-Nucleating Ability of Aerosol Particles. Science 312, 1375–1378. doi:10.1126/science.1125261

Ervens, B., Carlton, A.G., Turpin, B.J., Altieri, K.E., Kreidenweis, S.M., Feingold, G., 2008. Secondary organic aerosol yields from cloud-processing of isoprene oxidation products. Geophysical Research Letters 35, 4–8. doi:10.1029/2007GL031828

Ervens, B., Turpin, B.J., Weber, R.J., 2011. Secondary organic aerosol formation in cloud droplets and aqueous particles (aqSOA): A review of laboratory, field and model studies. Atmospheric Chemistry and Physics 11, 11069–11102. doi:10.5194/acp-11-11069-2011

Feng, J.L., Guo, Z.G., Zhang, T.R., Yao, X.H., Chan, C.K., Fang, M., 2012. Source and formation of secondary particulate matter in PM 2.5 in Asian continental outflow. Journal of Geophysical Research Atmospheres 117, 1–11. https://doi.org/10.1029/2011JD016400

Feng, Y., Ramanathan, V., Kotamarthi, V.R., 2013. Brown carbon: A significant atmospheric absorber of solar radiation. Atmospheric Chemistry and Physics 13, 8607–8621. doi:10.5194/acp-13-8607-2013

Forrister, H., Liu, J., Scheuer, E., Dibb, J., Ziemba, L., Thornhill, K.L., Anderson, B., Diskin, G., Perring, A.E., Schwarz, J.P., Campuzano-Jost, P., Day, D.A., Palm, B.B., Jimenez, J.L., Nenes, A., Weber, R.J., 2015. Evolution of brown

carbon in wildfire plumes. Geophysical Research Letters 42, 4623–4630. doi:10.1002/2015GL063897

Froyd, K.D., Murphy, D.M., Lawson, P., Baumgardner, D., Herman, R.L., 2010. Aerosols that form subvisible cirrus at the tropical tropopause. Atmospheric Chemistry and Physics 10, 209–218. doi:10.5194/acp-10-209-2010

Graber, E.R., Rudich, Y., 2006. Atmospheric HULIS: How humic-like are they? A comprehensive and critical review. Atmospheric Chemistry Physics 6, 729–753. https://doi.org/10.5194/acp-6-729-2006

Gustafsson, Ö., Kruså, M., Zencak, Z., Sheesley, R.J., Granat, L., 2009. Brown Clouds over South Asia: Biomass or Brown Clouds over South Asia: Science 84. doi:10.1126/science.1164857

Hallquist, M., Wenger, J. C., Baltensperger, U., Rudich, Y., Simpson, D., Claeys, M., Dommen, J., Donahue, N. M., George, C., Goldstein, A. H., Hamilton, J. F., Herrmann, H., Hoffmann, T., Iinuma, Y., Jang, M., Jenkin, M. E., Jimenez, J. L., Kiendler-Scharr, A., Maenhaut, W., McFiggans, G., Mentel, Th. F., Monod, A., Prévôt, A. S. H., Seinfeld, J. H., Surratt, J. D., Szmigielski, R., and Wildt, J., 2009. The formation, properties and impact of secondary organic aerosol: current and emerging issues. Atmospheric Chemistry Physics 9, 5155-5236, https://doi.org/10.5194/acp-9-5155-2009

Hamilton, J.F., Baeza-Romero, M.T., Finessi, E., Rickard, A.R., Healy, R.M., Peppe, S., Adams, T.J., Daniels, M.J.S., Ball, S.M., Goodall, I.C.A., Monks, P.S., Borrás, E., Muñoz, A., 2013. Online and offline mass spectrometric study of the impact of oxidation and ageing on glyoxal chemistry and uptake onto ammonium sulfate aerosols. Faraday Discussions 165, 447–472. doi:10.1039/c3fd00051f

Hansen, J., Sato, M., Ruedy, R., 1997. Radiative forcing and climate response. Journal of Geophysical Research: Atmospheres 102, 6831–6864. doi:10.1029/96JD03436

Hecobian, A., Zhang, X., Zheng, M., Frank, N., Edgerton, E.S., Weber, R.J., 2010. Water-soluble organic aerosol material and the light-absorption characteristics of aqueous extracts measured over the Southeastern United States. Atmospheric Chemistry Physics 10, 5965–5977. https://doi.org/10.5194/acp-10-5965-2010

Hems, R.F., Abbatt, J.P.D., 2018. Aqueous Phase Photo-oxidation of Brown Carbon Nitrophenols: Reaction Kinetics, Mechanism, and Evolution of Light Absorption. ACS Earth and Space Chemistry 2, 225–234. https://doi.org/10.1021/acsearthspacechem.7b00123

Herich, H., Hueglin, C., Buchmann, B., 2011. A 2.5 year's source apportionment study of black carbon from wood burning and fossil fuel combustion at urban and rural sites in Switzerland. Atmospheric Measurement Techniques 4, 1409–1420. https://doi.org/10.5194/amt-4-1409-2011

Hoffer, A., Gelencsér, A., Guyon, P., Kiss, G., Schmid, O., Frank, G.P., Artaxo, P., Andreae, M.O., 2006. Optical properties of humic-like substances (HULIS) in biomass-burning aerosols. Atmospheric Chemistry Physics 6, 3563–3570. https://doi.org/10.5194/acp-6-3563-2006

Hoyle, C.R., Boy, M., Donahue, N.M., Fry, J.L., Glasius, M., Guenther, A., Hallar, A.G., Huff Hartz, K., Petters, M.D., Petäjä, T., Rosenoern, T., Sullivan, A.P., 2011. A review of the anthropogenic influence on biogenic secondary organic aerosol. Atmospheric Chemistry and Physics 11, 321–343. doi:10.5194/acp-11-321-2011

Hu, Q.H., Xie, Z.Q., Wang, X.M., Kang, H., Zhang, P., 2013. Levoglucosan indicates high levels of biomass burning aerosols over oceans from the Arctic to Antarctic. Scientific Reports 3, 1–7. https://doi.org/10.1038/srep03119

Jacobson, M.C., Hansson, H.-C.C., Noone, K.J., Charlson, R.J., 2000. Organic Atmospheric Aerosols: Review and State of the Science. Reviews of Geophysics, 267–294. doi:10.1029/1998RG000045

Jacobson, M.Z., 2014. Effects of biomass burning on climate, accounting for heat and moisture fluxes, black and brown carbon, and cloud absorption effects. Journal of Geophysical Research: Atmospheres 1–23. doi: 10.1002/2014JD021861.Received

Jiang, X.Q., Mei, X.D., Feng, D., 2016. Air pollution and chronic airway diseases: What should people know and do? Journal of Thoracic Disease 8, E31–E40. doi: 10.3978/j.issn.2072-1439.2015.11.50

Jimenez, J.L., Canagaratna, M.R., Donahue, N.M., Prevot, a. S.H., Zhang, Q., Kroll, J.H., DeCarlo, P.F., Allan, J.D., Coe, H., Ng, N.L., Aiken, a. C., Docherty, K.S., Ulbrich, I.M., Grieshop, A.P., Robinson, a. L., Duplissy, J., Smith, J.D., Wilson, K.R., Lanz, V. a., Hueglin, C., Sun, Y.L., Tian, J., Laaksonen, A., Raatikainen, T., Rautiainen, J., Vaattovaara, P., Ehn, M., Kulmala, M., Tomlinson, J.M., Collins, D.R., Cubison, M.J., Dunlea, J., Huffman, J.A., Onasch, T.B., Alfarra, M.R., Williams, P.I., Bower, K., Kondo, Y., Schneider, J., Drewnick, F., Borrmann, S., Weimer, S., Demerjian, K., Salcedo, D., Cottrell, L., Griffin, R., Takami, a., Miyoshi, T., Hatakeyama, S., Shimono, A., Sun, J.Y., Zhang, Y.M., Dzepina, K., Kimmel, J.R., Sueper, D., Jayne, J.T., Herndon, S.C., Trimborn, a. M., Williams, L.R., Wood, E.C., Middlebrook, A.M., Kolb, C.E., Baltensperger, U., Worsnop, D.R., Dunlea, E.J., Huffman, J.A., Onasch, T.B., Alfarra, M.R., Williams, P.I., Bower, K., Kondo, Y., Schneider, J., Drewnick, F., Borrmann, S., Weimer, S., Demerjian, K., Salcedo, D., Cottrell, L., Griffin, R., Takami, a., Miyoshi, T., Hatakeyama, S., Shimono, A., Sun, J.Y., Zhang, Y.M., Dzepina, K., Kimmel, J.R., Sueper, D., Jayne, J.T., Herndon, S.C., Trimborn, a. M., Williams, L.R., Wood, E.C., Middlebrook, A.M., Kolb, C.E., Baltensperger, U., Worsnop, D.R., Dunlea, J., Huffman, J.A., Onasch, T.B., Alfarra, M.R., Williams, P.I., Bower, K., Kondo, Y., Schneider, J., Drewnick, F., Borrmann, S., Weimer, S., Demerjian, K., Salcedo, D., Cottrell, L., Griffin, R., Takami, a., Miyoshi, T., Hatakeyama, S., Shimono, A., Sun, J.Y., Zhang, Y.M., Dzepina, K., Kimmel, J.R., Sueper, D., Jayne, J.T., Herndon, S.C., Trimborn, a. M., Williams, L.R., Wood, E.C., Middlebrook, A.M., Kolb, C.E., Baltensperger, U., Worsnop, D.R., Dunlea,

E.J., Huffman, J.A., Onasch, T.B., Alfarra, M.R., Williams, P.I., Bower, K., Kondo, Y., Schneider, J., Drewnick, F., Borrmann, S., Weimer, S., Demerjian, K., Salcedo, D., Cottrell, L., Griffin, R., Takami, a., Miyoshi, T., Hatakeyama, S., Shimono, A., Sun, J.Y., Zhang, Y.M., Dzepina, K., Kimmel, J.R., Sueper, D., Jayne, J.T., Herndon, S.C., Trimborn, a. M., Williams, L.R., Wood, E.C., Middlebrook, A.M., Kolb, C.E., Baltensperger, U., Worsnop, D.R., 2009. Evolution of Organic Aerosols in the Atmosphere. Science 326, 1525–1529. doi:10.1126/science.1180353

Kanakidou, M., 2005. Organic aerosol and global climate modelling: A review, Atmospheric Chemistry Physics 5, 1053–1123.

Karl, M., Tsigaridis, K., Vignati, E., Dentener, F., 2009. Formation of secondary organic aerosol from isoprene oxidation over Europe. Atmospheric Chemistry and Physics 9, 7003–7030. doi:10.5194/acp-9-7003-2009

Kaul, D.S., Gupta, T., Tripathi, S.N., Tare, V., Collett, J.L., 2011. Secondary organic aerosol: A comparison between foggy and nonfoggy days. Environmental Science and Technology 45, 7307–7313. doi:10.1021/es201081d

Kirchstetter, T.W., Novakov, T., Hobbs, P. V., 2004. Evidence that the spectral dependence of light absorption by aerosols is affected by organic carbon. Journal of Geophysical Research D: Atmospheres 109, 1–12. doi:10.1029/2004JD004999

Kirillova, E.N., Andersson, A., Han, J., Lee, M., Gustafsson, Ö, 2014a. Sources and light absorption of water-soluble organic carbon aerosols in the outflow from northern China. Atmospheric Chemistry Physics 14, 1413–1422. https://doi.org/10.5194/acp-14-1413-2014

Kirillova, E.N., Andersson, A., Tiwari, S., Srivastava, A.K., Bisht, D.S., Gustafsson, Ö., 2014. Water-soluble organic carbon aerosols during a full New Delhi winter: Isotope-based source apportionment and optical properties.

Journal of Geophysical Research: Atmospheres 19, 3476-3485. https://doi.org/10.1002/2013JD020041.Received

Krishnamurthy, A., Moore, J.K., Mahowald, N., Luo, C., Zender, C.S., 2010. Impacts of atmospheric nutrient inputs on marine biogeochemistry. Journal of Geophysical Research 115, G01006. doi:10.1029/2009JG001115

Lack, D.A., Cappa, C.D., 2010. Impact of brown and clear carbon on light absorption enhancement, single scatter albedo and absorption wavelength dependence of black carbon. Atmospheric Chemistry and Physics 10, 4207–4220. doi:10.5194/acp-10-4207-2010

Lack, D. A., Langridge, J.M., Bahreini, R., Cappa, C.D., Middlebrook, a. M., Schwarz, J.P., 2012. Brown carbon and internal mixing in biomass burning particles. Proceedings of the National Academy of Sciences 109, 14802–14807. https://doi.org/10.1073/pnas.1206575109

Lack, D.A., Bahreini, R., Langridge, J.M., Gilman, J.B., Middlebrook, A.M., 2013. Brown carbon absorption linked to organic mass tracers in biomass burning particles. Atmospheric Chemistry and Physics 13, 2415–2422. doi:10.5194/acp-13-2415-2013

Lambe, A.T., Cappa, C.D., Massoli, P., Onasch, T.B., Forestieri, S.D., Martin, A.T., Cummings, M.J., Croasdale, D.R., Brune, W.H., Worsnop, D.R., Davidovits, P., 2013. Relationship between oxidation level and optical properties of secondary organic aerosol. Environmental Science and Technology 47, 6349–6357. doi:10.1021/es401043j

Laskin, A., Laskin, J., Nizkorodov, S.A., 2015. Chemistry of Atmospheric Brown Carbon. Chemical Reviews 115, 4335–4382. https://doi.org/10.1021/cr5006167

Lee, H.J., Aiona, P.K., Laskin, A., Laskin, J., Nizkorodov, S.A., 2014. Effect of solar radiation on the optical properties and molecular composition of

laboratory proxies of atmospheric brown carbon. Environmental Science and Technology. 48, 10217–10226. https://doi.org/10.1021/es502515r

Leeuw, G. De, Cohen, L., Frohn, L.M., Geernaert, G., Hertel, O., Jensen, B., Jickells, T., Klein, L., Kunz, G.J., Lund, S., Moerman, M., Müller, F., Pedersen, B., Salzen, K. Von, Heinke Schlünzen, K., Schulz, M., Skjøth, C.A., Sorensen, L.L., Spokes, L., Tamm, S., Vignati, E., 2001. Atmospheric input of nitrogen into the North Sea: Anice project overview. Continental Shelf Research 21, 2073–2094. doi:10.1016/S0278-4343(01)00043-7

Lin, G., Penner, J.E., Flanner, M.G., Sillman, S., Xu, L., Zhou, C., 2014. Radiative forcing of organic aerosol in the atmosphere and on snow: Effects of SOA and brown carbon. Journal of Geophysical Research: Atmospheres 119, 7453–7476. doi:10.1002/2013JD021186

Lin, P., Aiona, P.K., Li, Y., Shiraiwa, M., Laskin, J., Nizkorodov, S.A., Laskin, A., 2016. Molecular Characterization of Brown Carbon in Biomass Burning Aerosol Particles. Environmental Science and Technology 50, 11815–11824. https://doi.org/10.1021/acs.est.6b03024

Lin, P., Bluvshtein, N., Rudich, Y., Nizkorodov, S.A., Laskin, J., Laskin, A., 2017. Molecular Chemistry of Atmospheric Brown Carbon Inferred from a Nationwide Biomass Burning Event. Environmental Science and Technology 51, 11561−11570. https://doi.org/10.1021/acs.est.7b02276

Lin, P., Laskin, J., Nizkorodov, S.A., Laskin, A., 2015a. Revealing Brown Carbon Chromophores Produced in Reactions of Methylglyoxal with Ammonium Sulfate. Environmental Science and Technology 49, 14257–14266. https://doi.org/10.1021/acs.est.5b03608

Lin, P., Liu, J., Shilling, J.E., Kathmann, S.M., Laskin, J., Laskin, A., 2015b. Molecular characterization of brown carbon (BrC) chromophores in secondary organic aerosol generated from photo-oxidation of toluene. Physical

Chemistry Chemical Physics 17, 23312–23325. https://doi.org/10.1039/C5CP02563J

Liu, J., Bergin, M., Guo, H., King, L., Kotra, N., Edgerton, E., Weber, R.J., 2013. Size-resolved measurements of brown carbon in water and methanol extracts and estimates of their contribution to ambient fine-particle light absorption. Atmospheric Chemistry Physics 13, 12389–12404. https://doi.org/10.5194/acp-13-12389-2013

Liu, J., Lin, P., Laskin, A., Laskin, J., Kathmann, S.M., Wise, M., Caylor, R., Imholt, F., Selimovic, V., Shilling, J.E., 2016. Optical properties and aging of light-absorbing secondary organic aerosol. Atmospheric Chemistry Physics 16, 12815–12827. https://doi.org/10.5194/acp-16-12815-2016

Liu, J., Scheuer, E., Dibb, J., Diskin, G.S., Ziemba, L.D., Thornhill, K.L., Anderson, B.E., Wisthaler, A., Mikoviny, T., Devi, J.J., Bergin, M., Perring, A.E., Markovic, M.Z., Schwarz, J.P., Campuzano-Jost, P., Day, D.A., Jimenez, J.L., Weber, R.J., 2015. Brown carbon aerosol in the North American continental troposphere: Sources, abundance, and radiative forcing. Atmospheric Chemistry Physics 15, 7841–7858. https://doi.org/10.5194/acp-15-7841-2015

Lu, J.W., Flores, J.M., Lavi, A., Abo-Riziq, A., Rudich, Y., 2011. Changes in the optical properties of benzo[a]pyrene-coated aerosols upon heterogeneous reactions with NO_2 and NO_3. Physical Chemistry Chemical Physics 13, 6484–6492. doi:10.1039/c0cp02114h

Lukács, H., Gelencsér, A., Hammer, S., Puxbaum, H., Pio, C.A., Legrand, M., Kasper-Giebl, A., Handler, M., Limbeck, A., Simpson, D., Preunkert, S., 2007. Seasonal trends and possible sources of brown carbon based on 2-year aerosol measurements at six sites in Europe. Journal of Geophysical Research: Atmospheres 112, 1–9. https://doi.org/10.1029/2006JD008151

Luo, C., Zender, C.S., Bian, H., Metzger, S., 2007. Role of ammonia chemistry and coarse mode aerosols in global climatological inorganic aerosol distributions. Atmospheric Environment 41, 2510–2533. doi: 10.1016/j.atmosenv.2006.11.030

Mahanta, R., Sarma, D., Choudhury, A., 2013. Heavy rainfall occurrences in northeast India. International Journal of Climatology 33, 1456–1469. https://doi.org/10.1002/joc.3526

Mauderly, J.L., Chow, J.C., 2008. Health effects of organic aerosols, Inhalation Toxicology. doi:10.1080/08958370701866008

Nikulin, A.Y., Davis, J.R., 1998. Refraction phenomena in X-ray scattering experiments performed with a narrow collimator aperture. Optics Communications 155, 231–235. doi:10.1016/S0030-4018(98)00375-7

Ng, N.L., Kwan, A.J., Surratt, J.D., Chan, A.W.H., Chhabra, P.S., Sorooshian, A., Pye, H.O.T., Crounse, J.D., Wennberg, P.O., Flagan, R.C., Seinfeld, J.H., 2008. Secondary organic aerosol (SOA) formation from reaction of isoprene with nitrate radicals (NO_3). Atmospheric Chemistry and Physics 8, 4117–4140. doi:10.5194/acp-8-4117-2008

Ofner, J., Kŕuger, H.U., Grothe, H., Schmitt-Kopplin, P., Whitmore, K., Zetzsch, C., 2011. Physico-chemical characterization of SOA derived from catechol and guaiacol - A model substance for the aromatic fraction of atmospheric HULIS. Atmospheric Chemistry and Physics 11, 1–15. doi:10.5194/acp-11-1-2011

Pope, C.A., Ezzati, M., Dockery, D.W., 2009. Fine-Particulate Air Pollution and Life Expectancy in the United States. New England Journal of Medicine 360, 376–386. doi:10.1056/NEJMsa0805646

Rajput, P., Sarin, M., Kundu, S.S., 2013. Atmospheric particulate matter (PM2.5), EC, OC, WSOC and PAHs from NE–Himalaya: abundances and chemical

characteristics. Atmospheric Pollution Research 4, 214–221. https://doi.org/10.5094/APR.2013.022

Rajput, P., Sarin, M.M., 2014. Polar and non-polar organic aerosols from large-scale agricultural-waste burning emissions in Northern India: Implications to organic mass-to-organic carbon ratio. Chemosphere 103, 74–79. https://doi.org/10.1016/j.chemosphere.2013.11.028

Rajput, P., Gupta, T., Kumar, A., 2016. The diurnal variability of sulfate and nitrate aerosols during wintertime in the Indo-Gangetic Plain: Implications for heterogeneous phase chemistry. RSC Advances 6. https://doi.org/10.1039/c6ra19595d

Ram, K., Sarin, M.M., 2009. Absorption coefficient and site-specific mass absorption efficiency of elemental carbon in aerosols over urban, rural, and high-altitude sites in India. Environmental Science and Technology 43, 8233–8239. doi:10.1021/es9011542

Ram, K., Sarin, M.M., 2011. Day-night variability of EC, OC, WSOC and inorganic ions in urban environment of Indo-Gangetic Plain: Implications to secondary aerosol formation. Atmospheric Environment 45, 460–468. https://doi.org/10.1016/j.atmosenv.2010.09.055

Rastogi, N., Sarin, M.M., 2009. Quantitative chemical composition and characteristics of aerosols over western India: One-year record of temporal variability. Atmospheric Environment 43, 3481–3488. doi: 10.1016/j.atmosenv.2009.04.030

Rastogi, N., Singh, A., Singh, D., Sarin, M.M., 2014. Chemical characteristics of PM2.5 at a source region of biomass burning emissions: Evidence for secondary aerosol formation. Environmental Pollution 184, 563–569. https://doi.org/10.1016/j.envpol.2013.09.037

Rastogi, N., Patel, A., Singh, A., Singh, D., 2015. Diurnal variability in secondary organic aerosol formation over the Indo-Gangetic Plain during winter using online measurement of water-soluble organic carbon. Aerosol Air Quality Research 15, 2225–2231. https://doi.org/10.4209/aaqr.2015.02.0097

Rastogi, N., Singh, A., Satish, R., 2018. Characteristics of submicron particles coming from a big firecrackers burning event: Implications to atmospheric pollution. Atmospheric Pollution Research (inpress). doi: 10.1016/j.apr.2018.11.002

Rengarajan, R., Sarin, M.M., Sudheer, A.K., 2007. Carbonaceous and inorganic species in atmospheric aerosols during wintertime over urban and high-altitude sites in North India. Journal of Geophysical Research: Atmospheres 112, 1–16. doi:10.1029/2006JD008150

Riipinen, I., Pierce, J.R., Yli-Juuti, T., Nieminen, T., Häkkinen, S., Ehn, M., Junninen, H., Lehtipalo, K., Petäjä, T., Slowik, J., Chang, R., Shantz, N.C., Abbatt, J., Leaitch, W.R., Kerminen, V.M., Worsnop, D.R., Pandis, S.N., Donahue, N.M., Kulmala, M., 2011. Organic condensation: A vital link connecting aerosol formation to cloud condensation nuclei (CCN) concentrations. Atmospheric Chemistry and Physics 11, 3865–3878. doi:10.5194/acp-11-3865-2011

Robinson, N.H., Hamilton, J.F., Allan, J.D., Langford, B., Oram, D.E., Chen, Q., Docherty, K., Farmer, D.K., Jimenez, J.L., Ward, M.W., Hewitt, C.N., Barley, M.H., Jenkin, M.E., Rickard, A.R., Martin, S.T., McFiggans, G., Coe, H., 2011. Evidence for a significant proportion of secondary organic aerosol from isoprene above a maritime tropical forest. Atmospheric Chemistry and Physics 11, 1039–1050. doi:10.5194/acp-11-1039-2011

Sahai, S., Sharma, C., Singh, D.P., Dixit, C.K., Singh, N., Sharma, P., Singh, K., Bhatt, S., Ghude, S., Gupta, V., Gupta, R.K., Tiwari, M.K., Garg, S.C., Mitra, A.P., Gupta, P.K., 2007. A study for development of emission factors for trace gases and carbonaceous particulate species from in situ burning of wheat straw

in agricultural fields in india. Atmospheric Environment 41, 9173–9186. doi: 10.1016/j.atmosenv.2007.07.054

Sareen, N., Moussa, S.G., McNeill, V.F., 2013. Photochemical aging of light-absorbing secondary organic aerosol material. Journal of Physical Chemistry A 117, 2987–2996. https://doi.org/10.1021/jp309413j

Satish, R., Shamjad, P., Thamban, N., Tripathi, S., Rastogi, N., 2017. Temporal Characteristics of Brown Carbon over the Central Indo-Gangetic Plain. Environmental Science and Technology 51, 6765–6772. https://doi.org/10.1021/acs.est.7b00734

Schkolnik, G., Falkovich, A.H., Rudich, Y., Maenhaut, W., Artaxo, P., 2005. New analytical method for the determination of levoglucosan, polyhydroxy compounds, and 2-methylerythritol and its application to smoke and rainwater samples. Environmental Science and Technology 39, 2744–2752. https://doi.org/10.1021/es048363c

Seinfeld, J. H. and Pandis, S. N., 2006. Atmospheric Chemistry and Physics: From Air Pollution to Climate Change, John Wiley & Sons, New York, 2nd edition, 1232 pp., ISBN-13: 978-0-471- 72018-8.

Seinfeld, J.H., Pankow, J.F., 2003.Organic Atmospheric Particulate matter. Annual Review of Physical Chemistry 54, 121–140. doi: 10.1146/annurev.physchem.54.011002.103756

Shamjad, P.M., Tripathi, S.N., Pathak, R., Hallquist, M., Arola, A., Bergin, M.H., 2015. Contribution of Brown Carbon to Direct Radiative Forcing over the Indo-Gangetic Plain. Environmental Science and Technology 49, 10474–10481. doi: 10.1021/acs.est.5b03368

Simoneit, B.R.T., Schauer, J.J., Nolte, C.G., Oros, D.R., Elias, V.O., Fraser, M.P., Rogge, W.F., Cass, G.R., 1999. Levoglucosan, a tracer for cellulose in biomass burning and atmospheric particles. Atmospheric Environment 33, 173–182. https://doi.org/10.1016/S1352-2310(98)00145-9

Singh, A., Rajput, P., Sharma, D., Sarin, M.M., Singh, D., 2014. Black carbon and elemental carbon from postharvest agricultural-waste burning emissions in the Indo-Gangetic plain. Advance Meteorology 2014. https://doi.org/10.1155/2014/179301

Singh, A., Rastogi, N., Patel, A., Satish, R.V., Singh, D., 2016. Size-Segregated Characteristics of Carbonaceous Aerosols over the Northwestern Indo-Gangetic Plain: Year Round Temporal Behavior. Aerosol Air Quality Research 16, 1615–1624. https://doi.org/10.4209/aaqr.2016.01.0023

Spracklen, D. V., Jimenez, J.L., Carslaw, K.S., Worsnop, D.R., Evans, M.J., Mann, G.W., Zhang, Q., Canagaratna, M.R., Allan, J., Coe, H., McFiggans, G., Rap, A., Forster, P., 2011. Aerosol mass spectrometer constraint on the global secondary organic aerosol budget. Atmospheric Chemistry and Physics 11, 12109–12136. doi:10.5194/acp-11-12109-2011

Srinivas, B., Sarin, M.M., 2013. Light absorbing organic aerosols (brown carbon) over the tropical Indian Ocean: Impact of biomass burning emissions. Environmental Research Letters 8. https://doi.org/10.1088/1748-9326/8/4/044042

Srinivas, B., Sarin, M.M., 2014. Brown carbon in atmospheric outflow from the Indo-Gangetic Plain: Mass absorption efficiency and temporal variability. Atmospheric Environment 89, 835–843. https://doi.org/10.1016/j.atmosenv.2014.03.030

Srinivas, B., Rastogi, N., Sarin, M.M., Singh, A., Singh, D., 2016. Mass absorption efficiency of light absorbing organic aerosols from source region of paddy-residue burning emissions in the Indo-Gangetic Plain. Atmospheric Environment 125, 360–370. https://doi.org/10.1016/j.atmosenv.2015.07.017

Sudheer, A.K., Rengarajan, R., 2015. Time-resolved inorganic chemical composition of fine aerosol and associated precursor gases over an urban environment in western India: Gas-aerosol equilibrium characteristics.

Atmospheric Environment 109, 217–227. https://doi.org/10.1016/j.atmosenv.2015.03.028

Sun, H., Biedermann, L., Bond, T.C., 2007. Color of brown carbon: A model for ultraviolet and visible light absorption by organic carbon aerosol. Geophysical Research Letters 34, 1–5. https://doi.org/10.1029/2007GL029797

Sun, J., Zhi, G., Hitzenberger, R., Chen, Y., Tian, C., Zhang, Y., Feng, Y., Cheng, M., Zhang, Y., Cai, J., Chen, F., Qiu, Y., Jiang, Z., Li, J., Zhang, G., Mo, Y., 2017. Emission factors and light absorption properties of brown carbon from household coal combustion in China. Atmospheric Chemistry and Physics 17, 4769–4780. doi:10.5194/acp-17-4769-2017

Tripathi, S.N., Tare, V., Chinnam, N., Srivastava, A.K., Dey, S., Agarwal, A., Kishore, S., Lal, R.B., Manar, M., Kanawade, V.P., Chauhan, S.S.S., Sharma, M., Reddy, R.R., Gopal, K.R., Narasimhulu, K., Reddy, L.S.S., Gupta, S., Lal, S., 2006. Measurements of atmospheric parameters during Indian Space Research Organization Geosphere Biosphere Program Land Campaign II at a typical location in the Ganga Basin: 2. Chemical properties. Journal of Geophysical Research 111. doi:10.1029/2006JD007278

Updyke, K.M., Nguyen, T.B., Nizkorodov, S.A., 2012. Formation of brown carbon via reactions of ammonia with secondary organic aerosols from biogenic and anthropogenic precursors. Atmospheric Environment 63, 22–31. https://doi.org/10.1016/j.atmosenv.2012.09.012

Verma, S., Payra, S., Gautam, R., Prakash, D., Soni, M., Holben, B., Bell, S., 2013. Dust events and their influence on aerosol optical properties over Jaipur in Northwestern India. Environmental Monitoring and Assessment 185, 7327–7342. doi:10.1007/s10661-013-3103-9

Wang, G., Kawamura, K., Xie, M., Hu, S., Gao, S., Cao, J., An, Z., Wang, Z., 2009. Size-distributions of n-alkanes, PAHs and hopanes and their sources in the urban, mountain and marine atmospheres over East Asia. Atmospheric Chemistry Physics 9, 8869–8882. https://doi.org/10.5194/acp-9-8869-2009

Wang, H., Kawamura, K., Shooter, D., 2005. Carbonaceous and ionic components in wintertime atmospheric aerosols from two New Zealand cities: Implications for solid fuel combustion. Atmospheric Environment 39, 5865–5875. https://doi.org/10.1016/j.atmosenv.2005.06.031

Wang, Y., Hu, M., Lin, P., Guo, Q., Wu, Z., Li, M., Zeng, L., Song, Y., Zeng, L., Wu, Y., Guo, S., Huang, X., He, L., 2017. Molecular Characterization of Nitrogen-Containing Organic Compounds in Humic-like Substances Emitted from Straw Residue Burning, Environmental Science and Technology 51, 5951−5961. doi: 10.1021/acs.est.7b00248

Wang, Y., Zhuang, G., Xu, C., An, Z., 2007. The air pollution caused by the burning of fireworks during the lantern festival in Beijing. Atmospheric Environment 41, 417–431. https://doi.org/10.1016/j.atmosenv.2006.07.043

Williams, J., Reus, M. De, Krejci, R., Fischer, H., Ström, J., 2002. Application of the variability-size relationship to atmospheric aerosol studies: Estimating aerosol lifetimes and ages. Atmospheric Chemistry and Physics 2, 133–145. doi:10.5194/acp-2-133-2002

Xie, M., Chen, X., Hays, M.D., Lewandowski, M., Offenberg, J., Kleindienst, T.E., Holder, A.L., 2017. Light Absorption of Secondary Organic Aerosol: Composition and Contribution of Nitroaromatic Compounds. Environmental Science and Technology 51, 11607–11616. https://doi.org/10.1021/acs.est.7b03263

Yan, J., Wang, X., Gong, P., Wang, C., Cong, Z., 2018. Science of the Total Environment Review of brown carbon aerosols: Recent progress and perspectives. Science of Total Environment 634, 1475–1485. https://doi.org/10.1016/j.scitotenv.2018.04.083

Zhang, X., Lin, Y.H., Surratt, J.D., Weber, R.J., 2013. Sources, composition and absorption angstrom exponent of light-absorbing organic components in

aerosol extracts from the Los Angeles basin. Environmental Science and Technology 47, 3685–3693. https://doi.org/10.1021/es305047b

Zhang, X., Lin, Y.H., Surratt, J.D., Zotter, P., Prevot, A.S.H., Weber, R.J., 2011. Light-absorbing soluble organic aerosol in Los Angeles and Atlanta: A contrast in secondary organic aerosol. Geophysical Research Letters 38, 49385. https://doi.org/10.1029/2011GL049385

Zhao, R., Lee, A.K.Y., Huang, L., Li, X., Yang, F., Abbatt, J.P.D., 2015. Photochemical processing of aqueous atmospheric brown carbon. Atmospheric Chemistry Physics 15, 6087–6100. https://doi.org/10.5194/acp-15-6087-2015

Zhong, M., Jang, M., 2014. Dynamic light absorption of biomass-burning organic carbon photochemically aged under natural sunlight. Atmospheric Chemistry Physics 14, 1517–1525. https://doi.org/10.5194/acp-14-1517-2014

List of Publications:

Rastogi, N., Singh, A., **Satish, R**., 2018. Characteristics of submicron particles coming from a big firecrackers burning event: Implications to atmospheric pollution (Inpress). Atmospheric Pollution Research. doi:10.1016/j.apr.2018.11.002

Satish, R., Shamjad, P., Thamban, N., Tripathi, S., Rastogi, N., 2017. Temporal Characteristics of Brown Carbon over the Central Indo-Gangetic Plain. Environmental Science and Technology 51, 6765–6772. doi:10.1021/acs.est.7b00734

Shamjad, P.M., **Satish, R**., Thamban, N.M., Rastogi, N., Tripathi, S.N., 2018. Absorbing Refractive Index and Direct Radiative Forcing of Atmospheric Brown Carbon over Gangetic Plain. ACS Earth and Space Chemistry 2, 31–37. doi:10.1021/acsearthspacechem.7b00074

Singh, A., Rastogi, N., Patel, A., **Satish, R**, Singh, D., 2016. Size-segregated characteristics of carbonaceous aerosols over the northwestern Indo-Gangetic plain: Year round temporal behavior. Aerosol and Air Quality Research 16, 1615–1624. doi:10.4209/aaqr.2016.01.0023

Satish, R., Rastogi N, On the Use of Brown Carbon Spectra as a Tool to Understand Their Broader Composition and Characteristics: A Case Study from Crop-residue Burning Samples, 2018 (Under review)

CHAPTER 5

Summary and Future Scope

5.1 Summary

BrC immersed in cloud droplets can absorb light and facilitate evaporation/dispersion of clouds (Hansen et al., 1997, Laskin et al., 2015). It contributes ~35% of the direct radiative forcing warming by carbonaceous aerosols (Lin et al., 2014). However, to assess the effects of BrC on air quality and climate, a proper understanding of its sources and characteristics on temporal and spatial scales is very important (Satiah et al., 2017). In this study, we have characterized atmospheric brown carbon using both offline and online techniques. With an aim to understand the characteristics of BrC over different regions dominated by different emission sources and/or meteorological conditions, many sampling regions and periods for sampling were selected. Further, we have investigated the BrC variability concerning its sources, chemical composition, optical properties, and atmospheric evolution.

This study suggests that primary emissions from biomass burning (BB) and fossil fuel burning (FFB) are the major sources of highly absorbing BrC. Secondary BrC and aged/oxygenated OA are relatively less absorbing. Further, BrC absorption decreases as the day progresses achieving a minimum during afternoon hours. It is also shown that BrC composition is not uniform throughout the day. Our observations suggest that BrC chromophores are a variable mixture of at least HULIS and nitrogen-containing organic compounds over the study regions. These results have implications in regional radiation budget. This study qualitatively depicts the possible role of meteorological parameters on the abundances of BrC, which may be useful in assessing meteorological effects on similar atmospheric species.

Site specific summary of BrC characteristics are given below.

5.1.1 Patiala during Biomass Burning:

In this study, day/night (10-hour integration time) pair of ambient $PM_{2.5}$ samples (n = 69) were collected every day before (n = 21), during (n = 36) and after (n = 8) a large-scale paddy-residue burning during October-November 2014. BrC was

extracted using water and methanol, and subsequently, BrC absorption spectra were stored for 300-700 nm wavelength range for all the samples. Major observations/inferences/conclusions from this work are:

- The $PM_{2.5}$ mass concentration ranged from ~90 to 500 μg m^{-3} (average ± 1$\boldsymbol{\sigma}$ standard deviation: 230 ± 114) with the average values of 154 ± 57, 271 ± 122, 156 ± 18 μg m^{-3} during pre-burning (T1), burning (T2) and post-burning (T3) periods, respectively, reflecting the effect of BB emissions on ambient air quality.
- The $b_{abs\_365\_Water}$ and $b_{abs\_365\_Methanol}$ ranged ~2 to 112 Mm^{-1} (avg: 37±27) and ~3 to 457 Mm^{-1} (avg: 121±108), respectively, suggesting a considerable presence of water-insoluble BrC.
- In linear regression plots of WSOC vs $b_{abs\_365\_Water}$, and OC vs $b_{abs\_365\_Methanol}$, their slopes for day (Water: m = 0.94 ± 0.05, Methanol: m = 1.64 ± 0.06) and night (Water: m = 1.33 ± 0.06, Methanol: m = 2.52 ± 0.12) samples were significantly different. This observation suggests that a significant fraction of water-insoluble chromophores was emitted from BB emissions.
- In the present study, Levoglucosan and K^+ showed a strong correlation with a slope (0.94 ± 0.04, r^2 = 0.87, n = 62) different than those reported for domestic wood burning (Levo/ K^+<0.2), savanna fires (Levo/ K^+~20), and biofuel (Levo/ K^+ = 0.37 ± 0.1) in literature. This ratio (slope) can be used as a fingerprint for the paddy-residue burning over the IGP.
- We observed that BB emits a significant fraction of water-soluble fraction that absorb at the UV region, whereas the water-insoluble fraction absorbs at both UV and visible region. Further, the highest fraction (~86%) of water-insoluble BrC was observed during BB emissions (T2 period).
- At 370 nm, the contribution from MAE of BrC (Water) is ~16-46% and MAE of BrC (Methanol) is~30-88% relative that of EC, indicating the role of BrC in climate forcing.
- %-Water-insoluble fraction was calculated over their different wavelength ranges (R1: 360-400 nm, R2: 410-500 nm, and R3: 510-600 nm). Over Patiala

(BB period), the observed %-water-insoluble fraction during pre-burning (T1: R1 = 63%, R2 = 69%, and R3 = 79%), burning (T2: R1 = 72%, R2 = 77%, and R3 = 85%) and post-burning (T3: R1 = 70%, R2 = 75%, and R3 = 82%) periods were considerable.

5.1.2 Parallel measurements over Patiala and Kanpur during winter period:

In this study, ambient $PM_{2.5}$ samples (24-hour integration time) were collected over Patiala (n = 43) and Kanpur (n = 59) during winter Dec, 2015 to Feb, 2016 period. BrC was extracted using water and methanol and BrC absorption spectra was stored from 300-700 nm for all the samples. Major observations/inferences/conclusions from this study are:

- The $PM_{2.5}$ concentration ranged from ~58 to 251 μg m^{-3} (131 ± 50) and 79 to 336 (167 ± 53) over Patiala and Kanpur, respectively, during the winter period. Primary emission and secondary formation associated with BB and FFB were prominent during winter period over these regions.
- The $b_{abs\_365\_Water}$ and $b_{abs\_365\_Methanol}$ ranged from ~4 to 44 Mm^{-1} (avg: 20 ± 9) and ~13 to 76 Mm^{-1} (avg: 30 ± 16) over Patiala, and ~12 to 60 Mm^{-1} (avg: 27 ± 10) and ~20 to 107 Mm^{-1} (avg: 48 ± 21) over Kanpur, respectively. Both water and methanol soluble BrC concentrations were relatively high over Kanpur. This suggests that Kanpur is more influenced by different emission sources.
- In linear regression plots of WSOC vs $b_{abs\_365\_Water}$ and OC vs $b_{abs\_365\_Methanol}$, their slopes for water (m = 1.11 ± 0.05) and methanol (m= 1.02 ± 0.05) were similar over Patiala. Further, both water and methanol extracted BrC also showed similar spectral characteristics over Patiala. However, the water-soluble BrC is found to be more absorbing compared to methanol soluble BrC, which contradicts the observations made over other sampling sites. This suggests that BrC chromophores over Patiala were highly water soluble.
- In linear regression plots of WSOC vs $b_{abs\_365\_Water}$ and OC vs $b_{abs\_365\_Methanol}$ over Kanpur, slopes for water (m= 0.88 ± 0.06) and methanol (m= 1.44 ± 0.14) plots were significantly different. Methanol Extracted BrC shows higher

absorption compared to water extracted BrC. This observation suggests that water-insoluble BrC chromophores were dominant over Kanpur.

- Mass absorption efficiency (MAE) fraction of BrC over EC is estimated and found to be very high over Kanpur than that over Patiala. At 365 nm, the ratios were ~ 6 times higher at Kanpur than that at Patiala. It is important to note that over Kanpur region, the ambient BrC was also more absorbing.
- %-Water-insoluble fraction was calculated over their different wavelength ranges (R1: 360-400 nm, R2: 410-500 nm, and R3: 510-600 nm). The observed % water-insoluble fractions were 40%, 43% and 45% at R1, R2, and R2, respectively, over Patiala. Similarly, the observed % water-insoluble fractions were 45%, 51% and 60% at R1, R2, and R2, respectively, over Kanpur.

5.1.2.1 Kanpur (Online BrC measurements):

In this study, we conducted semi-continuous measurements of water-soluble organic carbon (WSOC) and BrC using particle-into-liquid sampler coupled with liquid waveguide capillary cell and total carbon analyzer (PILS-LWCC-TOC) over Kanpur during winter season (December 2015 to February 2016). Major observations/inferences/conclusions from this work are:

- Considerable diurnal and day-to-day variability in WSOC concentration and $b_{abs\_365\_Water}$ values were observed. The WSOC varied from 1.0 to 72 µg m^{-3} (avg ± sd: 20 ± 13, 1σ) and b_{abs_365} ranged from 0.02 to 98 Mm^{-1} (24 ± 19) during the study period. This suggests the BrC chromophores concentrations were highly variable during the study period.
- WSOC exhibited a strong correlation with b_{abs_365} (slope =1.22 ± 0.007, r^2 = 0.70, n = 13265, intercept= -0.69 ± 0.17), suggesting that a significant fraction of WSOC is BrC chromophores, which are absorbing at 365 nm.
- Diurnal variability in the absorption coefficient of BrC at 365 nm ($b_{abs\_365\_Water}$) showed higher values (35 ± 21 Mm^{-1}) during late evening to early morning hours and was attributed to primary emissions from biomass burning (BB) and fossil fuel burning (FFB). The b_{abs_365} reduced by more than 80% as the day progressed, which was ascribed to photobleaching/volatilization of BrC and/or due to raising planetary boundary layer (PBL) heights.

- In order to understand the day-to-day variability in BrC composition through absorption spectra, the absorptions at 405, and 420 nm wavelength (representing absorption by different nitro-aromatics) were normalized to the absorption at 365 nm (representing absorption by HULIS compounds). Strong diurnal variability was observed for the ratios of b_{abs_405}/b_{abs_365} and b_{abs_420}/b_{abs_365} which suggests that BrC composition was not uniform throughout the day.
- Mass absorption efficiency (MAE) values of WSOC ranged from 0.003 to 5.26 $m^2\ g^{-1}$ (1.16 ± 0.60) during the study period. This result suggests that the sampling region contains different types of BrC chromophores.
- A moderate correlation (r^2 = 0.50, slope = 1.58 ± 0.019, n = 6471) of $b_{abs\_365\_Water}$ was observed with the semi-volatile oxygenated organic aerosol (SV-OOA) fraction of BB resolved from positive matrix factorization (PMF) analysis of organic mass spectral data obtained from an HR-ToF-AMS. This result suggests that the majority of the BrC chromophores over study region were SV-OOA.
- The low-volatility OOA (LV-OOA) fraction of BB had a similar correlation to $b_{abs\_365\_Water}$ (r^2 = 0.54, slope 0.38 ± 0.004, n = 6442), but appears to have a smaller contribution to the absorption.
- In the scatter plot between WSOC µg $m^{-3}$and $b_{abs\_365\_Water}$, the color axis plotted using elemental ratios (H:C and O:C). We observed high H:C corresponds high $b_{abs\_365nm\_Water}$ and high O:C corresponds to lower $b_{abs\_365nm\_Water}$. It is inferred that over study region primary emitted BrC is more absorbing and absorption reduces as OA gets oxidized.
- Further, higher $b_{abs\_365\_Water}$ value for data points showed a positive relationship with higher WSOC/OA ratios suggests that water-soluble chromophores from respective sources are relatively more absorbing.

5.1.3 Delhi (Winter):

Semi-continuous measurements of water-soluble organic carbon (WSOC) and BrC were also performed using PILS-LWCC-TOC over Delhi during winter season

(December 2017 to February 2018). Major observations/inferences/conclusions from this work are:

- Considerable diurnal and day-to-day variability were observed in WSOC concentration and $b_{abs\_365nm\_Water}$ values. The WSOC varied from 1.0 to 62 µg m^{-3} (avg ± sd: 16 ± 9, 1σ) and b_{abs_365nm} ranged from 0.05 to 65 Mm^{-1} (18 ± 12) during the study period. This result suggests that BrC chromophores are highly variable over the study region.
- WSOC exhibited a strong correlation with an absorption coefficient ($b_{abs\_365\_Water}$) (slope = 1.21 ± 0.007, r^2 = 0.72, n = 11635, intercept = −0.66 ± 0.12), suggesting the presence of a significant but variable fraction of water-soluble chromophores.
- MAE ranged from 0.005 to 3.34 m^2 g^{-1} (1.12 ± 0.46) during the study period. Further, MAE value calculated at different wavelengths; it shows a decreasing trend with increasing wavelength (365 nm: m = 1.20, r^2 = 0.72; 405 nm: m = 0.60, r^2 = 0.72; 420 nm: m = 0.48, r^2 = 0.70; 450 nm: m = 0.371, r^2 = 0.64; 490 nm: m = 0.30, r^2 = 0.52; and 550 nm: m = 0.1, r^2 = 0.46).
- The photochemical secondary organic aerosol formation was evident during morning hours (08:00 to 10:00 hours) whereas variability during late evening/night hours (19:00 to 23:00 hours) is attributed to both due to primary emission and secondary formation of WSOC and $b_{abs\_365\_Water}$.
- Diurnal pattern of MAE also followed similar trends with WSOC and $b_{abs\_365\_Watter}$, and these trends are similar to those observed over Kanpur site.
- Further, diurnal pattern of $b_{abs\_365nm\_Water}$/CO suggests that secondary BrC was dominant throughout the day from 00:00 to 12:00 hours and it reduced during early evening rush hours.
- In January, BrC spectra showed a dual hump with the first peak at 300 nm (likely due to HULIS) and second at 500 nm (likely due to secondary nitroaromatics). The second hump disappeared during day hours, and overall BrC absorption at shorter wavelengths also decreased, which was ascribed to photo-bleaching/volatilization.

5.1.4 NE-Himalayan region (Shillong):

In this study, ambient $PM_{2.5}$ samples (24-hour integration time) were collected over Barapani, Shillong region (n = 35) during Jan-Apr, 2017. BrC was extracted using water and methanol and BrC absorption spectra stored from 300-700 nm for all the samples. Major observations/inferences/conclusions from this work are:

- $PM_{2.5}$ mass concentration ranged from 44 - 144 (avg ± sd: 88 ± 25) during the study period with the highest concentrations in January (100 ± 20) than the rest of the period. January month was influenced by local BB emissions.
- The $b_{abs\_365\_Water}$ and $b_{abs\_365\_Methanol}$ ranged from 5 to 31 M m^{-1} (14 ± 6 M m^{-1}) and 5 – 70 M m^{-1} (27 ± 17 M m^{-1}), respectively, over Shillong region, suggesting the dominance of water-insoluble BrC likely due to local BB emissions during the winter period.
- In linear regression plots of WSOC vs $b_{abs\_365\_Water}$ and OC vs $b_{abs\_365\_Methanol}$, their slopes for water (m = 0.74 ± 0.06) and methanol (m = 1.25 ± 0.12) were significantly different. The methanol-soluble BrC slope is two times higher than water-soluble BrC. The majority (~ 60%) BrC is found to be insoluble in water. The observed % of the water-insoluble fraction was 52%, 60% and 64% at R1, R2, and R2, respectively, over Shillong region.
- Fractional contribution MAE of BrC (Water and Methanol) over that of EC was low.

5.1.5 Port Blair region conclusion of the study:

In this study, ambient PM_{10} samples (24-hour integration time, n = 50) were collected over Port Blair region (Andaman Nicobar group of Islands) during Feb-Mar, 2013. BrC was extracted using water and methanol, and BrC absorption spectra was stored from 300-700 nm for all the samples. Major observations/inferences/conclusions from this work are:

- The $PM_{2.5}$ mass concentration ranged from 23 to 65 μg m^{-3} (42 ± 11) with the average values of 47 ± 5, 43 ± 12, and 38 ± 9 μg m^{-3} during February, March, and April, respectively.

- The $b_{abs\_365\_Water}$ and $b_{abs\_365\_Methanol}$ ranged from 0.4 to 4.2 M m^{-1} (1.4 ± 0.8 M m^{-1}) and 0.8–11.3 M m^{-1} (3.2 ± 1.9 M m^{-1}), respectively. The methanol-soluble BrC was more than two times higher than water-soluble BrC. However, linear regression plots of WSOC vs $b_{abs\_365\_Water}$, and OC vs $b_{abs\_365\_Methanol}$ showed similar slopes for water (0.64 ± 0.06) and methanol (0.74 ± 0.06) extracts. The difference in these slopes suggests that water-soluble chromophores were dominant.
- Further, the monthly variation of $b_{abs\_365\_Water}$ and $b_{abs\_365\_Methanol}$ during February (1.8 ± 0.6 M m^{-1}; 3.5 ± 0.9 M m^{-1}), March (1.6 ± 1.0 M m^{-1}; 3.7 ± 2.4 M m^{-1}), April (0.9 ± 0.3 M m^{-1}; 2.1 ± 0.8 M m^{-1}) showed a decreasing trend. From February to April, both water and methanol-soluble BrC values reduced significantly.
- Both water and methanol extracted BrC showed similar MAE values. Further, EC was found to be well correlated with $b_{abs\_365\_water}$ (r^2 = 0.75) and $b_{abs\_365\_Methanol}$ (r^2 = 0.70), suggesting both water and methanol soluble chromospheres came from the similar source and/or transport pathway. Similarly, BrC absorption relative to EC values also found to be similar for water and methanol extracted BrC.
- The observed %- water-insoluble fraction was 57%, 62% and 65% at R1, R2, and R2, respectively, over Port Blair.

5.1.6 Ahmedabad (November 2015):

Semi-continuous measurements of WSOC and BrC were also performed using PILS-LWCC-TOC over Delhi during November, 2014. Major observations/inferences/conclusions from this work are:

- A considerable day-to-day variability was observed in WSOC concentration and $b_{abs\_365\_Water}$ values. The WSOC varied from 1.0 to 116 µg m^{-3} (avg ± sd: 11 ± 9, 1σ) and $b_{abs\_365\_Water}$ ranged from 1 to 126 Mm^{-1} (10 ± 12) during the study period. This result suggests that BrC chromophores were highly variable during the study period.
- WSOC exhibited a moderate correlation with $b_{abs\_365\_Water}$ (slope = 0.79 ±

0.01, r^2 = 0.44, n = 3949), suggesting that a fraction of WSOC is BrC chromophores, which are absorbing at 365 nm.

- The observed diurnal pattern of $b_{abs\_365\_Water}$ and WSOC was slightly different over Ahmedabad compared to those observed over Kanpur and Delhi sites. During winter period, Kanpur and Delhi sites were largely influenced by BB and FFB emissionswith relatively high concentrations during night over these regionscompared to that over Ahmedabad.
- Diurnal pattern of $b_{abs\_365\_Water}$ peaked in the morning (06:00-09:00) and evening (17:00-22:00), which was attributed to rush hours. However, morning peak for WSOC lasted for more extended period (07:00 to 12:00) compared to $b_{abs\_365\_Water}$.
- Diurnal pattern of WSOC/CO ratio showed a substantial increase from morning to afternoon hours of the day (08:00-16:00), which suggests that SOA formation was dominant during day hours.
- MAE ranged from 0.03 to 3.90 $m^2\ g^{-1}$ (0.97 ± 0.78) during the study period with lower MAE values during day time (attributed to Photo bleaching/ expansion of boundary layer) and high values during night hours.

5.2 Future Scope

This study provides the BrC characteristics of ambient aerosols ($PM_{2.5}$) from urban, rural and high-altitude sites in India using online and offline techniques. However, there is still much work that needs to be done to understand the role of brown carbon in the atmosphere. Understanding photobleaching of BrC chromophores in the atmosphere is one the challenging research area. Also, the increase in the wavelength dependence of BrC absorption suggests that not all BrC molecules respond similarly to photobleaching. Further studies on the molecular speciation of BrC could yield valuable insights into both primary and secondary BrC. Vertical profiles of BrC composition and characteristics through aircraft measurements needs attention. It will allow one to assess the role of BrC on clouds and climate forcing. BrC properties from specific sources can also be assessed through chamber based experiments.